STUDY OF MECHANICAL, ELECTRICAL AND THERMAL PROPERTIES OF CARBON NANOTUBE INCORPORATED CELLULOSE NANOCOMPOSITES

URENA MOSTAFA

MASTER OF SCIENCE IN PHYSICS

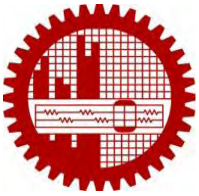

DEPARTMENT OF PHYSICS

BANGLADESH UNIVERSITY OF ENGINEERING AND TECHNOLOGY

DHAKA-1000, BANGLADESH

MAY, 2018

STUDY OF MECHANICAL, ELECTRICAL AND THERMAL PROPERTIES OF CARBON NANOTUBE INCORPORATED CELLULOSE NANOCOMPOSITES

A dissertation submitted to the Department of Physics, Bangladesh University of Engineering and Technology, Dhaka in partial fulfillment of the requirements for the degree of Master of Science (M.Sc.) in Physics

by

URENA MOSTAFA

ROLL NO.: 0416142504F

SESSION: APRIL, 2016

DEPARTMENT OF PHYSICS

BANGLADESH UNIVERSITY OF ENGINEERING AND TECHNOLOGY

DHAKA-1000, BANGLADESH

MAY, 2018

BANGLADESH UNIVERSITY OF ENGINEERING & TECHNOLOGY (BUET)
DHAKA
DEPARTMENT OF PHYSICS

CERTIFICATION OF THESIS

The thesis titled "**Study of Mechanical, Electrical and Thermal Properties of Carbon Nanotube Incorporated Cellulose Nanocomposites**" submitted by **Urena Mostafa**, Roll No: 0416142504F, Session: **April/2016**, has been accepted as satisfactory in partial fulfillment of the requirement for the degree of **Master of Science (M.Sc.) in Physics** on **27 May, 2018.**

BOARD OF EXAMINERS

1. _____
Dr. Mohammad Jellur Rahman — **Chairman (Supervisor)**
Assistant Professor,
Department of Physics, BUET, Dhaka-1000

2. _____
Dr. Md. Forhad Mina — **Member (Ex-Officio)**
Professor & Head
Department of Physics, BUET, Dhaka-1000

3. _____
Dr. Md. Abu Hashan Bhuiyan — **Member**
Professor
Department of Physics, BUET, Dhaka-1000

4. _____
Dr. Jiban Podder — **Member**
Professor
Department of Physics, BUET, Dhaka-1000

5. _____
Dr. Md. Mizanur Rahman — **Member (External)**
Associate Professor
Department of Physics, University of Dhaka, Dhaka-1000

CANDIDATE'S DECLARATION

It is hereby declared that this thesis or any part of it has not been submitted elsewhere for the award of any degree or diploma.

Signature of the candidate

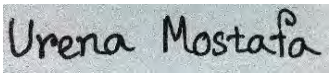

Urena Mostafa

Roll No.: 0416142504F

Session: April, 2016

Dedicated

To

My Dear Parents

Who have made innumerable sacrifices

For me

CONTENTS

		Page No.
CANDIDATE'S DECLARATION		i
DEDICATION		ii
LIST OF FIGURES		vi
LIST OF TABLES		viii
LIST OF ABBREVIATIONS		ix
ACKNOWLEDGEMENTS		x
ABSTRACT		xi
CHAPTER 1		
GENERAL INTRODUCTION		**1 – 19**
1.1	Introduction	2
1.2	Introduction to Carbon Nanotubes	3
1.3	Nanocomposites	5
1.4	Cellulose	6
1.5	Cellulose Nanocomposites	7
1.6	Paper based Nanocomposites	8
1.7	Literature Review	9
1.8	Objectives of this Study	16
1.10	Outline of this Thesis	17
	References	18
CHAPTER 2		
THEORITICAL BACKGROUND		**20 – 49**
2.1	Polymers	21
	2.1.1 Natural Polymers	21
	2.1.2 Structure of Cellulose Fiber	23
2.2	Properties of Carbon Nanotubes	24
2.3	Dispersion of Carbon Nanotubes	25
	2.3.1 Dispersion of CNTs in Water by Surfactants	26
2.4	Surface Morphology	28
	2.4.1 Electron Microscope	28
	2.4.2 Scanning Electron Microscope	29

2.4.3 Transmission Electron Microscope 30
2.5 Elemental Analysis 31
2.5.1 Energy Dispersive X-ray Spectroscopy 31
2.6 Structural Analysis 33
2.6.1 X-Ray Diffraction 33
2.6.2 Fourier-Transform Infrared spectroscopy 34
2.7 Thermal Analysis 37
2.7.1 Thermogravimetric Analysis (TGA) 37
2.7.2 Differential scanning calorimetry (DSC) 38
2.8 Electrical Conduction in Polymer Nanocomposites 40
2.8.1 Theory of Percolation 41
2.8.2 Composite Behavior above the Percolation Threshold 41
2.8.3 Composite Behavior at the Percolation Threshold 41
2.8.4 Composite Behavior below the Percolation Threshold 42
2.8.5 Factors Influencing the Conductivity of CNT/polymer Composites 42

References 46

CHAPTER 3
EXPERIMENTAL DETAILS 50 – 59

3.1 Materials 51
3.1.1 Cellulose 51
3.1.2 Multi-Walled Carbon Nanotubes (MWCNTs) 51
3.1.3 Sodium Dodecyl Sulfate (SDS) 51
3.1.4 Ethanol 51
3.2 Apparatus used for the Fabrication of the Composites 51
3.3 Composite Fabrication 53
3.4 Composite Characterization 55
3.4.1 Surface Morphology 55
3.4.2 Elemental Analysis 55
3.4.3 Structural Characterization 56
3.4.3.1 X-ray Diffraction 56
3.4.3.2 Fourier Transform Infrared Spectroscopy 57
3.4.4 Thermal Stability Analyses 57
3.4.4.1 TGA and DTG 57

3.4.5 Electrical Measurements 58

CHAPTER 4
RESULTS AND DISCUSSION 60−91

4.1 Introduction 61
4.2 Surface Morphology 61
4.2.1 Surface Morphology of *p*-CNTs 61
4.2.2 Surface Morphology of the CNT/cellulose Nanocomposites 62
4.3 Elemental Analysis 67
4.3.1 Energy Dispersive X-ray Analysis (EDX) 67
4.4 Structural Analyses 70
4.4.1 Fourier Transform Infrared Spectroscopy (FTIR) Analysis 70
4.4.2 X-ray Diffraction (XRD) Analysis 71
4.5 Thermal Analyses 73
4.5.1 TGA and DTG 73
4.5.2 Flame Retardancy Test 75
4.6 DC Electrical Properties 77
4.6.1 Sheet Resistance 77
4.6.2 Current Density ─ Voltage Characteristics 78
4.6.3 Electrical Conductivity 82
4.6.4 Activation Energy 84
4.7 Flexibility Test 86
References 89

CHAPTER 5
CONCLUSIONS AND SUGGESTIONS FOR FUTURE WORK 92 − 94

5.1 Conclusions 93
5.2 Recommendations for Future Work 94

LIST OF FIGURES

Fig No.		Page No.
1.1	Different types of CNTs depending on the chiral indices.	4
1.2	Different types of CNTs depending on the number of rolled-up graphene sheets.	4
1.3	Chemical structure of cellulose.	6
2.1	Classification of fibers.	22
2.2	The structure of cellulose sheet showing the intra- and inter-chain hydrogen bonds.	23
2.3	Different types of possibilities of the functionalization of CNTs.	25
2.4	Schematic representations of the mechanism by which surfactants help to disperse CNT.	27
2.5	Chemical structure of SDS.	28
2.6	Schematic diagram of the working principle of a scanning electron microscope.	29
2.7	Schematic diagram of the working principle of a transmission electron microscope.	31
2.8	Schematic diagram of the principle of EDS.	32
2.9	Schematic diagram of the Bragg's equation.	33
2.10	Different types of molecular vibrations.	35
2.11	Block diagram of an FTIR spectrometer.	36
2.12	Schematic diagram of thermogravimetric analysis.	37
2.13	Schematic diagram of heat flux type DSC.	39
2.14	Schematic diagram of power compensation type DSC.	40
2.15	Integration of nanotubes into the polymer cross-linked structure.	42
3.1	A photograph of a magnetic stirrer.	52
3.2	A photograph of a hot air oven machine.	53
3.3	Flow chart of preparation procedure of CNT/Cellulose nanocomposites.	54
3.4	Field emission scanning electron microscope set up.	55
3.5	X-ray diffractometer set up.	56
3.6	Simultaneous thermal analyzer set up.	57
3.7	A schematic circuit diagram of DC measurement.	58
3.8	DC measurement set up.	59
4.1	(a), (c) TEM images of *p*-CNTs at ×25k and ×120k magnifications and (b), (d) FESEM images of *p*-CNTs at ×30k and ×50k magnifications.	61
4.2	FESEM images of (a) Cellulose sheet and (b) CNT coated cellulose fibers at ×1k magnification.	62
4.3	FESEM images of cellulose fiber at (a) ×10k magnifications and (b) ×30k magnifications.	63
4.4	FESEM images of 0.5 wt% CNT/Cellulose nanocomposites at (a) ×10k and (b) ×30k magnifications.	64

4.5	FESEM images of 1.0 wt% CNT/Cellulose nanocomposites at (a) ×10k and (b) ×30k magnifications.	65
4.6	FESEM image of 1.5 wt% CNT/Cellulose nanocomposites at (a) ×10k and (b) ×30k magnifications.	66
4.7	EDX spectrum of Cellulose sheet.	67
4.8	EDX spectrum of (a) 0.5 wt% and (b) 1.0 wt% CNT/Cellulose nanocomposites.	68
4.9	EDX spectrum of 1.5 wt% CNT/Cellulose nanocomposites.	69
4.10	FTIR spectra of the *p*-CNTs, cellulose sheet and 2.0 wt% CNT/Cellulose nanocomposites.	70
4.11	XRD patterns of the *p*-CNTs, cellulose sheet and 0.5 wt%, 1.0 wt%, 1.5 wt% CNT/cellulose nanocomposites.	72
4.12	TGA curves of the cellulose sheet and 0.5 wt%, 1.0 wt%, 1.5 wt% CNT/Cellulose nanocomposites.	73
4.13	DTG curves of the cellulose sheet and 0.5 wt%, 1.0 wt%, 1.5 wt% CNT/cellulose nanocomposites.	74
4.14	Flammability comparison of cellulose sheet (left) and CNT/cellulose composite sheet.	76
4.15	Sheet resistance vs composites with different weight percentages of CNTs.	77
4.16	Plots of J-V characteristics for cellulose sheet and CNT/cellulose nanocomposites with various CNT content at (a) 298 K and (b) 358 K temperature.	78
4.17	Plots of J-V characteristics at different temperature for (a) cellulose sheet and (b) 0.5 wt% CNT/cellulose nanocomposites.	79
4.18	(a) Conductivity vs wt% of CNTs and (b) Conductivity vs temperature for cellulose sheet (0 wt%) and different wt% of CNT/cellulose nanocomposites.	83
4.19	(a) Variation of current density with 1000/T.	84
4.19	(b) Activation energy vs wt% of MWCNT in the cellulose matrix.	85
4.20	(a) Variation of sheet resistance of the nanocomposites according to the number of bending cycles.	86
4.20	(b) Sheet resistance vs CNT concentration curves during flat and bending states.	87

LIST OF TABLES

Table 1.1	Some basic properties of cellulose.	7
Table 4.1	Elemental analysis for cellulose sheet and CNT/cellulose nanocomposites.	69
Table 4.2	Data of weight loss calculation for cellulose sheet and CNT/cellulose nanocomposites.	75
Table 4.3	Activation energy values of nanocomposites in two temperature regions	85

LIST OF ABBREVIATIONS

CNTs	Carbon nanotubes
MWCNTs	Multi-walled carbon nanotubes
p-CNTs	Pristine carbon nanotubes
SDS	Sodium dodecyl sulfate
λ	Wavelength
θ	Bragg angle
k_B	Boltzmann constant
ΔE	Activation energy
σ	Electrical conductivity
J	Current density
R_s	Sheet resistance
D	Crystallite size
β	Full width half maximum
R	Electrical resistance
T	Temperature

ACKNOWLEDGEMENTS

First and foremost praise is to the Almighty Allah for continuous blessings and for providing me the opportunity, determination, strength and patience to complete the research work.

I would like to thank all the people that have contributed directly or indirectly and without their help this work would have never been possible to complete.

I would like to convey my immense gratitude to my respected supervisor Dr. Mohammad Jellur Rahman, Assistant Professor, Department of Physics, Bangladesh University of Engineering and Technology (BUET) for his meticulous guidance, invaluable suggestions, encouragement, friendly supervision and strong support throughout the entire period of research. I am also very thankful for his belief in me and introducing me to the exciting world of nanotechnology.

I am humbly grateful to Professor Dr. Md. Forhad Mina, Head, Department of Physics, BUET, for providing me necessary research facilities available in the Department and also for his useful suggestions and insightful comments.

I owe an enormous debt of gratitude to Professor Dr. Md. Abu Hashan Bhuiyan, Department of Physics, BUET, for all his advice, enlightening discussions, essential instructions and also for inspiring me to always learn and strive for excellence.

I would also like to express gratitude to all the faculty members for their inspiration and suggestions.

I would like to especially acknowledge Professor Dr. Tetsu Mieno, GSST, Shizuoka University, Japan for providing the carbon nanotubes.

I am gratefully acknowledge the financial support for this research work from the authority of BUET.

I am very grateful to my teacher Mrs. Nasima Banu for her helpful suggestions, support, care and all the things that I could have learned from her. I would also like to thank Ahaduzzaman Deeraz, Md. Abdul Momin, Meherun Nesa, Md. Forhad Hossain, Md. Aminul Islam and my other senior and junior researchers of Material Science Laboratory for their help and support in completing the dissertation.

I wish to thank all the staff members, Department of Physics for their kind assistance.

Finally, I would like to express my infinite gratitude to my parents and younger brother for their unconditional love, incredible motivation and sincere support throughout my life.

Urena Mostafa

May, 2018.

Abstract

Low cost, biodegradable, thin and flexible carbon nanotube (CNT)/cellulose nanocomposites have been prepared by varying the concentration of multi-walled carbon nanotubes (MWCNTs) up to 3.0 wt%. To attain effective CNT/cellulose composites uniform CNT dispersion is made by the adsorption of sodium dodecyl sulfate (SDS) on the CNT surface. The implications of incorporating CNTs in cellulose and electrical, structural and thermal properties of the composites are evaluated in this work. The field emission scanning electron microscope micrographs of the CNT/cellulose composites display the uniform attachment of CNTs on the surfaces of all the fibers of cellulose sheet. The energy-dispersive x-ray spectroscopy analysis reveals that all the samples are composed of high content of C and O. The Fourier-transform infrared spectroscopy spectrum of the CNT/cellulose composites do not show any significant changes in the band position but the band intensities of -OH and -CH_2 groups are increased. X-ray diffraction patterns indicate that the crystallinity of the composites is improved with increasing CNT concentration. The dominant weight loss of all the samples is observed between 566-663 K. A gradual decrease of sheet resistance of the composites can be observed due to the formation of electrically conducting CNT network on the surfaces of the all fibers of the cellulose sheet and the nanocomposites exhibit remarkably low sheet resistance varying from 6.5 kΩ/sq. to 0.04 kΩ/sq. The conductivity of the nanocomposites increases with the increase of incorporating wt% of MWCNTs and becomes 2.34 S/m. The conductivity of the nanocomposites also increases with the increase in temperature indicating the semiconducting nature of the composites. The activation energy of all the samples are decreased in high temperature region (358 K) compared to the low temperature region (298 K). Flame retardancy test indicates that the CNT/cellulose sheet exhibits an improved flame retardant performance. The sheet resistance is slightly increased in bending state compared to the flat condition of the composites. CNT/cellulose composites shows mechanical flexibility, which is desirable for flexible electronic devices. The CNT/cellulose nanocomposites will find applications in foldable energy storage electronic devices as well as in other advanced technological fields.

CHAPTER 1

GENERAL INTRODUCTION

1.1 Introduction

The enormous potential of natural polymer based biodegradable nanocomposites for creating new applications in advanced technological sectors is the reason behind the increasing scientific attention. Also, they offer alternatives to maintaining sustainable development of economic and environmentally attractive technology. The combination of the unique properties of natural polymers and nanofillers show the effective improvement of the properties of the composites and find applications as an advanced product. Natural polymers offer environmentally friendly benefits in that they have the capability to degrade naturally into organic substances without releasing any toxic components. In the recent years, the development of cellulose based materials have been an interesting topic in the field of advanced research. The main purpose of this research is to enhance the properties of regular cellulose sheet so that it finds application as an advanced product to satisfy the technological demand of next generation. By incorporating specific fillers with cellulose fibers, paper can take on conductive, magnetic, photoluminescent, antimicrobial, acoustic dampening, or flame retardant properties [18]. The versatility and multifunctionality of carbon nanotubes (CNTs) have made them promising for their use as nanofiller which can effectively transform the insulating cellulose into a conductive material. In addition to being of low cost, the CNT/cellulose nanocomposites are environmentally friendly, renewable, biodegradable, thin and flexible as well as having a low density. This CNT/cellulose nanocomposites may find applications in foldable energy storage electronic devices as well as in other advanced technological fields such as [11-14]:

- Paper battery
- Supercapacitors
- Transistors
- Actuators
- Multifunctional sensors
- Strain gauges
- Electric heater
- Power generators
- EMI shielding materials

1.2 Introduction to Carbon Nanotubes

After the discovery of CNTs in 1991 by Iijima [1], these fascinating materials have inspired the global research tremendously and opened up novel possibilities in nanotechnology, electronics, optics, material science, biotechnology and space science. CNTs are allotropes of sp^2 hybridized carbon with a hollow cylindrical nanostructure. These nanotubes can be visualized as rolled sheets of graphene with constant radius comprising of hexagonal network of carbon atoms, often capped by a fullerene-like hemisphere at each ends. CNTs are one-dimensional nanomaterials with large specific area and high aspect ratio. CNTs possess unique and remarkable properties which are varied with the structure, morphology, diameter and length of the tubes. The structure of CNTs depends on the chirality (the degree of twist of graphene sheet) of each nanotube where chirality can be expressed by the chiral vector $\boldsymbol{C_h}$ and the chiral angle θ. The chiral vector is defined as $\boldsymbol{C_h} = n\,\boldsymbol{a_1} + m\,\boldsymbol{a_2}$, where $\boldsymbol{a_1}$ and $\boldsymbol{a_2}$ are the unit vectors and n and m are the chiral indices.

Unit vector, $\boldsymbol{a} = \sqrt{3}L = 0.246$ nm, where L is the bond length taken as 0.142 nm [2].

Chiral angle, $\theta = \sin^{-1}\frac{(2n+m)}{2\sqrt{(n^2+m^2+nm)}}$

Nanotube diameter, $D = \frac{a}{\pi}\sqrt{(n^2 + m^2 + nm)}$

Depending on the chiral indices (n, m), CNTs can be classified to armchair, chiral and zigzag (Figure 1.1). When $n = m$, the nanotubes are called armchair ($\theta = 30°$). If $n = 0$ or $m = 0$, the nanotubes are named as zigzag ($\theta = 0°$) and when $n \neq m$, the nanotubes are called chiral ($0° < \theta < 30°$). At all times, the armchair nanotubes are metallic whereas zigzag nanotubes are either metallic or semiconducting in nature.

Depending on the number of concentrically rolled-up graphene sheets, CNTs are also classified to single-walled carbon nanotubes (SWCNTs), double-walled carbon nanotubes (DWCNTs), and multi-walled carbon nanotubes (MWCNTs) as shown in Figure 1.2. SWCNTs consist of a single graphite sheet seamlessly wrapped into a cylindrical tube. MWCNTs comprise an array of such nanotubes that are concentrically nested like rings of a tree trunk [3]. DWCNTs are considered as a special type of MWCNT where only two concentrically rolled up graphene sheets are present.

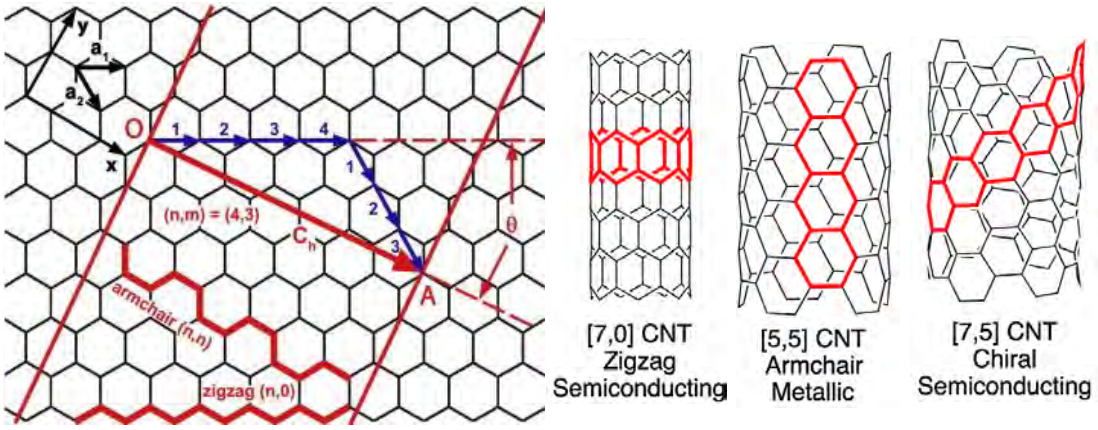

Figure 1.1: Different types of CNTs depending on the chiral indices [From internet].

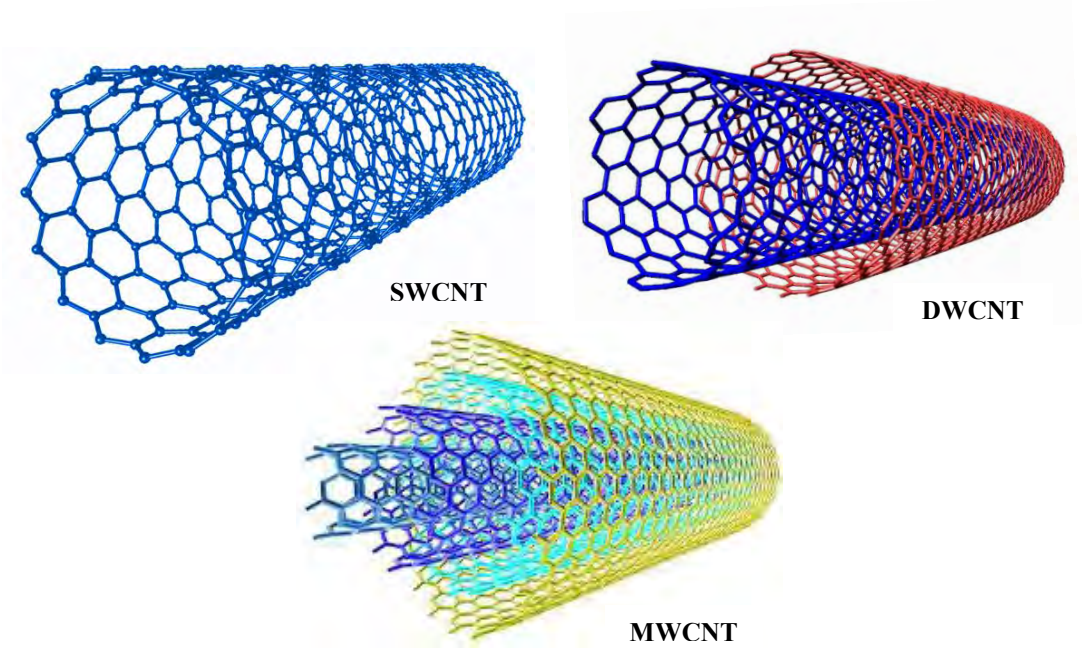

Figure 1.2: Different types of CNTs depending on the number of rolled-up graphene sheets [From internet].

1.3 Nanocomposites

Nanocomposites are multiphase solid materials derived from the combination of a matrix (continuous phase) and a nanoscale filler (reinforcing phase) such as nanoparticles, nanotubes, nanofibers, nanowhiskers, etc. to overcome the limitations of monolithic conventional materials.

The properties of nanocomposites rely on a range of variables, particularly the matrix material, which can exhibit nanoscale dimensions, loading, degree of dispersion, size, shape, and orientation of the nanoscale reinforcing phase and interactions between the matrix and the reinforcing phase. The properties of nanocomposites can display synergistic improvements over those of the component phases individually. The addition of nanofillers has drastic improvements in surface to volume ratio, mechanical strength, electrical or thermal conductivities, flame retardancy, optical clarity, gas barrier, etc. This rapidly expanding field is generating many exciting new materials with novel properties [4]. Based on matrix, there are generally three classes of nanocomposites [5]: (a) metal matrix nanocomposites, (b) ceramic matrix nanocomposites, (c) polymer matrix nanocomposites. Also, there are two modes of classification for nanocomposites. They are the organic and inorganic nanocomposites. Nanocomposites offer new technology and opportunities for several sectors. It has very high impact in developing a new generation of composites with enhanced functionality and a wide range of applications. Nanocomposites are currently being used in numerous fields and new applications are being continuously developed. Applications for nanocomposites include:

- Electronics
- Films
- Aerospace industries
- Automobile sectors
- Food packaging
- Environmental protection
- Biotechnology industries
- Gas barriers

1.4 Cellulose

Cellulose is the most prevalent organic polymer on earth and the main building block of the plant cell wall. Cellulose-based natural materials such as wood, cotton, rope, reinforce mud bricks and paper have played an important role in our societies over thousands of years [6]. Cellulose is a linear carbohydrate polymer chain consisting of several thousands of β (1-4) linked D-glucopyranose units. Chemical formula of cellulose is $(C_6H_{10}O_5)_n$. Each D-glucose unit has three free hydroxyl groups which can undergo chemical reactions but can also form intra- and intermolecular hydrogen bonds [7].

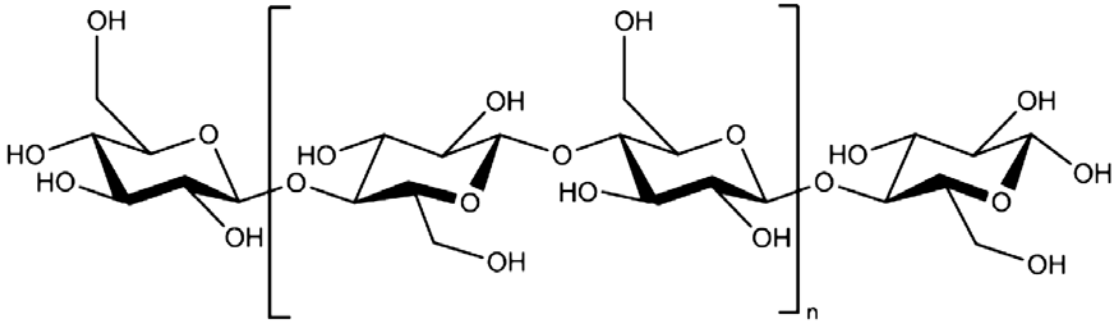

Figure 1.3: Chemical structure of cellulose.

The most stable confirmation about the β (1→4) linkage involves alternating 180 °C flips of every second glucose unit. This repeating unit of cellulose is cellobiose which is a dimer of glucose (Figure 1.3). The size of the cellulose molecule strongly depends on the source of the cellulose. Naturally, cellulose does not occur as an isolated molecule but is found in the form of fibrils. The structure of cellulose is stabilized by an intramolecular hydrogen bond network. This network makes cellulose a relatively stable polymer, which does not readily dissolve in aqueous solvents. Cellulose is composed of hemicelluloses and lignin which comprise 20-35% and 5-30% respectively of plant dry weight [8]. In a few cases such as cotton bolls, cellulose is present in a nearly pure state. Hemicelluloses are comprised of several different polysaccharides and lignin is a complex amorphous polymer consisting mainly of aromatic units. Biodegradability, non-toxicity, relatively low cost and plentiful supply are the main reasons for the attraction of more widespread utilization of cellulose.

Table 1.1: Some basic properties of cellulose [9].

Properties	
Molar Mass	162.1406 g/mol
Density	1.5 g/cm^3
Solubility in Water	Insoluble
Melting Point	260-270 °C
Crystalline Nature	Crystalline and Amorphous
Electrical Nature	Insulating polymer
Contact Angle	20–30 degrees (Hydrophilic)
Color	White

1.5 Cellulose Nanocomposites

The aim of manufacturing nanocomposites is to generate novel materials with improved properties in comparison to those of the individual constituents. Most of the industrial applications are found in polymer based nanocomposites. Polymer matrices are attractive as a continuous phase of nanocomposites for a variety of reasons.

The natural abundance, biodegradability, low density (1.5 g/cm^3) and relatively cheap production costs of materials are the reasons that researchers have and continue to use cellulose as a matrix for nanocomposites. A high aspect ratio and flexibility are characteristic for cellulose fibrils and functional hydroxyl groups in cellulose enable chemical modifications for further applications. Some physical features of cellulose are not satisfactory to extend its utilization in different advanced applications and it is necessary to modify them by adding specific fillers. The use of cellulose as a polymeric matrix typically requires either the dispersal or the dissolution of cellulose. In the successful preparation of polymer nanocomposites, uniform mixing of components is the most challenging issue [10]. Various approaches exist in order promote miscibility, such as using common solvents, high energy sonication treatments, surfactants,

chemical modification, etc. In the case of cellulose-based polymer nanocomposites, the cellulosic component may occupy the role of either nanoparticle filler or polymer host. The inherent properties of cellulose make it attractive for use in a wide range of advanced applications such as high-performance biodegradable material science, electronics, drug delivery, optoelectric, barrier catalysis, smart textiles, biodegradable packaging material, sensors, actuators etc. Besides, these nanocomposites are useful in various field of biomedical applications such as tissue engineering scaffolds, cardiovascular implants, biosensors, artificial skin and hydrogels for clinical and pharmacological applications.

1.6 Paper based Nanocomposites

One of the main focuses of bio-based composites is natural fibers and paper is the unique material that extend the uses of natural cellulose. Paper is still the major way to store information while we have the benefits of digital storage and it also offers many other traditional advantages. Papermaking is an ancient art that plays an important part in human history, Cellulose linear macromolecules aggregate to highly ordered structure referred to as elementary fibrils. These are packed into larger units to form microfibrils which in turn are assembled into cellulose fibers such as pulp fibers and paper is fabricated from cellulose pulp. By incorporating specific fillers with cellulose fibers, papers can take on properties of conductive, magnetic, photoluminiescent, catalytic, antimicrobial, acoustic dampening or flame retardant, which open the doors to myriad new potential applications. Paper nanocomposites based electronics provides possibilities for next generation devices with flexible, biodegradable, biocompatible, ecofriendly, lightweight and wearable electronics. High performance flexible paper based nanocomposites are researched extensively which can be used for the transistor, sensor, actuator, antistatic package, electric heater, electromagnetic interference shielding materials, foldable energy storage device.

1.7 Literature Review

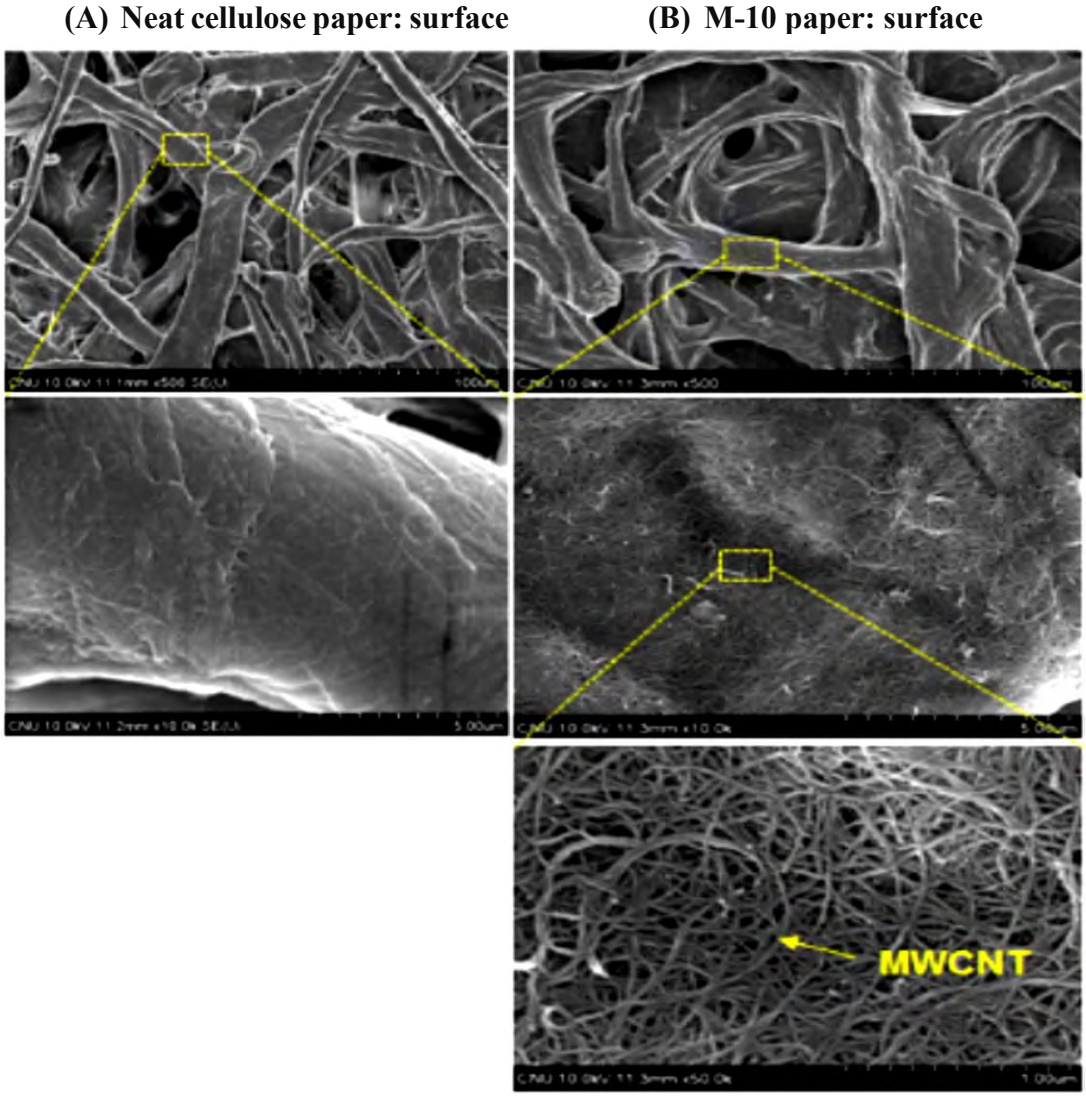

Figure 1.4: SEM images for surfaces of (A) neat cellulose paper and (B) M-10 paper [11].

Lee et al. [11] studied the CNT/cellulose sheets manufactured by dip coating process and observed their performance in electric heating and electromagnetic interference (EMI) shielding materials. The SEM images revealed that CNT/cellulose sheets were homogeneously coated with interconnected MWCNTs. For CNT/cellulose papers, the current increased linearly with the applied voltage and the slopes of the *I-V* curves increased significantly with the increase of the dip coating cycle. The apparent and practical electrical conductivity in the in-plane direction increased significantly from 0.02 S/cm to 1.11 S/cm with the increment of the dip-coating cycle. The CNT/cellulose papers were found to be thermally stable up to ~ 250 °C.

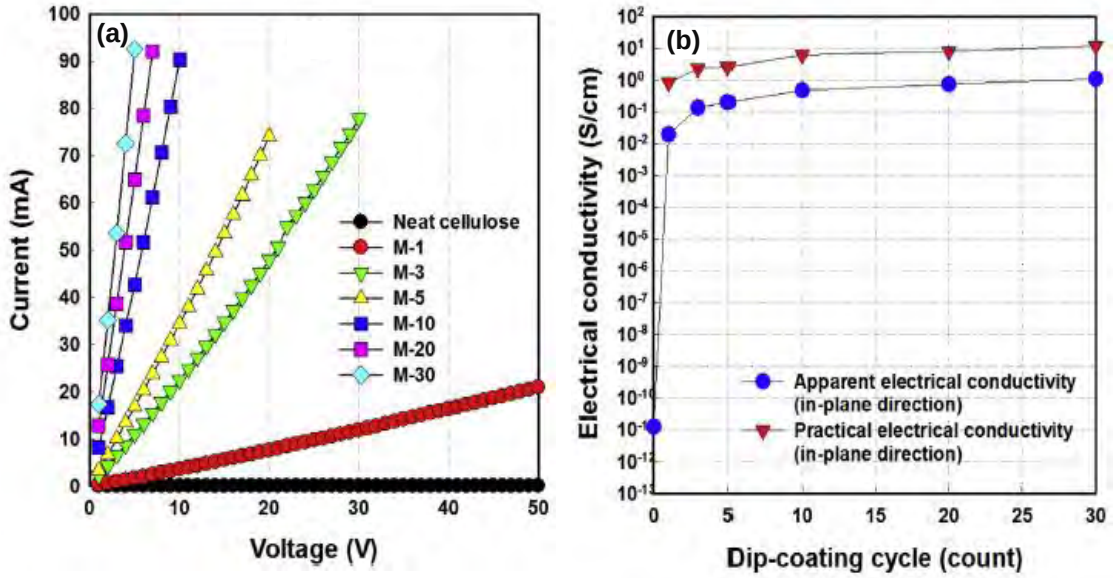

Figure 1.5: (a) Current-voltage *(I-V)* curves and (b) electrical conductivity of neat cellulose sheet and MWCNT/cellulose sheets in the in-plane direction [11].

Kim et al. [12] reported a flexible paper transistor fabricated with single-walled carbon nanotubes (SWCNTs) bonded cellulose (SCBC) composite. SWCNTs in SCBC composite were aligned by mechanical stretching process.

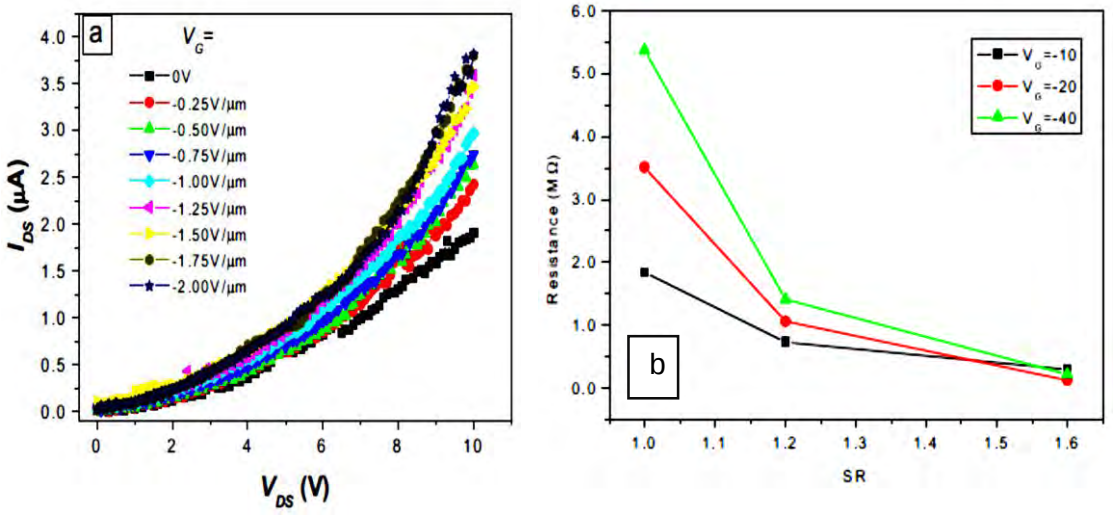

Figure 1.6: (a) Current-voltage *(I-V)* characteristic and (b) total resistance of SCBC paper transistor [12].

The electrical resistance was remarkably decreased. From the I_{DS}-V_{DS} plots of the SCBC paper transistors, the current between drain and source I_{DS} increased up to 10^{-1} μA in off state (V_G = 0V). FTIR spectra indicate the presence of covalent grafting of SWCNTs to cellulose chains.

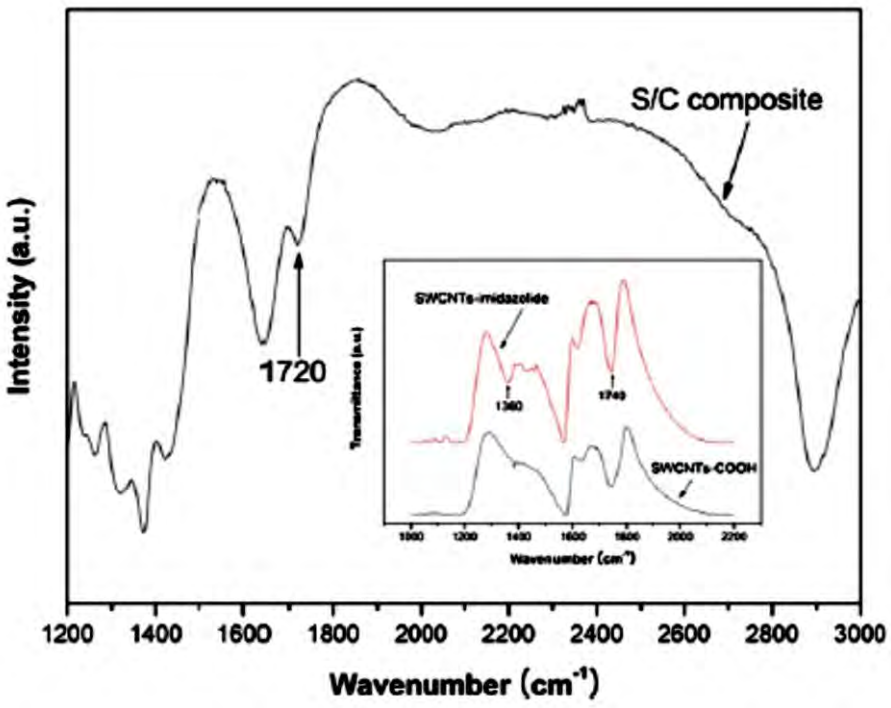

Figure 1.7: FT-IR spectra of SCBC composite and functionalized SWNTs [12].

Koga et al. [13] have demonstrated the flash reduced GO/cellulose sheet electrodes for a flexible supercapacitor. X-ray diffraction spectra of the GO/cellulose composites showed crystalline structure of native cellulose. The electrical conductivity of the composite increased with increasing irradiation time because of the conversion of electrically insulating GO to conductive rGO by the flash reduction. The conductivity reached 172 mS cm^{-1} after the flash reduction for 0.072s and specific capacitance of 212 Fg^{-1} at a flash reduction time 0.036s.

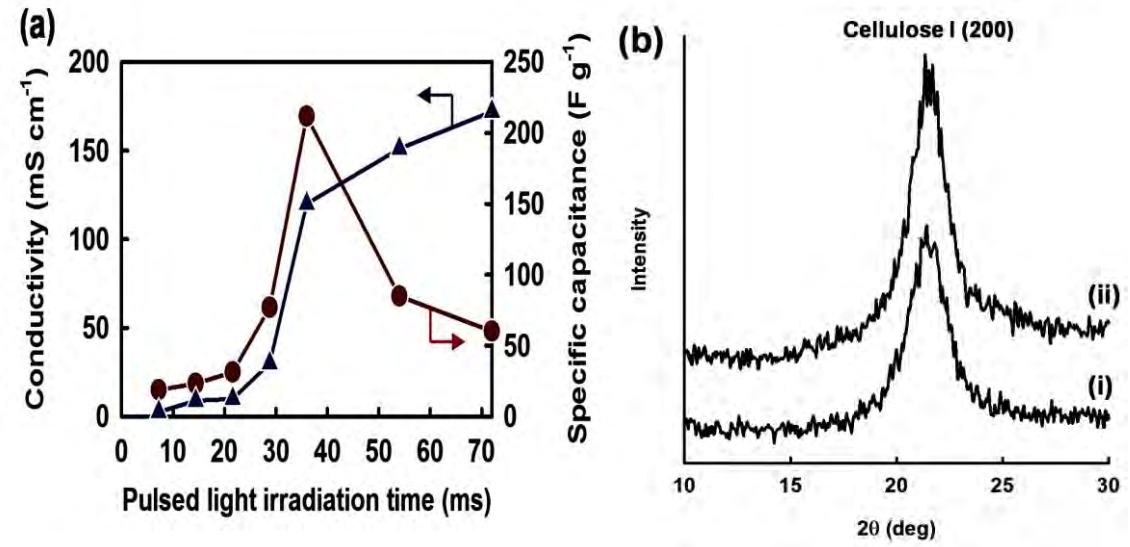

Figure 1.8: (a) Electrical conductivity and specific capacitance of the rGO/cellulose composite as a function of pulsed-light irradiation time and (b) X-ray diffraction spectra of the GO/cellulose composite (i) before and (ii) after pulsed light irradiation [13].

Lee and Jeong [14] investigated the regenerated cellulose/MWCNTs composite films manufactured by a simple solution-casting method and their application as electric heating materials. The composite were found to be thermally stable up to ~ 275 °C.

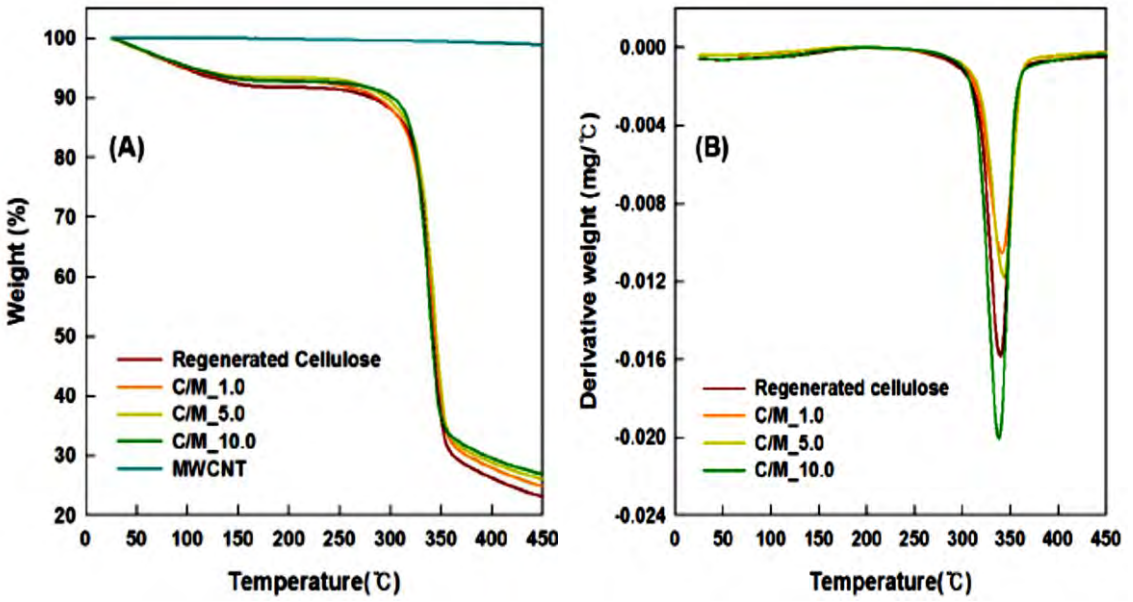

Figure 1.9: (A) TGA and (B) DTG curves of neat regenerated cellulose and its composite films with different MWCNT contents [14].

The composite films with MWCNT contents above 5 wt%, the electric current increased noticeably with the applied voltage and the slopes of the I-V curves became steeper with increasing the MWCNT content in the composite films (Figure 1.10). The electrical resistivity of the regenerated cellulose/MWCNT composite films decreased significantly from ~10^9 Ω cm to ~10^1 Ω cm with increasing the MWCNT loading. The composite films with 5-10 wt% MWCNT contents possessed low electrical resistivity of ~10^2-10^1 Ω cm.

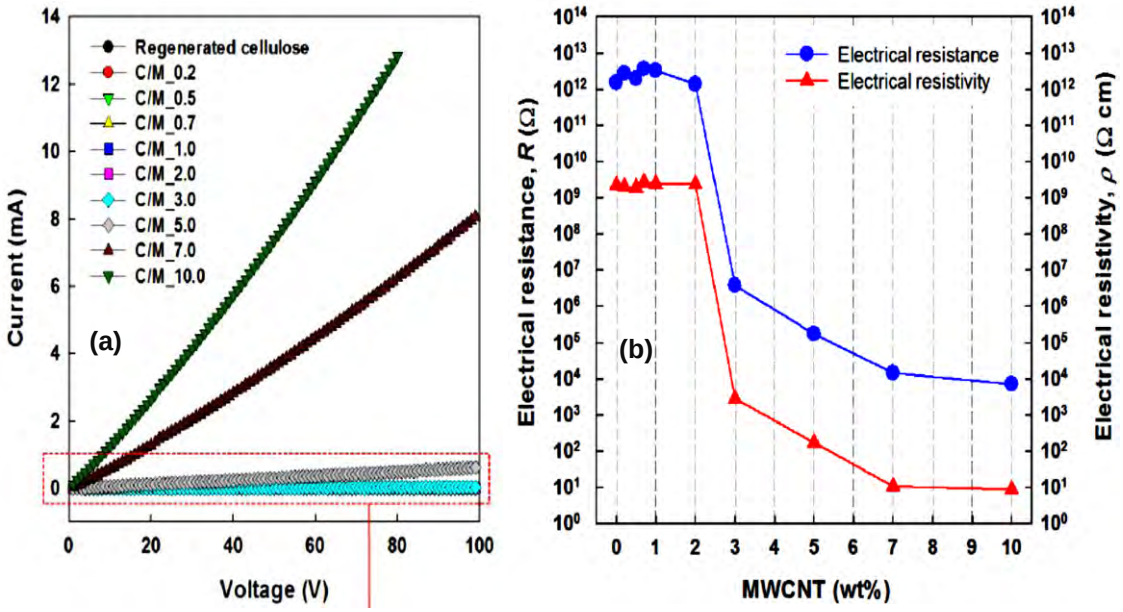

Figure 1.10: (a) Current-voltage curves and (b) Electrical resistance and resistivity of neat regenerated cellulose and its composite films with different MWCNT contents [14].

Salajkova et al. [15] studied the electrically conductive nanofibrillated cellulose (NFC)/CNT nanopapers prepared by a papermaking process. The FE-SEM image of pure NFC nanopaper showed weblike network structure of cellulose nanofibrils. The width of MWCNTs was estimated to be 3–4 times higher than the NFC nanofibrils. The NFC/CNT nanopaper with 9.1 wt% MWCNTs indicated homogenous incorporation of MWCNTs in the cellulose nanofibril network. The percolation composition (pc) clearly occurs between 6 and 9 wt% and the conductivity changes significantly.

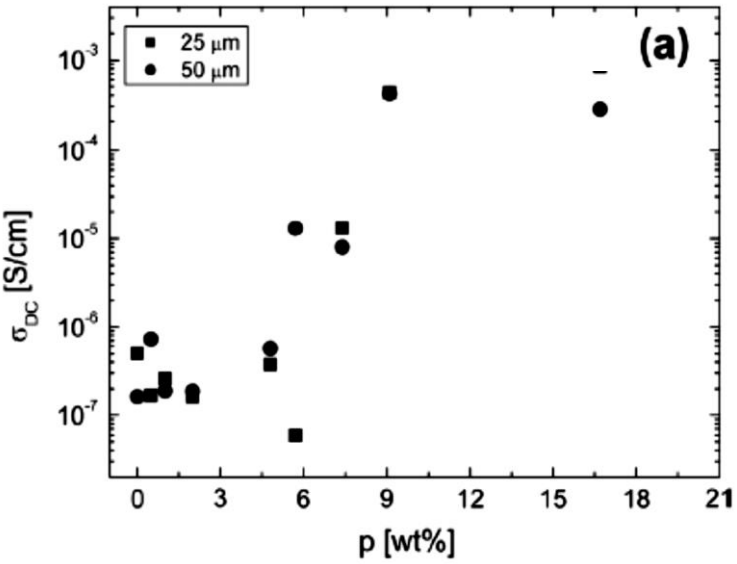

Figure 1.11: DC conductivity σ_{DC} versus MWCNT concentration p (wt%) for the prepared samples [15].

Lay et al. [16] stated the effect of MWCNTs and polypyrrole (PPy) on the electrical properties of cellulose nanopapers where 2,2,6,6,-tetramethylpiperidine-1-oxyl (TEMPO)-oxidized cellulose nanofibers (CNFs) were combined with MWCNTs and PPy polymer to produce binary and ternary formulations of conductive nanopapers.

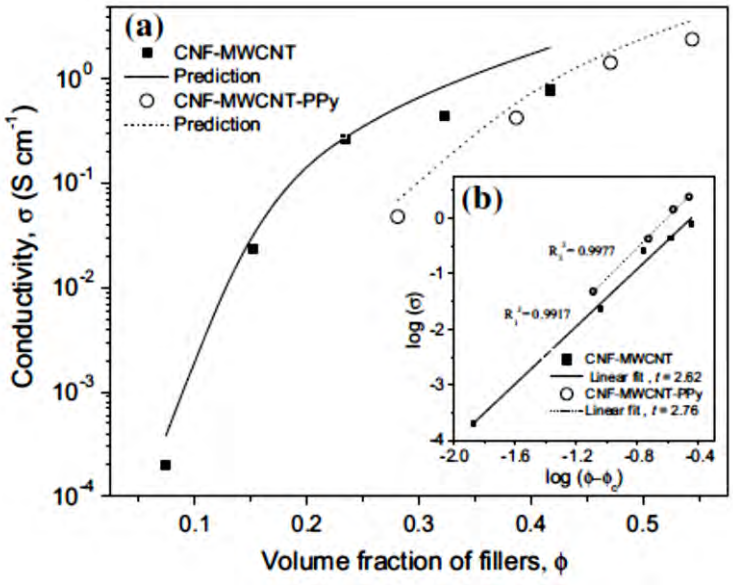

Figure 1.12: (a) Experimental and predicted electrical conductivities of CNF-MWCNT and CNF-MWCNT-PPy nanopapers (b) Linear correlation between log σ and log Φ-Φ_c [16].

High mechanical properties and good conductive response was found for these binary and ternary formulations. They reported that the ternary formulation produced nanopapers showed improved electrical conductivity of 2.41 S cm^{-1} (Figure 1.12) which was higher than those for the binary formulation with 50 wt% of MWCNTs (0.78 S cm^{-1}).

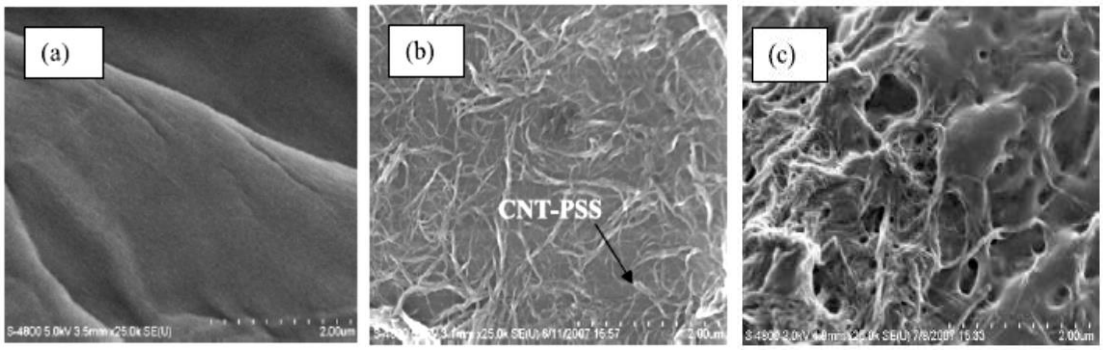

Figure 1.13: SEM images of the wood microfiber surface (a) uncoated; (b) coated with $(PEI/CNT\text{-}PSS)_4$; (c) microfiber coated with a composite film of $(PEI/CNT\text{-}PSS/PEI/PEDOT–PSS)_2$ [17].

Agarwal et al. [17] have developed conductive paper by layer-by-layer (LbL) nanoassembly technique where lignocellulose wood microfibers coated with anionic composite nanocoating of poly (3,4-ethylenedioxythiophene)-poly (styrenesulfonate) (PEDOT-PSS) and aqueous dispersion of carbon nanotubes (CNT-PSS) and cationic poly (ethyleneimine) (PEI).

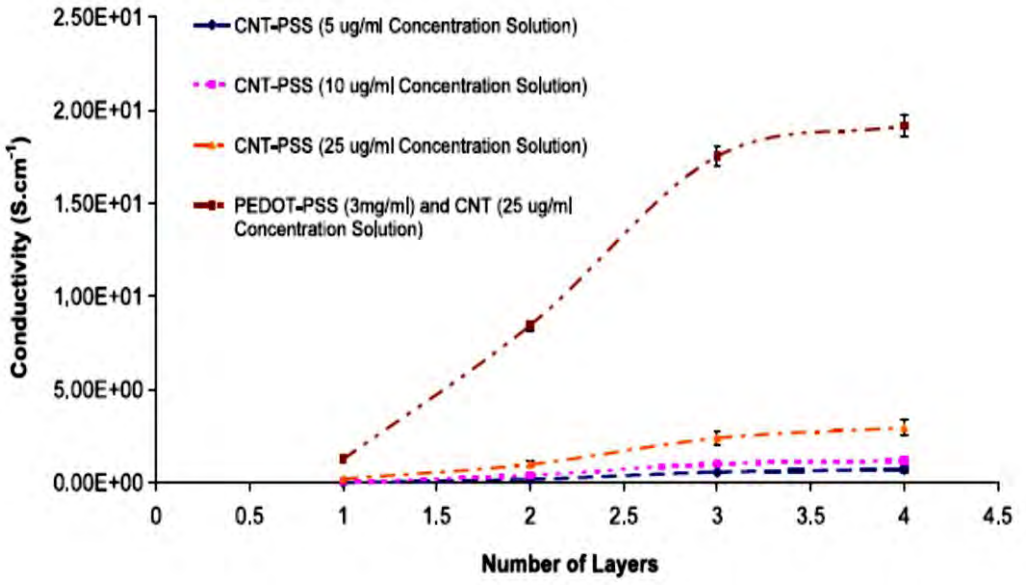

Figure 1.14: Conductivity of wood microfibers coated with four-bilayers of carbon nanotubes of different concentration [17].

They reported that the conductivity of the coated wood microfibers increased up to 20 S cm^{-1} by sandwiching multilayers of conductive co-polymer PEDOT–PSS with CNT–PSS through a polycation (PEI) interlayer. The SEM images showed the smooth surface of uncoated microfibers and CNTs were randomly dispersed on the entire CNT-PSS coated microfiber surface (Figure 1.13).

1.8 Objectives of this Study

The aim of the research is to prepare cost-effective, flexible, conductive CNT/Cellulose nanocomposites by incorporating CNTs uniformly dispersed into cellulose matrix. To identify the effects of the addition of CNTs in the cellulose polymer and study the variation of properties of the nanocomposites. The main purpose of this research work is to enhance the properties of typical cellulose sheet so that it finds new application as an advanced product for next generation. The objectives of this work are as follows:

To prepare CNT/cellulose nanocomposites by integrating different percentages of CNTs in cellulose pulp.
To measure DC electrical conductivity of the nanocomposites for different percentages of CNTs in the cellulose matrix.
To investigate the surface morphology and elemental composition of the prepared nanocomposites by field emission scanning electron microscopy (FESEM) and energy dispersive X-ray (EDX) analysis.
To analyze the thermal properties of the nanocomposites by thermogravimetric analysis (TGA), derivative thermogravimetric analysis (DTG) and differential scanning calorimetry (DSC).
To observe the crystalline nature, structural quality of the nanocomposites by X-ray diffraction (XRD).
To study the covalent bonding information of the nanocomposites by Fourier transform infrared spectroscopy (FTIR).

1.9 Outline of this Thesis

In chapter 1, a general introduction has been presented. This chapter also provides literature review.

Chapter 2 describes natural polymer, properties and dispersion of CNTs and the basic principles of characterization techniques.

Chapter 3 discusses about the sample preparation procedure and the composite characterization.

Chapter 4 covers the results and discussion part of this research work.

Chapter 5 includes conclusions of this work along with suggestions for future studies.

References

[1] Iijima, S., "Helical microtubules of graphitic carbon", Nature, Vol. 354, pp. 56–58, 1991.

[2] Wildoer, J., W., G., Venema, L., C., Rinzler, A., G., Smalley, R., E., Dekker, C., "Electronic structure of atomically resolved carbon nanotubes", Nature, Vol. 391, pp. 59-62, 1998.

[3] Baughman, R., H., Zakhidov, A., A., Heer, W., A., "Carbon Nanotubes—the route toward applications", Science, Vol. 297, pp. 787-792, 2002.

[4] Okpala, C., "Nanocomposites – An Overview", International Journal of Engineering Research and Development, Vol. 8, pp. 17-23, 2013.

[5] Camargo, P., H., Satyanarayana, K., G., Wypych, F., "Nanocomposites: Synthesis, Structure, Properties and New Application Opportunities", Materials Research, Vol. 12, pp.1-39, 2009.

[6] Moon, R. J., Martini, A., Nairn, J., Simonsen, J., Youngblood, J., "Cellulose nanomaterials review: structure, properties and nanocomposites", Chemical Society Reviews, Vol. 40, pp. 3941-3994, 2011.

[7] Krässig, H. A., "Cellulose: Structure Accessibility and Reactivity", Journal of Polymer Science, Vol. 32, pp. 2401, 1994.

[8] Lynd, L., R., Weimer, P., J., Zyl, W., H., Pretorius, I., S., "Microbial Cellulose Utilization: Fundamentals and Biotechnology", Microbiology and Molecular Biology Reviews, Vol. 66, pp. 506-577, 2002.

[9] https://en.wikipedia.org/wiki/Cellulose [Downloaded on 16:25, 19 May, 2018].

[10] Thostenson, E., T.; Li, C.; Chou, T.-W., "Nanocomposites in context", Composites Science and Technology, Vol. 65, pp. 491–516, 2005.

[11] Lee, T.-W., Lee, S.-E., Jeong, Y., G., "Carbon nanotube/cellulose papers with high performance in electric heating and electromagnetic interference shielding", Composites Science and Technology, Vol. 131, pp. 77-87, 2016.

[12] Kim, J.-H., Yun, S., Ko, H.-U, Kim, J., "A flexible paper transistor made with aligned single-walled carbon nanotube bonded cellulose composite", Current Applied Physics, Vol. 13, pp. 897-901, 2013.

[13] Koga, H., Tonomura, H., Nogi, M., Suganuma, K., Nishina, Y., "Fast, Scalable, and Eco-Friendly Fabrication of Energy Storage Paper Electrode", Green Chemistry, Vol. 18, pp. 1117-1124, 2015.

[14] Lee, T.-W., Jeong, Y., G., "Regenerated Cellulose/Multiwalled Carbon Nanotube Composite Films with Efficient Electric Heating Performance", Carbohydrate polymers, Vol. 133, pp. 456-463, 2015.

[15] Salajkova, M., Valentini, L., Zhou, Q., Berglund, L., A., "Tough nanopaper based on cellulose nanofibers and carbon nanotubes", Composites Science and Technology, Vol. 87, pp. 103-110, 2013.

[16] Lay, M., Méndez, J., A., Pèlach, M., À., Bun, K., N., Vilaseca, F., "Combined effect of carbon nanotubes and polypyrrole on the electrical properties of cellulose-nanopaper", Cellulose, Vol. 23, pp. 3925–3937, 2016.

[17] Agarwal, M., Xing, Q., Shim, B., S., Kotov, N., Varahramayan, K., Lovov, Y., "Conductive paper from lignocellulose wood microfibers coated with a nanocomposite of carbon nanotubes and conductive polymers", Nanotechnology, Vol. 20, pp. 215602 (8pp), 2009.

[18] Anderson, R., E., Guan, J., Ricard, M., Dubey, G., Su, J., Lopinski, G., Dorris, G., Bournea, O., Simard, B., "Multifunctional single-walled carbon nanotube–cellulose composite paper", Journal of Materials Chemistry, Vol. 20, pp. 2400–2407, 2010.

CHAPTER 2

THEORETICAL BACKGROUND

2.1 Polymers

The word "polymer" is derived from two Greek words, *poly* means 'many' and *mer* means 'unit' or 'part'. Polymers are referred to as macromolecules, which are formed by joining of repeating structural units on a large scale. The repeating structural units are derived from some simple and reactive molecules known as monomers and are linked to each other by covalent bonds. The process of formation of polymers from respective monomers is called polymerization. There are three different types of polymers based on the source.

Natural polymers

These polymers are found in plants and animals. Examples are proteins, cellulose, starch, some resins and rubber.

Semi-synthetic polymers

These polymers are mostly derived from naturally occurring polymers by chemical modifications. Cellulose derivatives as cellulose acetate (rayon) and cellulose nitrate, etc. are the usual examples of this category.

Synthetic polymers

A variety of synthetic polymers as plastic (polythene), synthetic polymers (nylon 6, 6) and synthetic rubbers (Buna – S), are examples of man-made polymers.

2.1.1 Natural Polymers

Increasing concern exists today about the preservation of our ecological systems. Most of today's synthetic polymers are produced from non-renewable petroleum resources and are not biodegradable. Persistent polymers generate significant sources of environmental pollution, causing harm to living things when they are dispersed in nature and are also responsible for the accumulation of polymeric solid waste materials. Natural polymers are available in large quantities from renewable sources, generally non-toxic and biodegradable. These polymers are formed in nature during the growth cycles of all organisms. Natural biodegradable polymers are called biopolymers. Polysaccharides such as cellulose, starch, chitosan, represent the most attribute family of these natural polymers. Polynucleotides such as DNA, RNA, polypeptides such as gelatin, proteins, polyisoprene such as rubber etc. are another types of biopolymers.

Natural polymers generally occur as fibers or grains. Starch composes grains, like wheat, roots, like cassava, tubercles, like potatoes, etc. All plant fibers are composed of cellulose while animal fibers consist of proteins (hair, silk and wool). Plant fibers are collected from different parts of the plant. Plant fibers include bast (or stem or soft sclerenchyma) fibers, leaf or hard fibers, seed, fruit, wood, cereal straw and other grass fibers. The purest fibers, like cotton and kapok, come from the threads that cover the skin of seeds. Fibers are divided based on their origins.

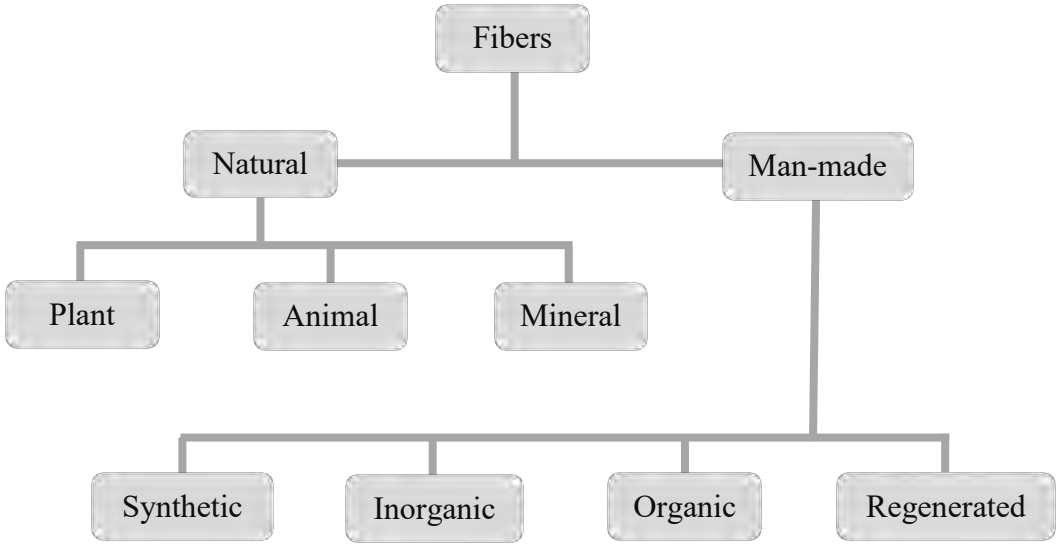

Figure 2.1: Classification of fibers.

The use of natural fibers in composite materials has increased due to their low cost, ability to recycle and better stiffness per weight which results in lighter components [1]. Natural plant fibers are consisting mainly of cellulose fibrils embedded in lignin. The cellulose fibrils are aligned in the longitudinal direction of the fiber, which render maximum tensile and flexural strengths, in addition to provide rigidity. The reinforcing efficiency of natural fiber is related to the nature of cellulose and its crystallinity. The main components of natural plant fibers are cellulose (α-cellulose), hemicelluloses, lignin, pectins and waxes [1].

Advantages of Natural Fiber

Low specific weight of fibers which results in a higher specific strength and stiffness. This is a benefit especially in parts designed for bending stiffness.

It is a renewable resource, the production requires little energy, and CO_2 is used while oxygen is given back to the environment.

Producible with low investment at low cost, which makes the material an interesting product for low-wage countries.

Eco-Friendly processing.

Good thermal properties.

2.1.2 Structure of Cellulose Fiber

Cellulose is a straight carbohydrate polymer chain consisting of several 1000 β(1→4)D-glucopyranose units. The β-configuration of the glycosidic bond allows the polymer to adopt a fully extended conformation. The extended cellulose chains from an array with the flat glucose units fixed edge to edge by hydrogen bonds (Figure 2.2).

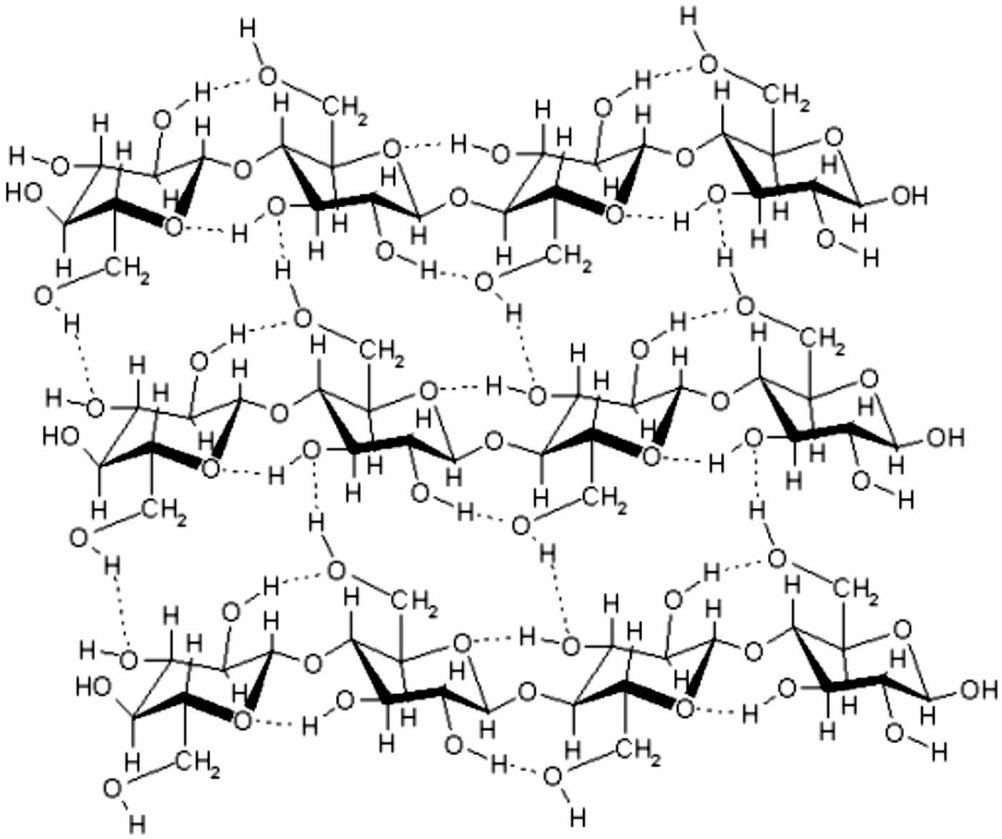

Figure 2.2: The structure of cellulose sheet showing the intra- and inter-chain hydrogen bonds [2].

These sheets are further stacked on top of each other and held together by hydrogen bonds and van der Waals interactions. This network of up to 40 cellulose chains makes up the crystalline core of the cellulose fibril. Native cellulose (cellulose I) has two

crystalline allomorphs, Iα and Iβ. The main difference between the two crystalline phases is the relative position of the chains with respect to each other. Cellulose in higher plants (woody tissue, cotton etc.) consists mainly of the Iβ phase whereas primitive organisms (bacteria, algae etc.) are enriched in the Iα phase [2]. If cellulose is recrystallized, cellulose I gives the thermodynamically more stable cellulose II structure with an antiparallel arrangement of the strands and some inter-sheet hydrogen bonding.

2.2 Properties of Carbon Nanotubes

The atomic arrangements of carbon atoms are responsible for the exceptional electrical, thermal, and mechanical properties of CNTs. These properties of CNTs are mentioned below:

Electrical properties

According to the chirality and diameter, CNTs can exhibit metallic or semiconducting properties and it has a direct influence on the electrical properties of CNTs. CNTs can carry an electric current density of 4×10^9 A/cm^2, which is more than 1000 times greater than copper [3]. CNTs are ideal one-dimensional conductors where electron transport occurs only along the axis of the tube due to its nanoscale cross-section. Owing to smaller diameter and higher length aspect ratio, the electrons inside the CNTs do not scatter much. As a result, they have extremely low electrical resistance.

Thermal properties

Nanotubes have very good thermal conductivity in the axial direction and they are insulators in the radial direction. At room-temperature, CNTs exhibit thermal conductivity of 3500 $Wm^{-1}K^{-1}$ along its axis which is 10 times higher than copper [4]. The thermal stability of CNTs can be up to 2800 °C in vacuum and about 750 °C in air.

Mechanical properties

Nanotubes are the strongest and stiffest of all known material. This strength is a direct consequence of covalent sp^2 bonds formed between the individual carbon atoms. CNTs exhibit exceptional mechanical properties that they are very strong and resilient at the same time. CNTs are very strong in the axial direction. Young's modulus of the CNTs is around 1 TPa and tensile strength is about 11-63 GPa [5]. They are 100 times stronger

than steel but six times lighter. CNTs are very soft in the radial direction. They can bend over 90° several times without breaking.

2.3 Dispersion of Carbon Nanotubes

CNTs are strongly entangled, forming aggregates due to strong van der Waals interaction energy of ca. 500 eV/μm of tube-tube contact [6]. Also, high aspect ratios, combined with high flexibilities [7], noticeably increase the possibility of nanotube entanglement. For such high interaction energy, CNT dispersion in aqueous and organic media is a challenging task. Besides, dispersion of CNTs is a prerequisite for their effective utilization in various applications. Basically, there are two approaches for dispersing CNTs. Such as - (i) Exohedral and (ii) Endohedral. Exohedral approach involves grafting of molecules on the outer surface of the nanotubes. . In endohedral approach, CNTs are treated by filling their inner empty cavity with different molecules or nanoparticles. Exohedral methods can be divided into two categories: (a) mechanical methods and (b) chemical dispersion methods. The mechanical approach includes ultrasonication and high-shear mixing. These processes are time-consuming and less efficient. Furthermore, ultrasonication can result in fragmentation of CNTs, in turn, decreasing their aspect ratio. Besides this the stability of the dispersion is poor. The chemical approach includes both covalent and non-covalent methods. Currently these two approaches are widely used in nanotube dispersion.

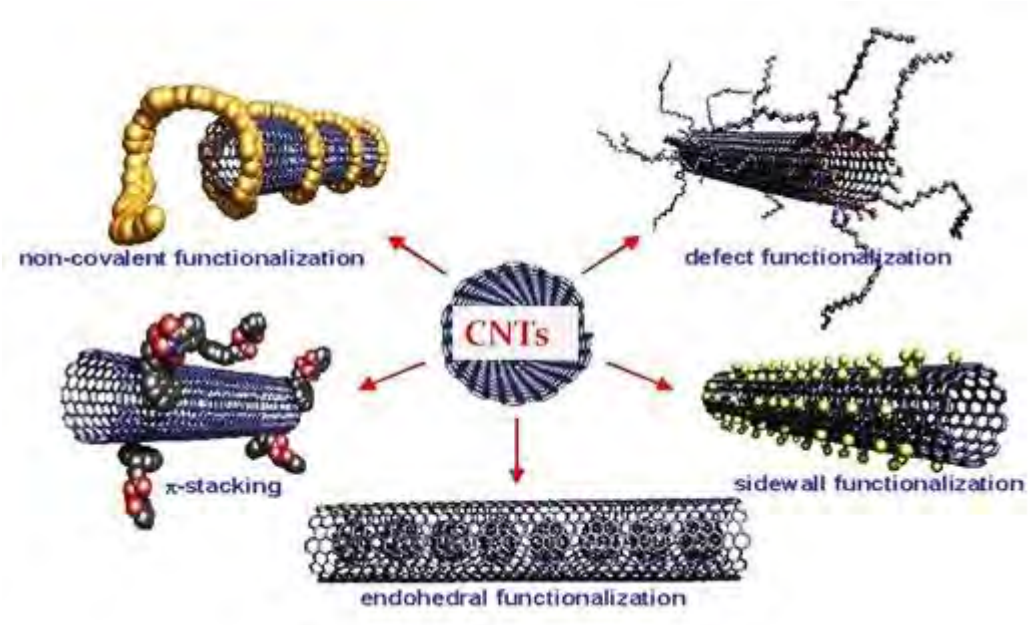

Figure 2.3: Different types of possibilities of the functionalization of CNTs.

Covalent functionalization of CNTs is the attachment of chemical moieties to the CNT tubular structure via the formation of covalent bonds. Depending upon the site of interaction, it can be of two types – covalent sidewall functionalization and defect functionalization. Direct covalent sidewall functionalization involves a change of hybridization from sp^2 to sp^3 and the loss of conjugation. Defect functionalization is based on the transformations of defect sites already present. Defect sites can be the open ends and holes in the sidewalls, terminated, for example by functional groups and Stone/Wales defects (5‑7 defects) in hexagonal graphene framework. In addition to these, oxidative purification generated oxygenated sites are also considered as defects. Covalent functionalization suffers from the drawback of damaging the structure of CNTs. Aggressive chemical functionalization such as the use of neat acids at high temperature might introduce structural defects at the nanotube surface, consequently altering the properties of carbon nanotubes [8].

A non-covalent approach involves adsorption of the chemical moieties onto the nanotube surface, either via π-π stacking interaction or through van der Waals' forces. The non-covalent approach is particularly attractive because of the possibility of adsorbing various groups on CNT surface without disturbing the π system of the graphene sheets, in turn preserving the properties of CNTs. In the last few years, surfactants and polymers has been widely utilized for this non-destructive functionalization of CNTs. Both of them get adsorbed onto nanotube surface, rendering them soluble in aqueous and organic solvents.

2.3.1 Dispersion of CNTs in Water by Surfactants

Water is a very important dispersing liquid for many uses of nanotubes and water soluble polymers also play a role in the importance of water dispersions of nanotubes. Surfactants are the most common dispersing agents used to disperse nanotubes in water because surfactants have a propensity to accumulate at surfaces. Surfactants are water soluble small molecules with a hydrophobic tail and a hydrophilic head group. Surfactants have the ability to disperse nanotubes in water because the hydrophobic tail is able to energetically interact with the nanotube favorably while the hydrophilic head is able to interact with the water. Surfactants are classified according to the sign of the charge of head in a surfactant molecule when it is dissolved in water. Generally, there are two groups of surfactants– non-ionic, with no charge in its head, and ionic: cationic,

anionic and zwitterionic. A wide variety of surfactants have been investigated for the dispersion of nanotubes such as sodium dodecyl sulfate (SDS), sodium dodecyl benzenesulfonate (SDBS), dodecyltrimethylammonium bromide (DTAB), hexadecyltrimethylammonium bromide (CTAB) and octyl phenol ethoxylate (Triton X-100). Generally, ionic surfactants are preferable for CNT/water-soluble solutions. Alternatively, nonionic surfactants are proposed when organic solvents have to be used. Ionic surfactants have hydrophobic chain lengths typically between 8 and 18 carbon atoms because shorter chains do not have surfactants properties, while longer chains are not water soluble. Nonionic surfactants can have much longer hydrophobic lengths. The adsorption mechanism of surfactants on nanotube surface is very interesting and different possibilities to produce specific self-organization of surfactant molecules are shown in Figure 2.3.

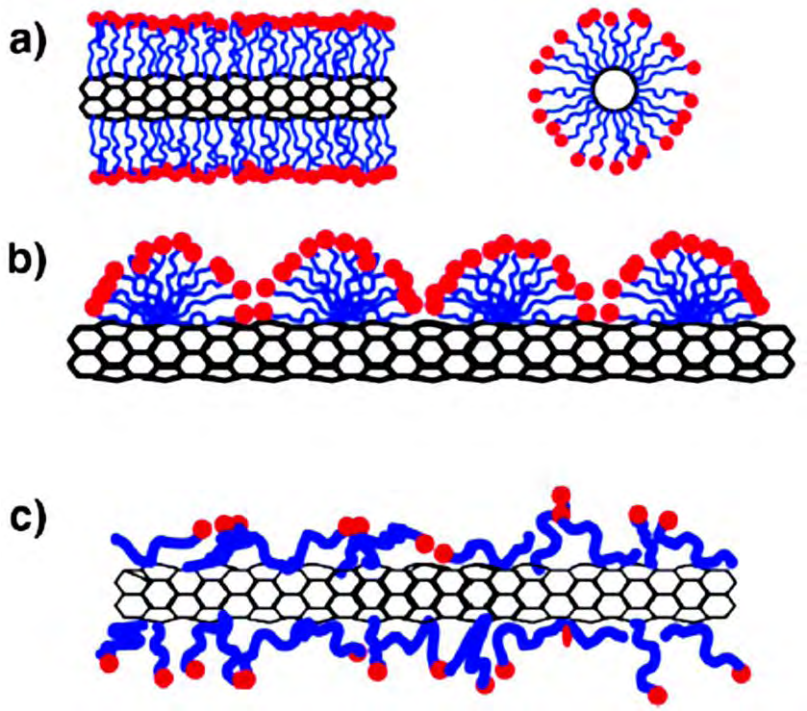

Figure 2.4: Schematic representations of the mechanism by which surfactants help to disperse CNT. (a) SWNT encapsulated in a cylindrical surfactant micelle (both cross section and side-view); (b) hemimicellar adsorption of surfactant molecules on a SWNT; (c) random adsorption of surfactant molecules on a SWNT [9].

In a typical dispersion procedure, after the surfactant has been adsorbed on the nanotube surface, ultrasonication for minutes or hours (with ultrasonication tip or bath) may help a surfactant to overcame van der Waals attraction and debundle nanotubes by steric or

electrostatic repulsions. The physical adsorption of surfactant on the CNT surface lowered the surface tension of CNTs, effectively preventing the formation of aggregates.

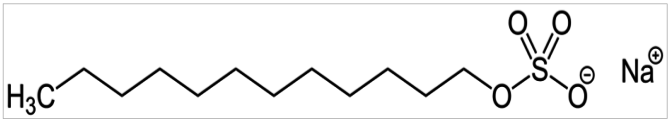

Figure 2.5: Chemical structure of SDS.

Nanotubes are better dispersed by anionic rather than cationic surfactant. Among the anionic surfactants, Sodium dodecyl sulfate (SDS) has been chosen to disperse MWCNTs in water because of its high dispersive efficiency. SDS is a synthetic organic compound and the chemical formula is $CH_3(CH_2)_{11}SO_4Na$. It consists of a 12-carbon tail attached to a sulfate group. As a result of its hydrocarbon tail, and anionic head group, it has amphiphilic properties that allow it to form micelles and so act as a detergent. This non-covalent modification of the CNT surface by SDS is helpful for the dispersion of CNTs in aqueous polymeric matrix.

2.4 Surface Morphology

In surface morphology, microscopic imaging techniques are used where three-dimensional high resolution imaging are analyzed which are not visible by normal human eye. Such images originates from the exposed surface of the sample.

2.4.1 Electron Microscope

Electron microscopes use high-speed electron beam instead of light waves to produce the image of the object and magnification is obtained by 'electromagnetic fields'. Electron microscope gives very high magnification and incredibly high resolution. Electron microscope generates larger (magnified) and more detailed (highly resolved) images of small objects or small areas of larger objects than light microscope. Electron microscopes use signals arising from the interaction of an electron beam with the sample to obtain information regarding structure, morphology and composition. The electronic beam passes through the specimen, then through a series of lenses that magnify the image. The image results from a scattering of electrons by atoms in the specimen. There are two main types of electron microscope – the scanning electron microscope and the transmission electron microscope.

2.4.2 Scanning Electron Microscope

The scanning electron microscope (SEM) is one of the very useful instrument to characterize morphology. The popularity of SEM is mainly due to its versatility and to the possibility to obtain three-dimension like images. The SEM is a type of electron microscope that uses a focused beam of high-energy electrons to generate a variety of signals at the surface of solid specimens. The signals that derive from electron-sample interactions reveal information about the sample including external morphology (texture), chemical composition, and crystalline structure and orientation of materials making up the sample. The types of signals generated by a SEM include secondary electrons (SE), back-scattered electrons (BSE), characteristics X-rays, light (cathodoluminescence), specimen current and transmitted electrons [10].

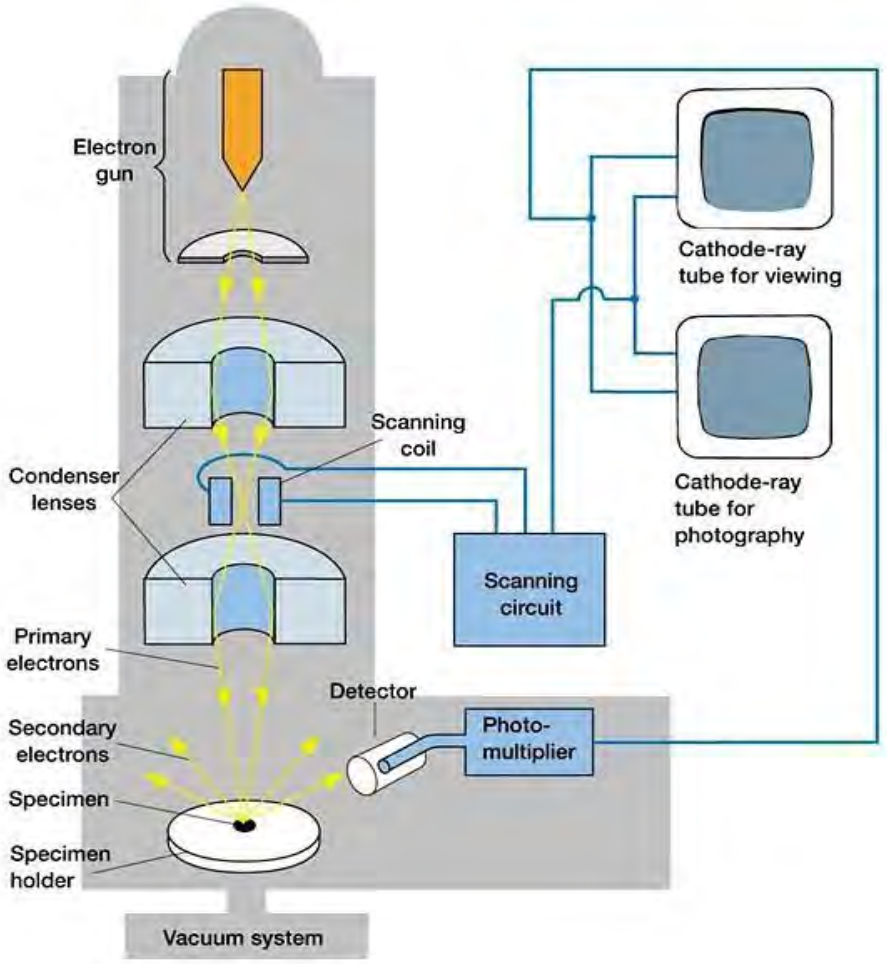

Figure 2.6: Schematic diagram of the working principle of a scanning electron microscope.

The SEM generates a beam of incident electrons in an electron column above the sample chamber. The electrons are produced by a thermal emission source, such as a heated tungsten filament, or by a field emission cathode. The electrons are focused into a small beam by a series of electromagnetic lenses in the SEM column. Scanning coils near the end of the column direct and position the focused beam onto the sample surface. The electron beam is scanned in a raster pattern over the surface for imaging. The emitted electrons are detected for each position in the scanned area by an electron detector. To avoid interference with the electron beam the whole system need to be in vacuum prior to measuring. The intensity of the emitted electron signal is displayed as brightness on a display monitor and/or in a digital image file. By synchronizing the position in the image scan to that of the incident electron beam, the display represents the morphology of the sample surface area. Magnification of the image is the ratio of the image display size to the sample area scanned by the electron beam. SEM analysis is considered to be "non-destructive"; that is, x-rays generated by electron interactions do not lead to volume loss of the sample, so it is possible to analyze the same materials repeatedly.

2.4.3 Transmission Electron Microscope

The transmission electron microscope (TEM) is a derivative of the light microscope, which uses a focused beam of high energy electrons instead of light and therefore achieves much better resolution. It reveals levels of detail and complexity inaccessible by light microscopy. TEMs provide topographical, morphological, compositional and crystalline information. The beam of electrons is ejected from the electron gun that travel through the specimen within a high vacuum column of the microscope. The beam then strikes the specimen and parts of it are transmitted depending upon the density and electron transparency of the specimen. This transmitted portion is focused by the objective lens into an image on phosphor screen or charge coupled device (CCD) camera. Optional objective apertures can be used to enhance the contrast by blocking out high-angle diffracted electrons. The image then passed down the column through the intermediate and projector lenses, is enlarged all the way. The image strikes the phosphor screen and light is generated, allowing the user to see the image. The darker areas of the image represent those areas of the sample that fewer electrons are transmitted through while the lighter areas of the image represent those areas of the sample that more electrons were transmitted through. TEM has become a powerful

analytical tool for a wide-range of applications and can be utilized in a variety of different scientific, educational and industrial fields.

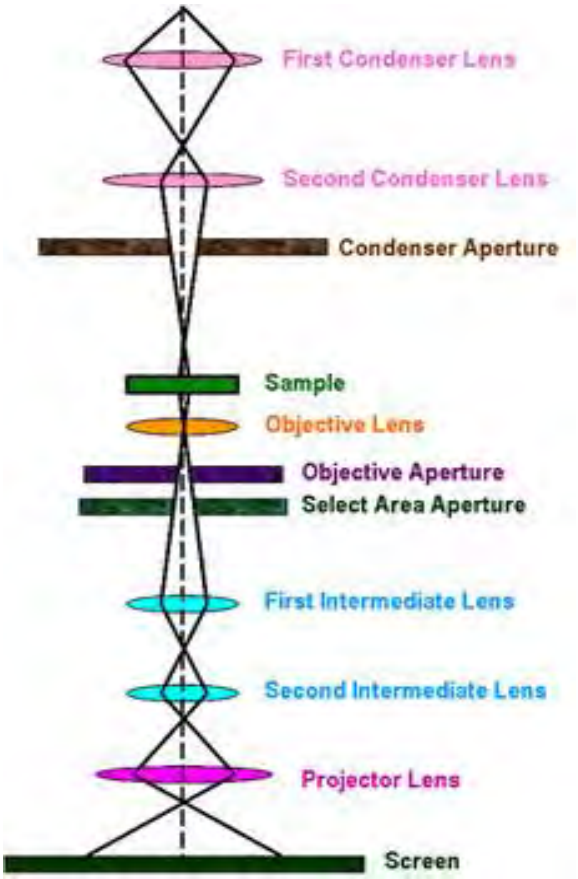

Figure 2.7: Schematic diagram of the working principle of a transmission electron microscope.

2.5 Elemental Analysis

Elemental analysis is an experiment that includes identification and quantification of elements in a sample, determination of the elemental composition and trace level elements**.** Energy Dispersive X-Ray Analysis (EDX), referred to as EDS or EDAX, is an x-ray technique used to identify the elemental composition of materials.

2.5.1 Energy Dispersive X-ray Spectroscopy

Energy dispersive X-ray spectroscopy (EDS, EDX or XEDS) is a qualitative and quantitative X-ray microanalytical technique that can provide information on the chemical composition of a sample for elements with atomic number (Z). An electron beam is focused on the sample in either a scanning electron microscope (SEM) or a transmission electron microscope (TEM). The electrons from the primary beam

penetrate the sample and interact with the atoms from which it is made. Two types of X-rays result from these interactions: 'Continuum or background X-rays', and 'Characteristic X-rays'.

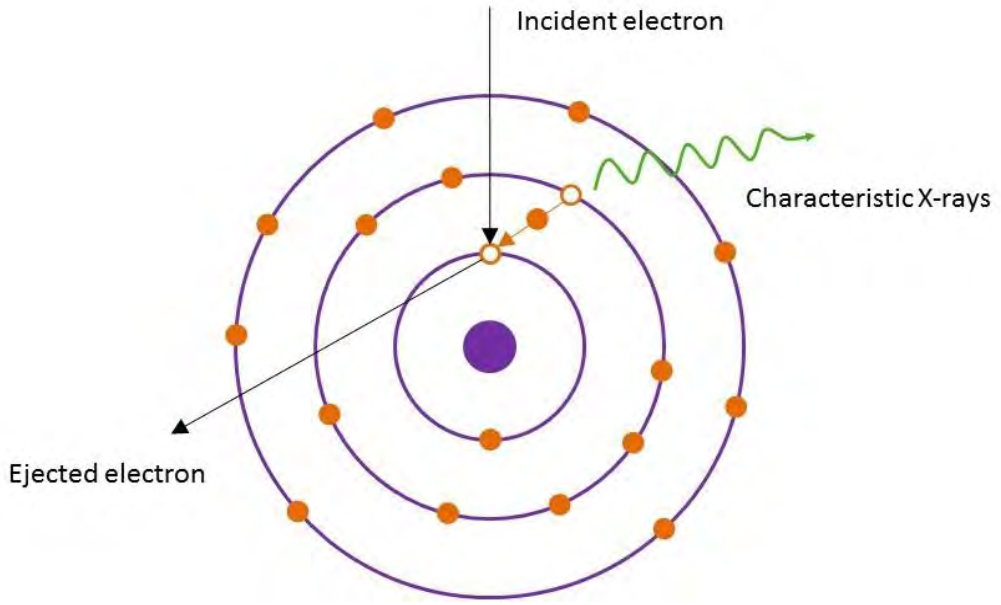

Figure 2.8: Schematic diagram of the principle of EDS.

Characteristic X-rays result from electron transitions between inner orbits, which are normally full. An electron must first be removed in order to create a vacancy into which another can fall from an orbit further out. The continuum X-rays result when the beam electrons interact with the nucleus of the specimen atoms. Continuum X-rays represent the background on which the characteristic X-ray peaks are imposed. The intensity of the continuum decreases monotonically with increasing X-ray energy, and is approximately proportional to Z. The X-rays are detected by an Energy Dispersive detector which displays the signal as a spectrum, or histogram, of intensity (number of X-rays or X-ray count rate) versus X-ray energy. The energies of the Characteristic X-rays allow the elements making up the sample to be identified, while the intensities of the Characteristic X-ray peaks allow the concentrations of the elements to be quantified. EDS is considered a non-destructive analytical technique, that is, the sample can be re-analyzed many times.

2.6 Structural Analyses

To describe a material uniquely, information like detailed structural properties are very important. Generally the answer of these type of questions: how are they arranged or what their functional groups are and other structural properties are obtained by various types of structural analysis such as X-ray diffraction, infrared spectroscopy, Raman spectroscopy etc.

2.6.1 X-Ray Diffraction

X-ray diffraction (XRD) is a rapid analytical technique for the investigation of the structure of matter and quantify the crystalline nature by measuring the diffraction of x-rays from the planes of atoms within the material. It provides information on crystal structure, phase, preferred crystal orientation (texture), and other structural parameters, such as average grain size, crystallinity, strain, and crystal defects.

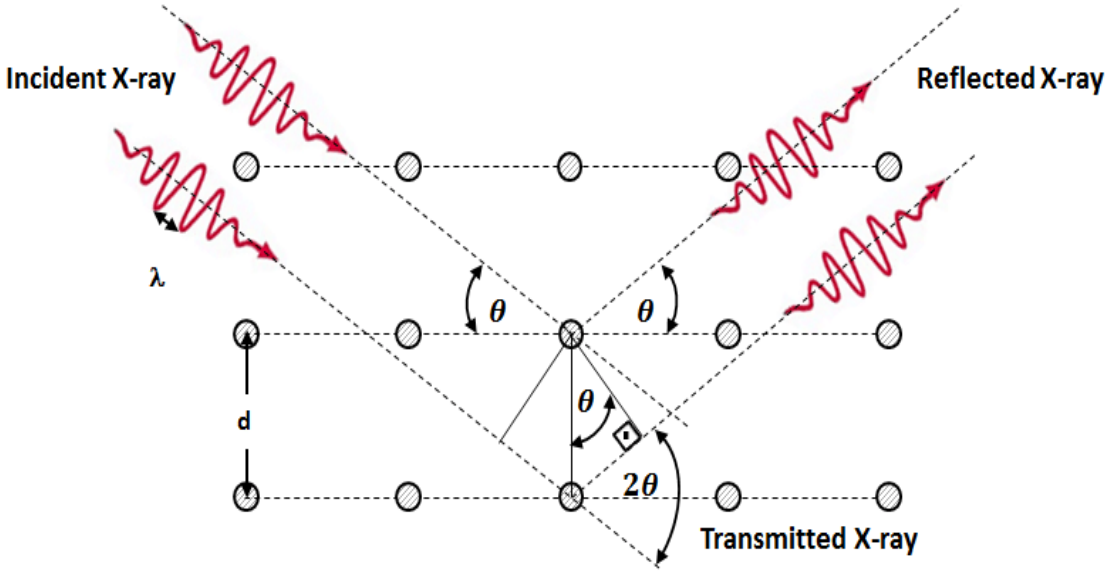

Figure 2.9: Schematic diagram of the Bragg's equation.

XRD relies on the dual wave/particle nature of X-rays to obtain information about the structure of crystalline materials. The technique was initiated by Laue's discovery in 1912 that crystals diffract X-rays [11]. By extending on the work of von Laue, William constructed an X-ray spectrometer that enabled the Bragg father and son pair to examine X-rays from crystals at various angles. Through analysing a variety of substances, Lawrence Bragg developed a simplified calculation, now known as Bragg's Law ($n\lambda=2d\sin\theta$), to determine the structure of a crystal [12,13]. It is still the most accurate way of determining molecular structures. This law relates the wavelength of

electromagnetic radiation to the diffraction angle and the lattice spacing in a crystalline sample. X-ray diffraction peaks are produced by constructive interference of a monochromatic beam of X-rays diffracted at specific angles from each set of lattice planes in a sample. X-rays are generated by a cathode ray tube, filtered to produce monochromatic radiation, collimated to concentrate, and directed toward the sample. Bragg conditions of diffraction: To maintain the same path length and remain in-phase, the x-rays must be deviated at an angle equal to the angle of incidence. The deviated rays combine to form a diffracted beam if they differ in phase by a whole number of the ray wavelength. The X-ray peak intensities are determined by the distribution of atoms within the lattice. Consequently, the X-ray diffraction pattern is the unique fingerprint of the periodic atomic arrangements in a given material. A search of the ICDD (International Centre for Diffraction Data) database of X-ray diffraction patterns enables the phase identification of a large variety of crystalline samples. XRD is the powerful and cost-effective diffraction technique for the identification of an unknown material.

2.6.2 Fourier-Transform Infrared spectroscopy

Fourier transform infrared spectroscopy (FTIR) is the most versatile analytical technique used to identify organic, polymeric, and in some cases, inorganic materials. FTIR test uses infrared light to scan test samples and observe chemical properties. It is an effective analytical method for detecting functional groups and characterizing covalent bonding information. Spectra of better quality normally can be obtained by using FTIR than dispersive IR spectroscopy because of its high speed of operation with superior signal to noise ratio and greater optical throughput. FTIR relies on the fact that the most molecules absorb light in the infra-red region of the electromagnetic spectrum. This absorption corresponds specifically to the bonds present in the molecule. The range of Infrared region is 12800 ~ 10 cm^{-1} and can be divided into near-infrared region (12800 ~ 4000 cm^{-1}), mid-infrared region (4000 ~ 200 cm^{-1}) and far-infrared region (200 ~ 10 cm^{-1}). However, the “mid-IR” region (4000 ~ 670 cm^{-1}) is the most attractive and common used region for chemical analysis because this region includes the frequencies corresponding to the fundamental vibrations of virtually all of the functional groups of organic molecules. Infrared spectrum is molecular vibrational spectrum. There are two kinds of molecular vibrations: stretching modes and bending modes.

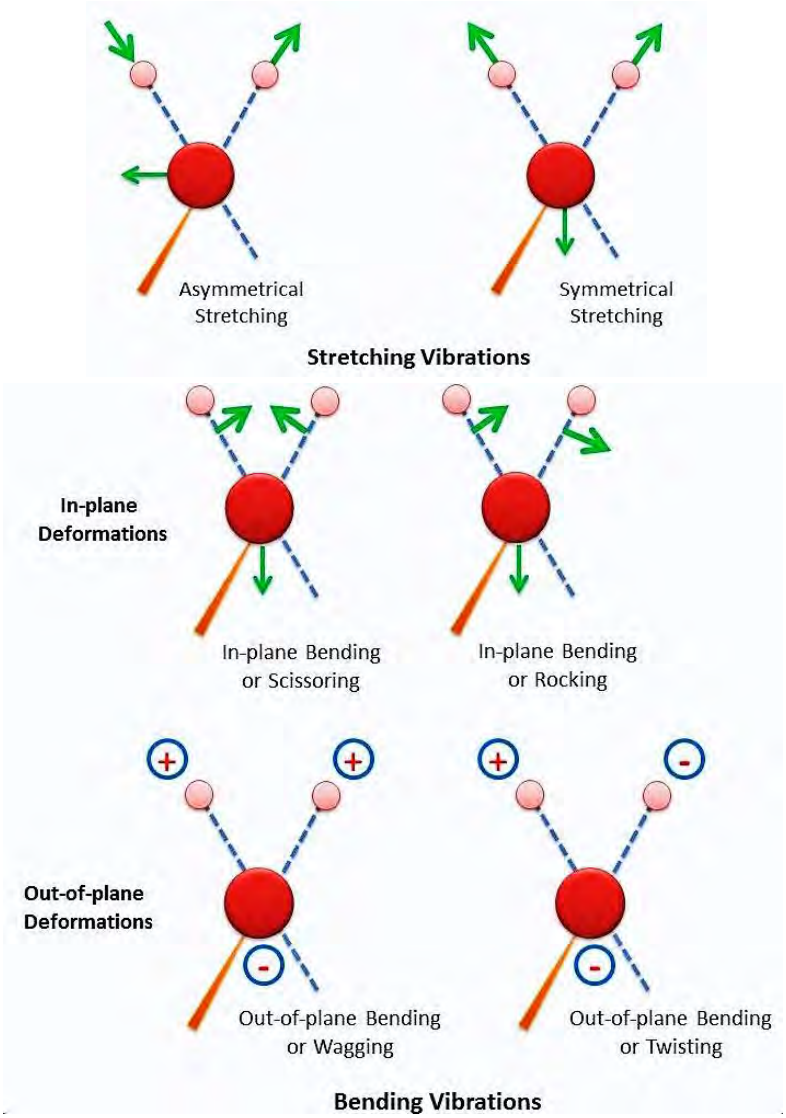

Figure 2.10: Different types of molecular vibrations.

When exposed to infrared radiation, sample molecules selectively absorb radiation of specific wavelengths which causes the change of dipole moment of sample molecules. Consequently, the vibrational energy levels of sample molecules transfer from ground state to excited state. The frequency of the absorption peak is determined by the vibrational energy gap. The number of absorption peaks is related to the number of vibrational freedom of the molecule. The intensity of absorption peaks is related to the change of dipole moment and the possibility of the transition of energy levels. Therefore, by analyzing the infrared spectrum, one can readily obtain abundant structure information of a molecule.

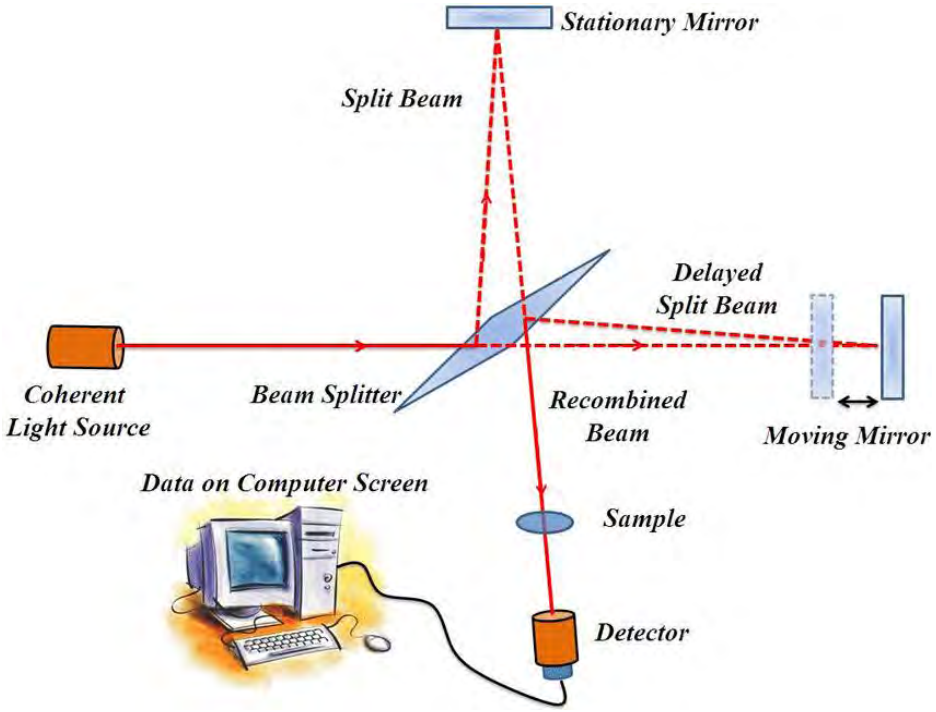

Figure 2.11: Block diagram of an FTIR spectrometer.

A common FTIR spectrometer comprises a source, interferometer, sample compartment, detector, and a computer.In FTIR analysis, infrared light from the light source passes through a Michelson interferometer. The major difference between an FTIR spectrometer and a dispersive IR spectrometer is the Michelson interferometer. The Michelson interferometer comprises a beam splitter, moving mirror, and fixed mirror. The light beam split into two by the beam splitter is reflected from the moving mirror and fixed mirror, before being recombined by the beam splitter. Then the beam enters the sample compartment where it is transmitted through or reflected off of the surface of the sample, depending on the type of analysis being accomplished. This is where specific frequencies of energy, which are uniquely characteristic of the sample, are absorbed. The beam finally passes to the detector for final measurement. The detectors used are specially designed to measure the special interferogram signal. The measured signal is digitized and sent to the computer where the Fourier transformation takes place. The final infrared spectrum is then presented to the user for interpretation and any further manipulation. The FTIR spectra are usually presented as plots of intensity versus wavenumber. Wavenumber is the reciprocal of the wavelength. The

intensity can be plotted as the percentage of light transmittance or absorbance at each wavenumber.

2.7 Thermal Analyses

Thermal Analysis deals with the theories of thermal analysis (thermodynamics, irreversible thermodynamics, and kinetics) as well as instrumentation and techniques (thermometry, differential thermal analysis, calorimetry, thermomechanical analysis and dilatometry, and thermogravimetry). Thermal analysis is used to determine the physical or chemical properties of a substance as it is heated, cooled or held at constant temperature in a controlled atmosphere. In advanced level, simultaneous thermal analysis (STA) refers to the simultaneous application of two different measurements to one and the same sample in a single run. Thermal analysis is a good analytical tool to measure: thermal decomposition of solids and liquids, solid-solid and solid-gas chemical reactions, material specification, purity and identification, inorganic solid material adsorption, phase transitions.

2.7.1 Thermogravimetric Analysis (TGA)

Thermogravimetry (TG) or thermogravimetric analysis (TGA) is a well proven thermal analysis technique in which the weight or the mass of a substance is monitored as a function of temperature or time as the specimen is subjected to a controlled temperature program in a controlled atmosphere. Inorganic materials, metals, polymers and plastics, ceramics, glasses, and composite materials can be analyzed by TGA.

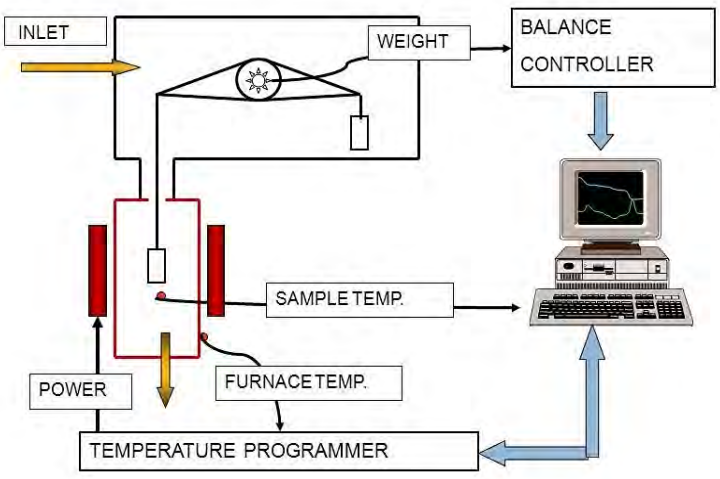

Figure 2.12: Schematic diagram of thermogravimetric analysis.

The thermogravimetric analyzer is an essential laboratory tool used for material characterization. The basic principle of TGA is that as a sample is heated, its mass changes. This change can be used to determine the composition of a material or its thermal stability. The sample is typically heated at a constant heating rate (so-called dynamic measurement) or held at a constant temperature (isothermal measurement), but may also be subjected to non-linear temperature programs such as those used in sample controlled TGA (so-called SCTA) experiments. The choice of temperature program will depend upon the type of information required about the sample. Additionally, the atmosphere used in the TGA experiment plays an important role and can be reactive, oxidizing or inert. Changes in the atmosphere during a measurement may also be made. Usually, a sample loses weight as it is heated up due to decomposition, reduction, or evaporation. A sample could also gain weight due to oxidation or absorption. A TGA consists of a sample pan that is supported by a precision balance. That pan resides in a furnace and is heated or cooled during the experiment. The mass of the sample is monitored during the experiment. A sample purge gas controls the sample environment. Purging gas can be provided from both horizontal and vertical directions. This gas may be inert or a reactive gas that flows over the sample and exits through an exhaust. The results of a TGA measurement are usually displayed as a TGA curve in which mass or per cent mass is plotted against temperature and/or time.

2.7.2 Differential scanning calorimetry (DSC)

Differential scanning calorimetry (DSC) is one of the thermo-analytical techniques which measures the amount of energy absorbed or released by a sample when it is heated or cooled or held isothermally, providing quantitative and qualitative data on endothermic (heat absorption) and exothermic (heat evolution) processes. Both the sample and reference are maintained at nearly the same temperature throughout the experiment. The reference sample should have a well-defined heat capacity over the range of temperatures to be scanned and analyzed. Usually, the reference is an inert material such as alumina or just an empty pan. Pans of Al, Cu, Au, Pt, alumina, and graphite are available and need to be chosen to avoid reactions with samples and with regard to the temperature range of the measurement. The most common purge gas is nitrogen. There are two types of DSC commercially available: heat flux (HF) type and power compensation (PC) type.

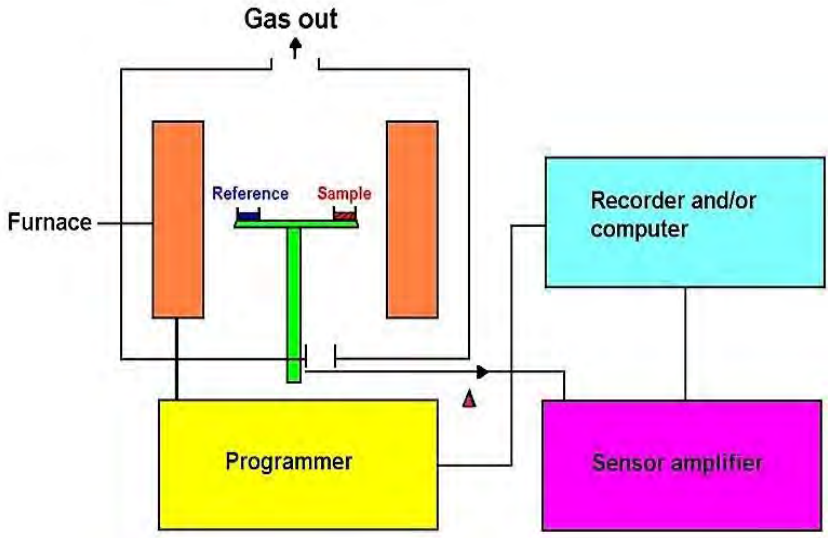

Figure 2.13: Schematic diagram of heat flux type DSC.

In HF type DSC, both sample and reference pans are heated by a single furnace through heat sink and heat resistor. Heat flow is proportional to the heat difference of heat sink and holders. The temperature versus time profile through a phase transition in a heat flux instrument is not linear. At a phase transition, there is a large change in the heat capacity of the sample, which leads to a difference in temperatures between the sample and reference pan. A set of mathematical equations convert the signal into heat flow information. By calibrating the standard material, the unknown sample quantitative measurement is achievable. In heat flux DSC, we can write the total heat flow $\frac{\mathrm{dH}}{\mathrm{dt}}$ as,

$$\frac{dH}{dt} = C_P \frac{dT}{dt} + f(T,t) \quad \ldots\ldots\ldots\ldots\ldots\ldots\ldots\ldots \quad (2.1)$$

Where, H = enthalpy in J mol^{-1}

Cp = specific heat capacity in JK^{-1} mol^{-1}

f (T,t) = kinetic response of the sample in J mol^{-1}

Thus, the total heat flow is the sum of the two terms, one related to the heat capacity, and one related to the kinetic response.

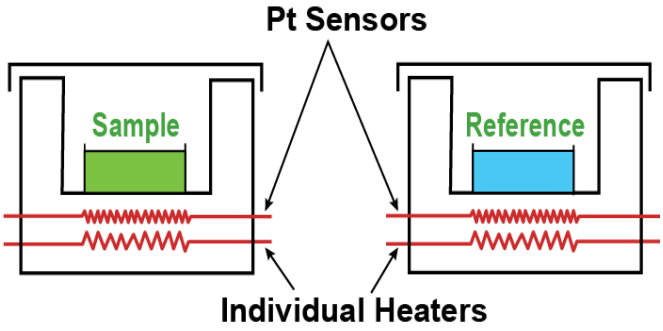

Figure 2.14: Schematic diagram of power compensation type DSC.

In PC type DSC, both sample and reference pans are heated by a different furnaces. When an event occurs in the sample, sensitive platinum resistance thermometer (PRT) detects the changes in the sample, and power (energy) is applied to or removed from the sample furnace to compensate for the change in heat flow to or from the sample. As a result, the system is maintained at a "thermal null" state at all times. The amount of power required to maintain system equilibrium is directly proportional to the energy changes occurring in the sample. No complex heat flux equations are necessary with a power compensation DSC because the system directly measures energy flow to and from the sample. The heating and cooling rate of PC types DSC can be as high as 500°C/min.

DSC analysis is used to measure melting temperature, heat of fusion, latent heat of melting, reaction energy and temperature, glass transition temperature, crystalline phase transition temperature and energy, precipitation energy and temperature, oxidation induction times, and specific heat or heat capacity.

2.8 Electrical Conduction in Polymer Nanocomposites

Electrically conductive composites consists of an insulating matrix material and conductive filler particles of various shape (spheres, flakes, fibers etc). Most polymers are inherently electrically insulating and conductive nano-fillers are found to impart significant conductivity to polymers and render them insulating to conductive. The electrical properties of nanocomposites are controlled through the material selection, volume fractions of components, conductivity, percolation behavior and anisotropy. Percolation theory has been a successful tool for describing the transition behavior of insulating polymers filled with conductive inclusions [14-16].

2.8.1 Theory of Percolation

The main factor influencing the composite conductivity is the concentration of the filler particles. At low filler content the conducting particles are separated and the electric current may flow only by means of hopping or tunneling through a non-conducting medium between the neighboring particles. The transport of charge carriers is inefficient and the overall conductivity of such a composite is low [17]. When particle concentration is increased the gaps between particles diminish and conductivity slowly increases because charge transport gets easier. At the percolation threshold the conductivity steeply rises. The percolation threshold is defined as a minimal concentration (volume fraction) of the conducting filler at which a continuous conducting network of macroscopic length appears in the system. Above this volume fraction, the electrical resistivity of the composite is relatively low.

There are different models and theories that define an insulator-conductor transition and a corresponding percolation threshold of the conductive filler concentration with regard to the DC and AC conductivity [18-20].

2.8.2 Composite Behavior above the Percolation Threshold

The relation between the composite conductivity, σ_c and the conductive filler concentration v_f, above the percolation threshold is described by the power law,

$$\sigma_c = \sigma_f (v_f - v_{crit})^{t}, \qquad v_f > v_{crit} \quad \ldots\ldots\ldots\ldots\ldots\ldots\ldots \quad (2.2)$$

Where σ_f is the filler conductivity, v_{crit} means the critical or threshold volume fraction of the filler and t is a critical exponent. It is usually supposed that these values do not depend on the percolation character but on the dimensionality of space [22]. Eq. (2.2) has been used by a variety of researchers to fit experimental data and to obtain the values of v_{crit} and t.

2.8.3 Composite Behavior at the Percolation Threshold

Several researchers have investigated the area of the percolation threshold [22,23,24]. They described the behavior of composites in this area and expressed the composite conductivity, σ_c, in terms of volume fraction as in Kirkpatrick's theory,

$$\sigma_c = \sigma_f \left(\frac{\sigma_m}{\sigma_f}\right)^{s}, \qquad v_f = v_{crit} \quad \ldots\ldots\ldots\ldots\ldots\ldots\ldots \quad (2.3)$$

Where σ_m means the matrix conductivity and s is a critical exponent for this area.

2.8.4 Composite Behavior below the Percolation Threshold

When the volume fraction of the filler in the composite is smaller than the percolation value, the conductivity of the composite is a slowly varying function whose values approach those of pure matrix σ_m [21]. The conductivity of the composite can thus be expressed

$$\sigma_c = \sigma_m \left(v_{crit} - v_f\right)^{-q}, \qquad v_f < v_{crit} \quad \ldots\ldots\ldots\ldots\ldots\ldots\ldots\ldots (2.4)$$

Where v_f is the conductive filler concentration, v_{crit} means the critical or threshold volume fraction of the filler and q is the critical exponent for this case.

The scaling hypothesis [22] gives the following relation between indexes t, s and q:

$$q = t\left(\frac{1}{s} - 1\right) \quad \ldots\ldots\ldots\ldots\ldots\ldots\ldots\ldots\ldots\ldots (2.5)$$

In the two-dimensional model (indicated by 2 in the subscript) $s_2 = 1/2$, and it follows from Eq. (2.2) that $q_2 = t_2$. In the three-dimensional model $q_3 \approx 1$, $t_3 \approx 1.6$ and from Eq. (2.2) we obtain $s_3 \approx 0.62$ [22].

2.8.5 Factors Influencing the Conductivity of CNT/polymer Composites

The electrical conductivity of composites mainly depends on the filler, matrix and temperature. From the filler point of view the type, size, volume fraction and orientation of particles in the matrix are crucial here.

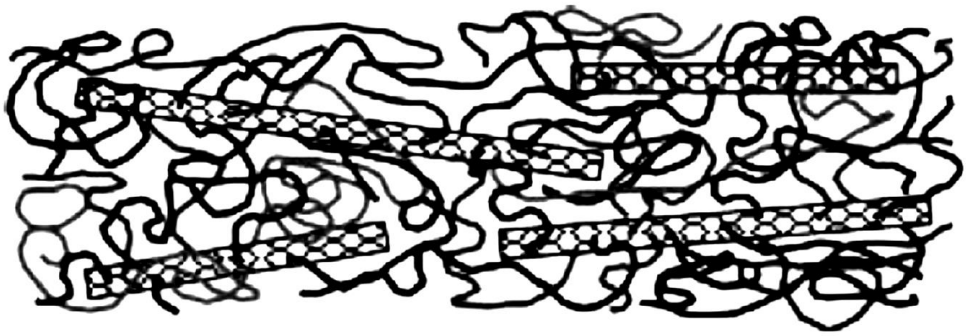

Figure 2.15: Integration of nanotubes into the polymer cross-linked structure [26].

According to Bigg [25], the fibrous fillers improve conductivity much more significantly than spheres, flakes of irregular particles, i.e. aspect ratio plays important roles here. In the nanocomposites reinforced by CNTs, nanotubes are covalently integrated into the polymer matrix and become part of the cross-linked structure rather than just a separated component [26], as shown schematically in Figure 2.12.

(i) Structure of CNTs

The aspect ratio is a proportion of maximum length, L to minimum diameter, D. According to this classification $L/D \approx 1$ for symmetrical particles (spheres, cubes and ellipsoids), $1 < L/D < 1000$ for short fibers and flakes and $L/D > 1000$ for long fibers [27]. The larger the particle aspect ratio is and the more randomly the particles are oriented, the smaller value of the threshold filler content, v_{crit}, appears. The larger values of L/D are more effective in enhancing the conductivity of composites. CNTs exhibit the highest potential for an efficient enhancement of the electrical conductivity, due to the relatively low surface area, chairality and high aspect ratio that enables a good dispersibility. At similar states of CNTs orientation, the higher the aspect ratio, the lower the CNTs concentration necessary to reach the percolation threshold, and to get conductive composies.

(ii) Volume Fraction of CNTs

With increasing MWNT loading, the nanocomposites undergo transition from electrically insulative to conductive and then the electrical conductivity was increase with additional weight percent of CNTs in the matrix [28,29]. The incorporation of a small quantity of CNTs into polymer composites could exhibit higher electrical conductivity due to the formation of an extra effective electrical network. However, higher CNTs loading in polymer composites may cause serious CNTs aggregation, and the bulk electrical conductivity will be leveled off, even decreased [30]. Thus, choosing a suitable CNTs percentage is very important. The CNT/polymer nanocomposites have critical exponent related to the system dimension ranges from 1.6 to 2.0 by theoretical prediction, while experimental values between 0.7 and 3.1 have been reported [29,31,32].

(iii) Dispersion of CNTs

The electrical conductivity will increase by improving the dispersion or reducing the aggregation of the CNTs. Good dispersion can bring good electrical conductivity due to the increasing number of complete conductive paths. Li [33] raised a model to summarize the effects of the dispersion, they thought that in practical nanocomposites, the percolation threshold of the nanocomposites can be expressed by

$$P_c = \frac{\xi\varepsilon\pi}{6} + \frac{(1-\xi)27\pi d^2}{4l^2} \quad \ldots\ldots\ldots\ldots\ldots\ldots\ldots\ldots \quad (2.6)$$

Where P_c is the percolation thresholds, d is the diameter of the CNTs, l is length of CNTs, ε is the localized volume content of CNTs in an agglomerate, ξ is the volume fraction of agglomerated CNTs. From this model we can found that the dispersion has great effect to the percolation.

(iv) Types of Polymer

Due to the different structures and different properties especially electrical conductivity of different kinds of polymers, when reinforced by CNTs, the nanocomposites will show different electrical percolation thresholds. The polymer matrix plays very important roles in a composite material: it acts as a path for stress transfer between fillers and protects the reinforcement from an adverse effect of the environment. The matrix has a major influence on the processing characteristics of composites. Several types of polymers have been used as matrix for reinforcement by CNTs.

(v) Temperature

The composite conductivity is influenced by temperature in various aspects, activation energy is the most important.

Activation Energy

The energy required to transfer charge from one initially neutral island to another is known as activation energy and denoted by ΔE. The temperature dependence of conductivity, σ can be expressed by the Arrhenius equation

$$\sigma = \sigma_0 exp\left(-\frac{\Delta E}{k_B T}\right) \quad \ldots\ldots\ldots\ldots\ldots\ldots\ldots\ldots \quad (2.7)$$

Where ΔE is the activation energy of conductivity, k_B stands for the Boltzmann constant, T is the temperature and σ_0 is a pre-exponential factor depending on mobility of charge carriers. Equation (2.7) can be written as

$$ln\sigma = -\frac{\Delta E}{k_B T} + ln\sigma_0 \quad \ldots\ldots\ldots\ldots\ldots\ldots\ldots\ldots \quad (2.8)$$

Equation (2.8) is equivalent to a straight line equation, y = mx + c. So that ΔE can be determined from the slope of the straight line. From the graph of lnσ vs. $\frac{1}{T}$, ΔE can be calculated by using the relation

$$\Delta E = -\left(\frac{ln\sigma}{\frac{1}{T}}\right) \times k_B(\text{eV}) \quad \ldots\ldots\ldots\ldots\ldots\ldots\ldots\ldots \quad (2.9)$$

The correlation between σ_0 and ΔE can be expressed by Meyer-Neldel rule [34], or according to Turvey as the compensation law [35],

$$ln\sigma_0 = a + b\Delta E \quad \ldots\ldots\ldots\ldots\ldots\ldots\ldots\ldots \quad (2.10)$$

Where *a* and *b* (with $b > 0$) are constants. Several authors [34-36] stated that the compensation law is generally valid not only for inorganic substances but for many semiconducting materials as well.

References

[1] John, M., J., "Biofibers and biocomposites", Carbohydrate Polymers, Vol. 71, pp. 343-364, 2008.

[2] Ahrenstedt, L., N., Licentiate thesis, Royal Institute of Technology, School of Biotechnology, Stockholm, 2007.

[3] Seunghun, H., Myung, S., "Nanotube electronics: a flexible approach to mobility", Nature Nanotechnology, Vol. 2, pp. 207–208, 2007.

[4] Pop, E., Mann, D., Wang, Q., Goodson, K. E., Dai, H. J., "Thermal conductance of an individual single-wall carbon nanotube above room temperature", Nano Letters, Vol. 6, pp. 96−100, 2006.

[5] Yu, M. F., Lourie, O., Dyer, M. J., Moloni, K., Kelly, T. F., Ruoff, R. S., "Strength and breaking mechanism of multiwalled carbon nanotubes under tensile load", Science, Vol. 287, pp. 637–640, 2000.

[6] Girifalco, L., A., Hodak, M., Lee, R., S., "Carbon nanotubes, buckyballs, ropes, and a universal graphitic potential", Physical Review B, Vol. 62, pp. 13104-13110, 2000.

[7] Lourie, O., Cox, D., M., Wagner, H., D., "Buckling and collapse of embedded Carbon nanotubes", Physical Review Letters, Vol. 81, pp. 1638-1641, 1998.

[8] Hilding, J., Grulke, E., A., Zhang, Z., G., Lockwood, F., "Dispersion of Carbon Nanotubes in liquids", Journal of Dispersion Science and Technology, Vol. 24, pp. 1–41, 2003.

[9] Yurekli, K., Mitchell, C., A., Krishnamoorti, R., "Small-angle neutron scattering from surfactant-assisted aqueous dispersions of Carbon nanotubes", Journal of the American Chemical Society, Vol. 126, pp. 9902-9903, 2004.

[10] Zhou, W., L., Wang, Z., L., "Scanning Microscopy for Nanotechnology", New York, NY: Springer; 2006.

[11] Friedrich, W., Knipping, P., Laue, M., "Interferenz-Erscheinungen bei Röntgenstrahlen", Sitzungsber. Kgl. Bayer: Akad. Wiss, pp. 303-322, 1912.

[12] Bragg, W., L., "The structure of some crystals as indicated by their diffraction of x-rays", Proceedings of the Royal Society A, Vol. 89, pp. 248-277, 1913.

[13] Bragg, W., H., Bragg, W., L., "The structure of the diamond", Proceedings of the Royal Society A, vol. 89, pp. 277-291, 1913.

[14] Balberg, I., Binenbaum, N., "Cluster structure and conductivity of three-dimensional continuum systems", Physical Review A, Vol. 31, pp. 1222–1225, 1985.

[15] Ma, H., M., Gao, X., L., "A three-dimensional Monte Carlo model for electrically conductive polymer matrix composites filled with curved fibers", Polymer, Vol. 49, pp. 4230–4238, 2008.

[16] Natsuki, T., Endo, M., Takahashi, T., "Percolation study of orientated short-fiber composites by a continuum model", Physica A, Vol. 352, pp. 498–508, 2005.

[17] Blythe, A., R., Electrical properties of polymers, Cambridge University Press, 1979.

[18] Kilbride, B. E., Coleman, J. N., Fraysse, J., Fournet, P., Cadek, M., Drury, A., Hutzler, S., Roth, S., Blau, W. J., "Experimental observation of scaling laws for alternating current and direct current conductivity in polymer-carbon nanotube composite thin films", Journal of Applied Physics, Vol. 92 , pp. 4024-4030, 2002.

[19] Potschke, P., Dudkin, S., M., Alig, I., "Dielectric spectroscopy on melt processed polycarbonate-multiwalled carbon nanotube composites", Polymer, Vol. 44, pp. 5023-5030, 2003.

[20] Potschke, P., Fornes, T. D., Paul, D., R., "Rheological behavior of multiwalled carbon nanotube/polycarbonate composites", Polymer, Vol. 43, pp. 3247-3255, 2002.

[21] Kirkpatrick, S., "Percolation and Conduction", Reviews of Modern Physics, Vol. 45, pp. 574-588, 1973.

[22] Efros, A., L., Shklovskii, B., I., "Critical behaviour of conductivity and dielectric constant near the metal-non-metal transition threshold", Physica Status Solidi B, Vol. 76, pp. 475, 1976.

[23] Shklovskii, B., I., "Anisotropy of percolation conduction", Physica Status Solidi B, Vol. 85, pp, 111, 1978.

[24] Chmutin, I., A., Shevchenko, V., G., Electroconducting Polymer Composites: Structure, Contact Phenomena, and Anisotropy", Polymer Science, Vol. 36, pp. 699-713, 1994.

[25] Bigg, D., M., "Conductive polymeric compositions" Polymer Engineering and Science, Vol. 17, pp. 842-847, 1977.

[26] Delozier, D., M., Watson, K., A., Smith, J., G., Clancy, T., C., Connell, J., W., "Investigation of aromatic/aliphatic polyimides as dispersants for single wall carbon nanotubes", Macromolecules, Vol. 39, pp. 1731–1739, 2006.

[27] Ponomarenko, A., T., Schevchenko, V., G., Enikolopyan, N., S., Advances in Polymer Science, Vol. 96, Springer-Verlag Berlin Heidelberg, 1990.

[28] Taib, M., H., Zainal, N., F., A., Jumali, N., S., Shaameri, Z., Hamzah, A., S., Rusop, M., "Effect of CNTs in the polymer base nano-composite thin films on the structure and electrical properties", Journal of Nanoscience and Nanotechnology, Vol. 1136, pp. 766–769, 2009.

[29] Feng, X., B., Liao, G., X., He, W., Sun, Q.M., Jian, X., G., Du, J., H., "Preparation and characterization of functionalized carbon nanotubes/poly(phthalazinone ether sulfone ketone)s composites", Polymer Composites, Vol. 30, pp. 365–373, 2009.

[30] Liao, S., H., Yen, C., Y., Weng, C., C., Lin, Y., F., Ma, C., C., M., Yang, C., H., Tsai, M., C., Yen, M., Y., Hsiao, M., C., Lee, S., J., Xie, X., F., Hsiao, Y., H., "Preparation and properties of carbon nanotube/polypropylene nanocomposite bipolar plates for polymer electrolyte membrane fuel cells", Journal of Power Sources, Vol. 185, pp. 1225–1232, 2008.

[31] Ounaies, Z., Park, C., Wise, K., E., Siochi, E., J., Harrison, J., S., "Electrical properties of single wall carbon nanotube reinforced polyimide composites", Composites Science and Technology, Vol. 63 (11), pp.1637–1646, 2003.

[32] Sandler, J., K., W., Kirk, J., E., Kinloch, I, A., Shaffer, M., S., P., Windle, A., H., "Ultra-low electrical percolation threshold in carbon-nanotube epoxy composites", Polymer, Vol. 44 (19), pp. 5893–5899, 2003.

[33] Li, J., Ma, P.C., Chow, W., S., To, C., K., Tang, B., Z., Kim, J., K., "Correlations between percolation threshold, dispersion state, and aspect ratio of carbon nanotubes", Advanced Functional Materials, Vol. 17, pp. 3207–3215, 2007.

[34] Rosenberg, B., Bhowmikh, B., B., Harder, C., Postow, E., "Pre-exponential Factor in semiconducting organic substances", Journal of Chemical Physics, Vol. 49, pp. 4108, 1968.

[35] Turvey, K., Allan, J., R., "Correlation between the pre-exponential factor and the activation energy for electrical conductivity in monomers and polymers containing the 4-Vinylpyridine molecule" Plastics and Rubber Processing and Applications, Vol. 15, pp. 273, 1991.

[36] Eley, D., D., "Energy gap and pre-exponential factor in dark conduction by organic semiconductors", Journal of Polymer Science Part C., Vol. 17, pp. 73-91, 1967.

CHAPTER 3

EXPERIMENTAL DETAILS

3.1 Materials

3.1.1 Cellulose

Commercial 80 GSM A4 size offset papers (Double A Public Company Limited, Thailand) are used to obtain cellulose pulp fibers. These papers were produced from bleached Eucalyptus Kraft pulp.

3.1.2 Multi-Walled Carbon Nanotubes (MWCNTs)

MWCNTs (CNano Technology Ltd.) of purity >95% were obtained from Shizuoka University, Japan as a gift. The diameter of the tubes are 10 ± 2.1 nm, and the length is between 1-10 μm. To prepare CNT/cellulose nanocomposites pristine MWCNTs (*p*-MWCNTs) are used as conductive additive.

3.1.3 Sodium Dodecyl Sulfate (SDS)

Sodium dodecyl sulfate (odorless, fine white powder, purity ≥ 90%) was manufactured by Merck Specialities Private Limited, Mumbai-400 018, India. Anionic surfactant SDS is used as dispersing agent to disperse *p*-MWCNTs in the distilled water. Distilled water was collected from Boiler and Steam Laboratory, BUET and used as solvent due to fabricate these nanocomposites.

3.1.4 Ethanol

Ethanol was manufactured by Merck KGaA, 64271 Darmstadt, Germany. Ethanol evaporates quickly, without leaving a residue and is very effective for surface cleaning applications. Distilled water and ethanol are used for cleaning purpose throughout the experiments.

3.2 Apparatus used for the Fabrication of the Composites

(i) Analytical Balance

Analytical balances are instruments used for accurate and precise determining weight of sample. Modern balances have built-in calibration weights to maintain accuracy. The balance that is used in this experiment is highly sensitive and can weigh samples to the nearest tenth of a milligram (0.0001g).

(ii) Ultrasonic Bath

Sonication is a process in which sound waves are used to agitate particles in solution. Ultrasonic frequencies (>20 kHz) are usually used in sonication, leading to the process also being known as ultrasonication or ultra-sonication. Sonication processes can be carried out by the use of a probe-type ultrasonic homogenizer or an ultrasonic bath. Ultrasonic bath is used in this research work for evenly dispersing CNTs in distilled water.

(iii) Blender

A blender machine is used to get cellulose pulp fibers from the shredded papers.

(iv) Hot Plate with Magnetic Stirrer

A magnetic stirrer is an equipment used to create rotating magnetic field, there is a small bar magnet and a stand or plate containing the rotating magnet. The way this works is the rapidly rotating magnetic field makes the bar magnet rotate which ends up stirring the liquid. This is very useful to mix component in a solution and get a homogeneous liquid mixture. Figure 3.4 illustrates a photograph of a combined hot-plate magnetic-stirrer device which is used in this experiment.

Figure 3.1: A photograph of a magnetic stirrer

(v) Hot Air Oven

A hot air oven is electrical operated equipment which is used widely in research and analysis works. It offers simple operation of heating and drying of the common material. The hot air oven (Cowbell, India) used in this research can be operated from 50 to 250 °C.

Figure 3.2: A photograph of a hot air oven machine

The temperature is controlled by using a thermostat and PID controller. Controller and automatically control units that helps to maintain the homogeneous temperature in the cabinet. It is constructed with double walled cabinet and inner chamber is made up of anodized aluminum/stainless steel. The double walled insulation keeps the heat in and conserves energy. For keeping samples, there are two trays fitted inside. Figure 3.5 shows a photograph of a hot air oven that is used to evaporate the solvent from the composite.

3.3 Composite Fabrication

Firstly, anionic surfactant sodium dodecyl sulfate (SDS) powder was dissolved in distilled water by sonication for 10 minutes. A certain amount of MWCNTs was dispersed in the SDS aqueous solution. The ratio of surfactant to CNTs was adjusted to 1.2/1 (w/w). The dispersion was homogenized using sonication treatment 30 minutes. In the second step, A4 size shredded paper was blended in distilled water and then the cellulose pulp was obtained. Then 25 ml of cellulose matrix was mixed with the uniform dispersion of CNTs (CNT ink). After mixing, the resultant solution was poured into a

petri dish and dried using an oven at 90 °C for 3 hours. Then the moist fibers was pressed to obtain nanocomposites having even and smooth surface. In this way, nanocomposites of different amount of CNTs (0.25, 0.5, 1, 1.5, 2, 2.5, 3 wt%) was prepared. A reference sample was also prepared by using 25 ml of the slurry without CNTs. Figure 3.6 represents a flow chart of CNT/Cellulose nanocomposites preparation procedure.

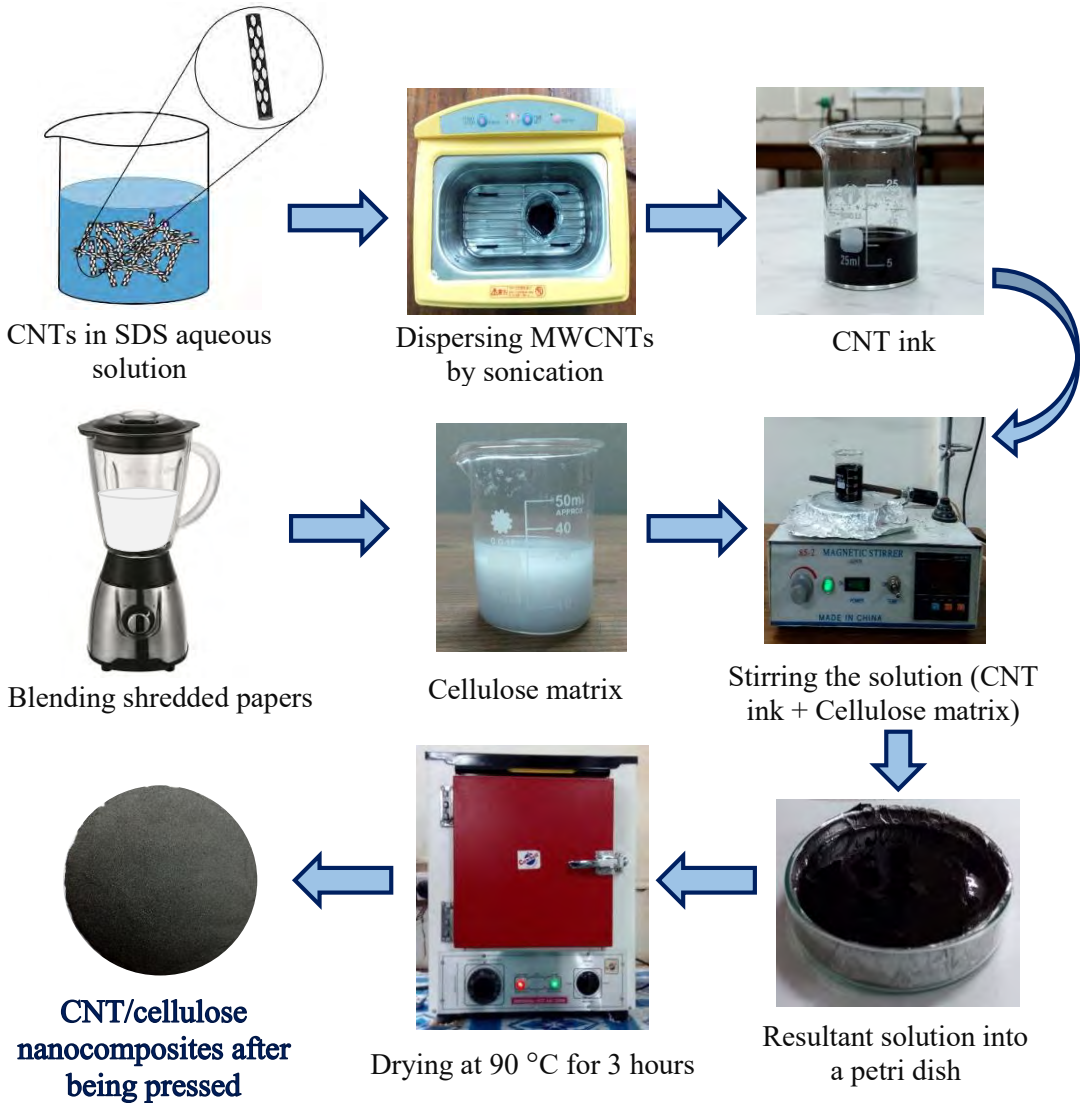

Figure 3.3: Flow chart of preparation procedure of CNT/Cellulose nanocomposites.

3.4 Composite Characterization

3.4.1 Surface Morphology

The surface morphology of the produced nanocomposites is observed by using field emission electron microscopy (FESEM, JEOL JSM-7600F). The electron microscope equipped with a field emission gun and the incorporation of the gentle beam mode, built-in r-filter and ultra-high vacuum for high resolution image acquisition. FESEM images (1,280 × 1,024 pixels) are captured at 5,000–30,000× magnifications, acceleration voltage of 5 kV and a constant working distance of 7.7 mm. Figure 3.7 indicates a field emission scanning electron microscope set up that is used in this research work.

Figure 3.4: Field emission scanning electron microscope set up.

3.4.2 Elemental Analysis

Energy Dispersive X-Ray Analysis (EDX) used in conjunction with FESEM to identify the elemental composition of the nanocomposites. The high probe current and high power optics irradiation system of the microscope delivers high-accuracy element

analysis. Acquisition parameters for the EDX analysis are as follows: accelerating voltage of 15 kV, probe current of 1 nA, energy range of 0 – 20 keV. Quantitative elemental concentrations are determined over 1 μm area of the composites samples.

3.4.3 Structural Characterization

3.4.3.1 X-ray Diffraction

Figure 3.5: X-ray diffractometer set up.

The X-ray diffraction (XRD) measurements of the fabricated composites are recorded with a PANalytical Empyrean model X-ray diffractometer (USA) equipped with curved graphite monochromator high-intensity CuKα radiation (λ = 1.540598 Å) and operated at 45 kV and 40 mA. The diffractograms are recorded in the range of angular region (2θ) from 10° to 90°. Step size 0.0066°, k2 1.544426.

3.4.3.2 Fourier Transform Infrared Spectroscopy

Functional group identification is carried out using a spectrometer (SIMADZU, FTIR-8400 spectrophotometer, Japan) in the region of 650-4000 cm^{-1} by KBr method.

3.4.4 Thermal Stability Analyses

3.4.4.1 Thermogravimetric Analysis (TGA) and Derivative Thermo-Gravimetric (DTG)

Thermal behavior of the prepared samples is examined by NETZSCH STA 449 F3 Jupiter. This simultaneous thermal analyzer is used for thermogravimetric analysis (TGA) and differential scanning calorimetric (DSC) analysis. Samples were placed in alumina crucibles and heated from 26 °C to 750 °C. A heating rate of 10 °C/minute is used under nitrogen atmosphere and at a flow rate of 40 ml/minute. The sample weight was about 5.5 mg. Derivative Thermo-Gravimetric (DTG) is obtained by using TGA instrument software.

Figure 3.6: Simultaneous thermal analyzer set up.

3.4.5 Electrical Measurements

Two-point DC Measurement

In order to get the electrical measurements, the nanocomposites of 0.6 mm thick, are cut into square of ($1\times1cm^2$) and then the sample is placed inside a pressure conductor. A digital multimeter (CD 800a, Sanwa, Japan) is used to measure the current, *I*, and a dc voltage is supplied by a stabilizer DC power supply (6545A, Agilent, Japan). The current of the prepared cellulose paper is measured by a digital Keithley 6517B electrometer (USA). A schematic circuit diagram for the DC measurement is shown in figure 3.10. The temperature-dependent electrical characteristics of the samples are studied for the temperature range of 298–358 K. For these measurements the samples are heated by a heating coil which is wrapped around the specific chamber.

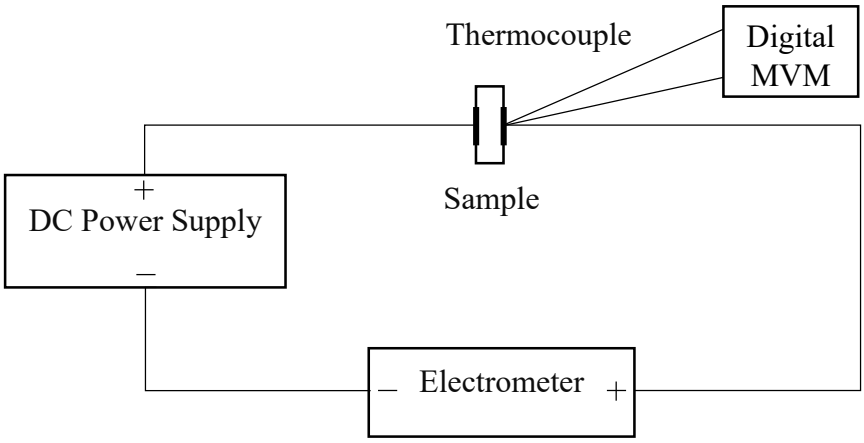

Figure 3.7: A schematic circuit diagram of DC measurement.

The temperature is measured by a Chromel-Alumel (Cr-Al) thermocouple placed very close to the sample which is connected to a GW Instek GDM- 451 digital multimeter (Taiwan). To avoid oxidation, all the measurements are performed in a vacuum of about 10^{-2} torr. DC measurement setup is shown in Figure 3.8.

Figure 3.8: DC measurement set up.

The electrical resistance, R, of the nanocomposites is obtained from $R = V/I$ and the conductivity is calculated from equation 3.1, where σ, A, and l are conductivity, electrode active area and length (thickness) of the sample, respectively.

$$\sigma = \frac{l}{RA} \quad \ldots\ldots\ldots\ldots\ldots\ldots\ldots\ldots\ldots\ldots \quad (3.1)$$

To measure the sheet resistance, R_s of the composites, two copper electrodes of width 1.97 cm are placed on the CNT/cellulose composites at a distance L. The sheet resistance of the composites is calculated by using the equation (3.2).

$$R_S = R \times \left(\frac{D}{L}\right) \quad \ldots\ldots\ldots\ldots\ldots\ldots\ldots\ldots \quad (3.2)$$

Where R, D, and L are the resistance, width of the electrodes and the distance between the electrodes, respectively. A digital multimeter (CD 800a, Sanwa, Japan) is used to measure the resistance across the sample by varying the distance between the electrodes.

CHAPTER 4

RESULTS AND DISCUSSION

4.1 Introduction

This chapter contains results and discussion on findings using different characterization techniques. The morphological, structural, thermal and electrical properties of the CNT/cellulose composites have been characterized by means of FESEM, XRD, FTIR, TGA/DTG and DC electrical measurements.

4.2 Surface Morphology

4.2.1 Surface Morphology of *p*-CNTs

Morphologies and structures of CNTs were observed through TEM and SEM micrographs. TEM images of *p*-CNTs are taken at ×25k and ×120k magnifications using JEOL JEM 1400 TEM at an acceleration voltage of 100 kV as shown in Figures 4.1 (a) and (c).

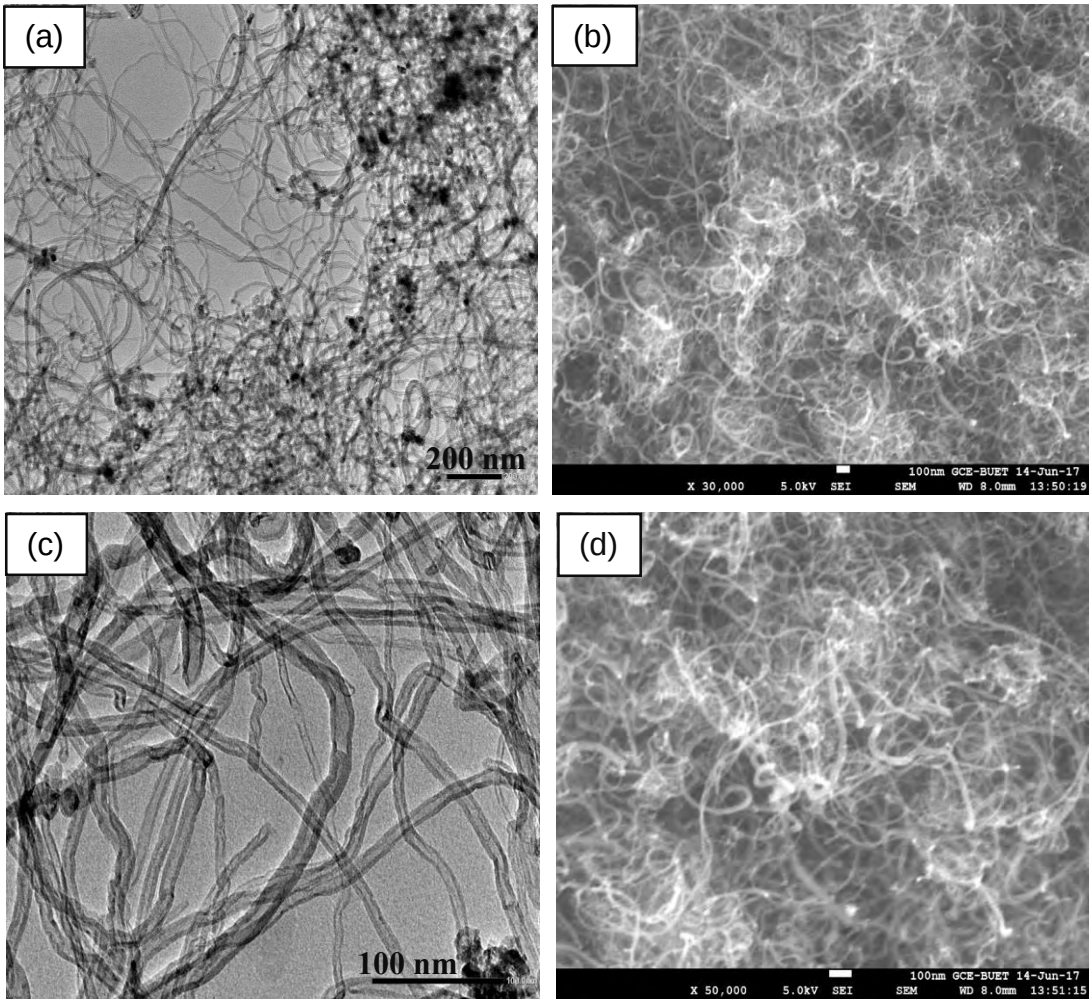

Figure 4.1: (a), (c) TEM images of *p*-CNTs at ×25k and ×120k magnifications and (b), (d) FESEM images of *p*-CNTs at ×30k and ×50k magnifications.

TEM images display CNTs with high aspect ratio, and apparent aggregation and entanglement nature of them. The length of the CNTs ranges from 1-10 μm, their outer diameter ranges from 10-30 nm and purity is above 90%. The FESEM images of *p*-CNTs shown in Figures 4.1 (b) and (d) also reveal the bundles of nanotubes which are sinuous and entangled.

4.2.2 Surface Morphology of the CNT/cellulose Nanocomposites

FESEM imaging is used to characterize the surface morphology of the cellulose sheet and CNT/cellulose nanocomposites. The low magnification FESEM image of the cellulose sheet presented in Figure 4.2 shows that the cellulose fibers are entangled together and the porous structure of the sheet is formed.

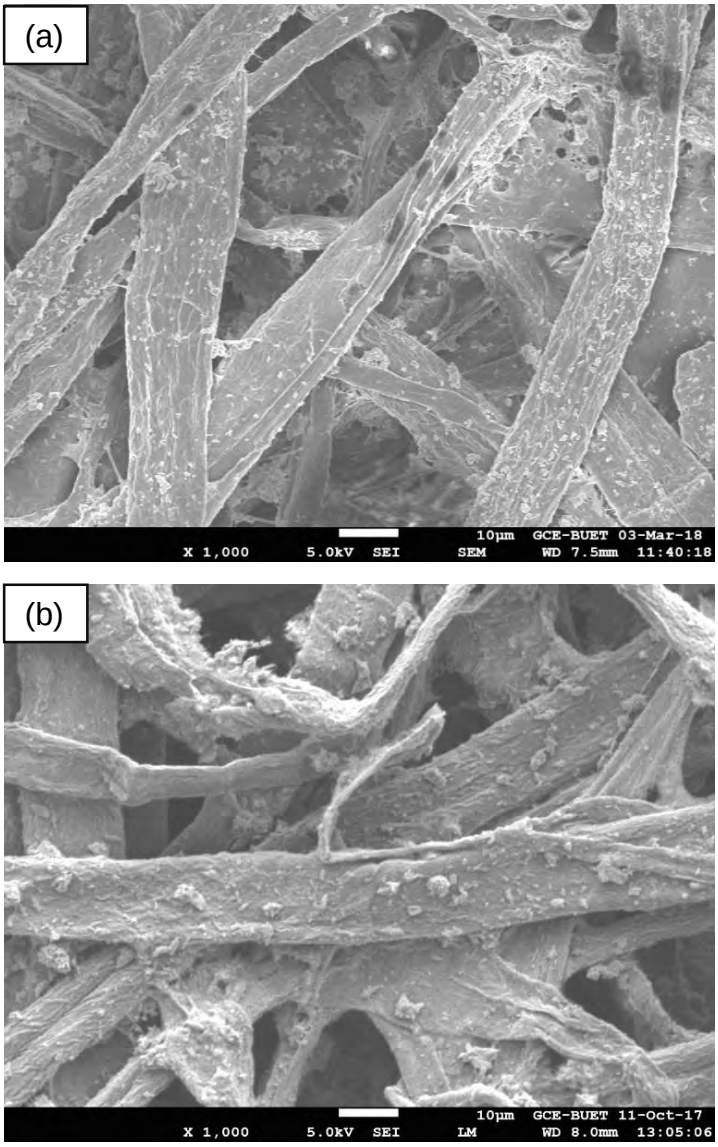

Figure 4.2: FESEM images of (a) cellulose sheet and (b) CNT coated cellulose fibers at ×1k magnification.

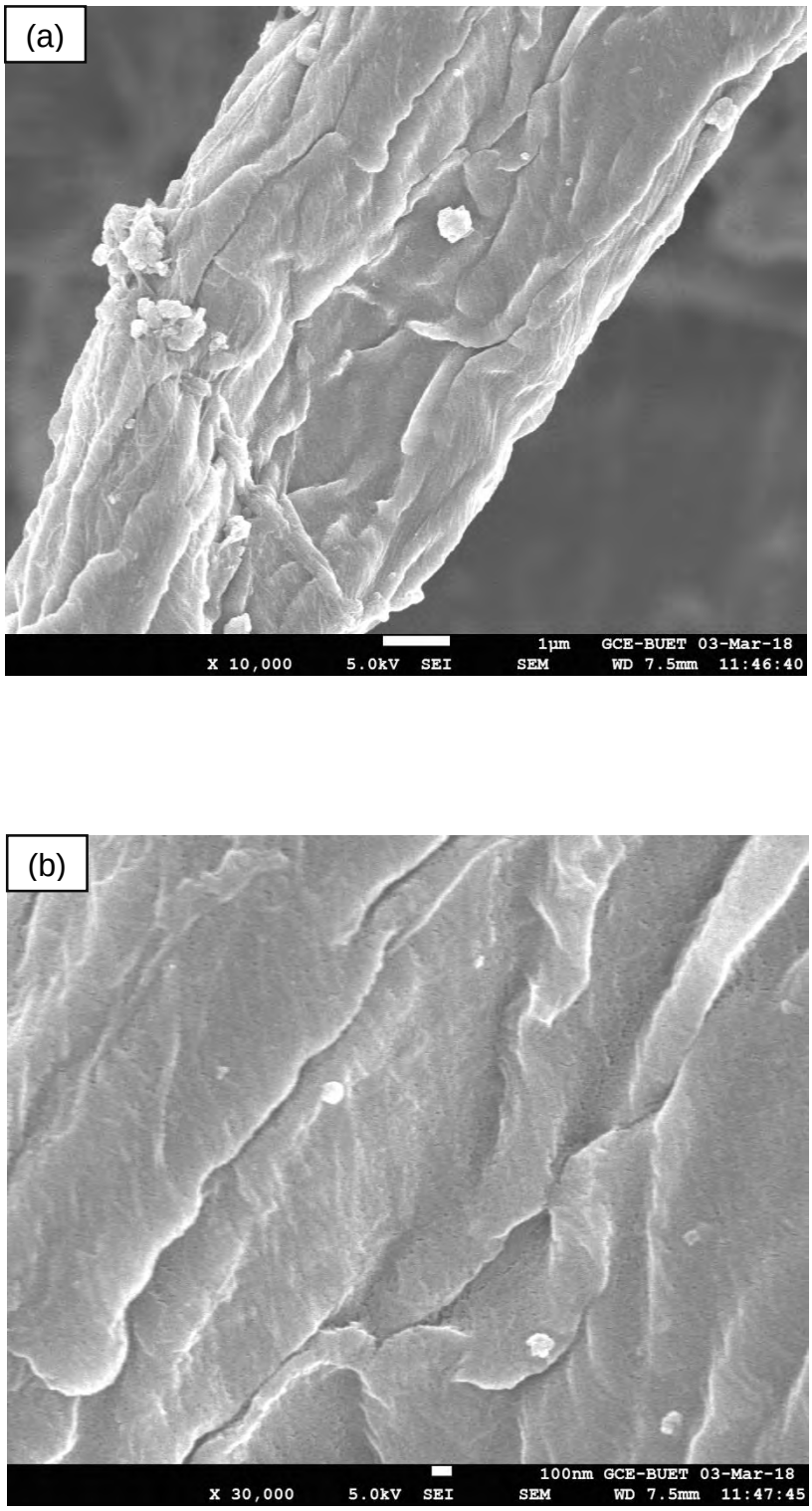

Figure 4.3: FESEM images of cellulose fiber at (a) ×10k magnifications and (b) ×30k magnifications.

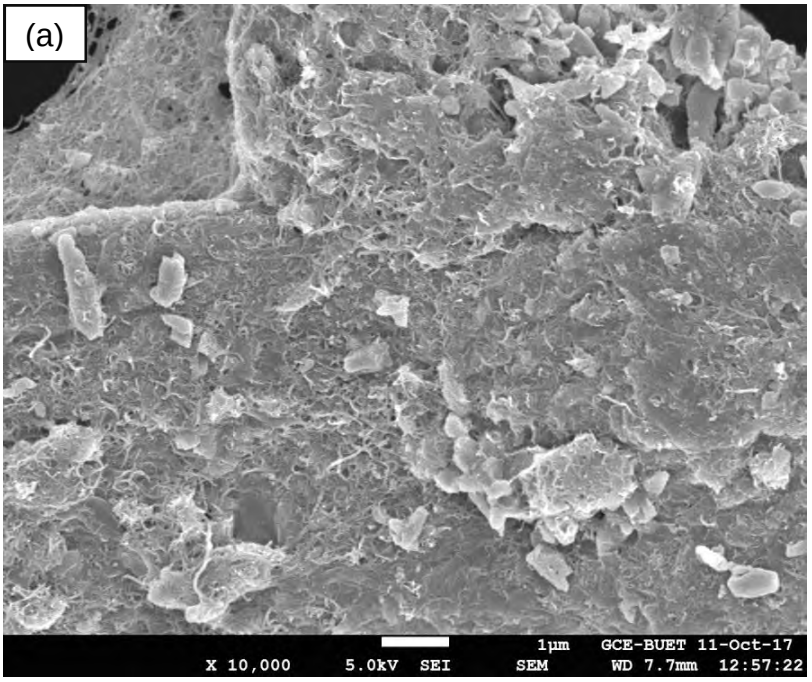

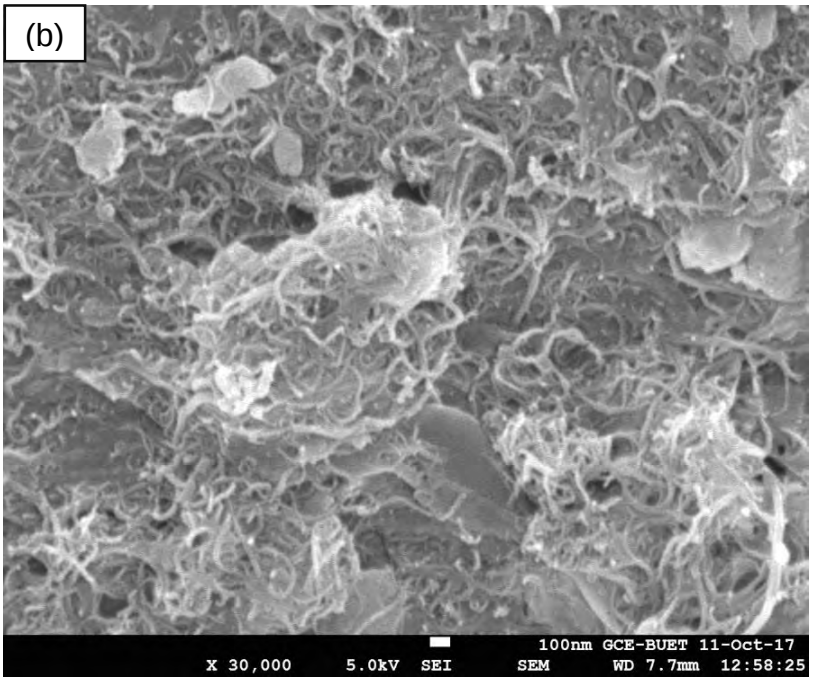

Figure 4.4: FESEM images of 0.5 wt% CNT/Cellulose nanocomposites at (a) ×10k magnifications and (b) ×30k magnifications.

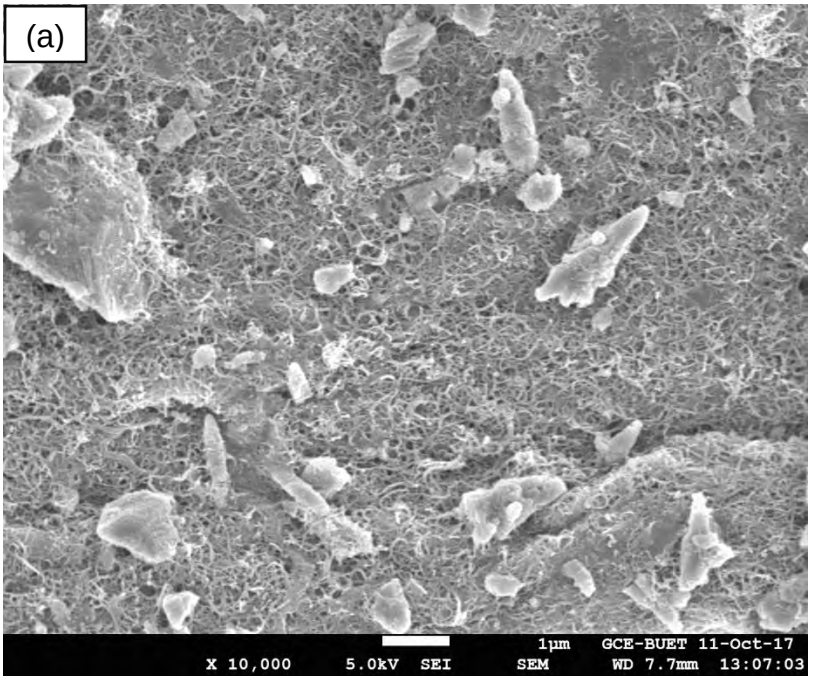

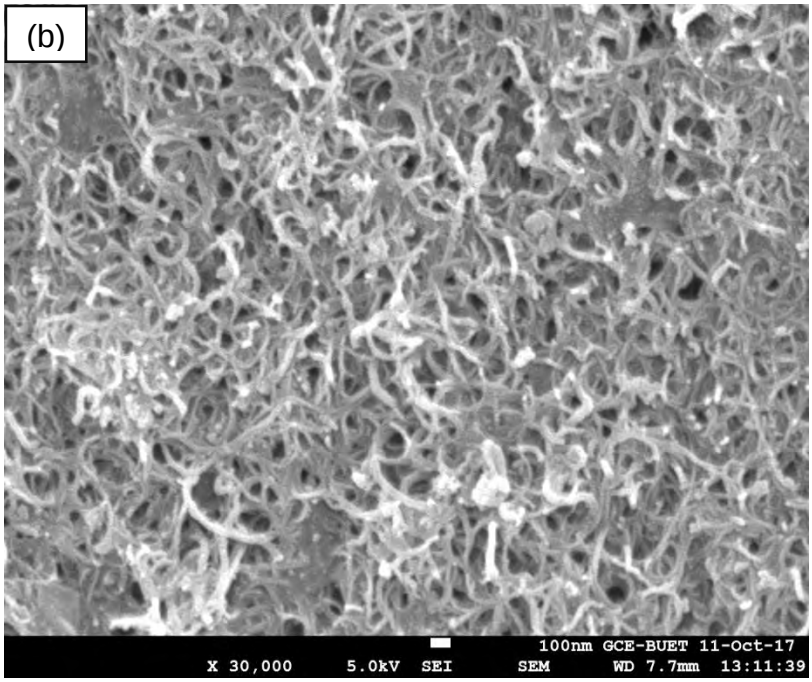

Figure 4.5: FESEM images of 1.0 wt% CNT/Cellulose nanocomposites at (a) ×10k magnifications and (b) ×30k magnifications.

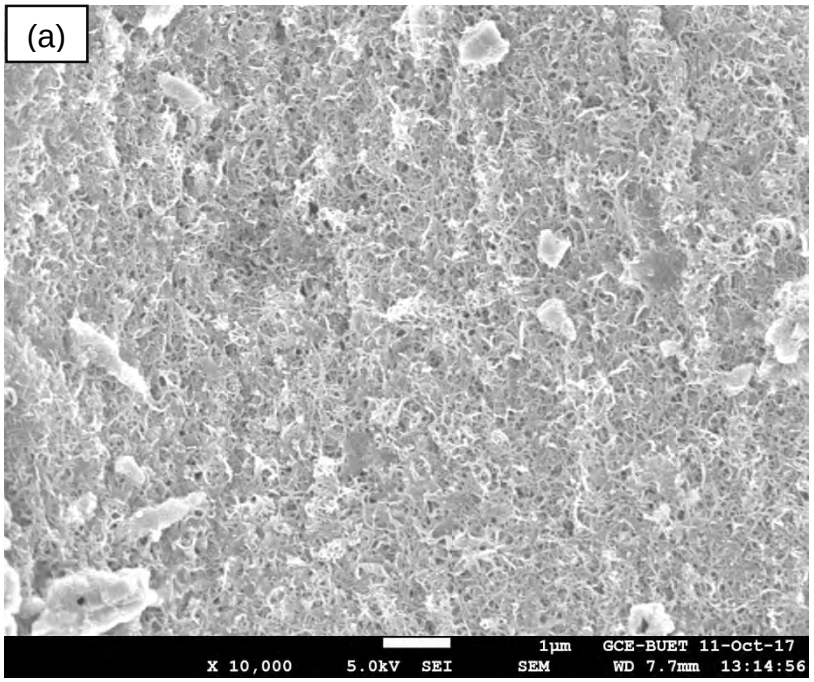

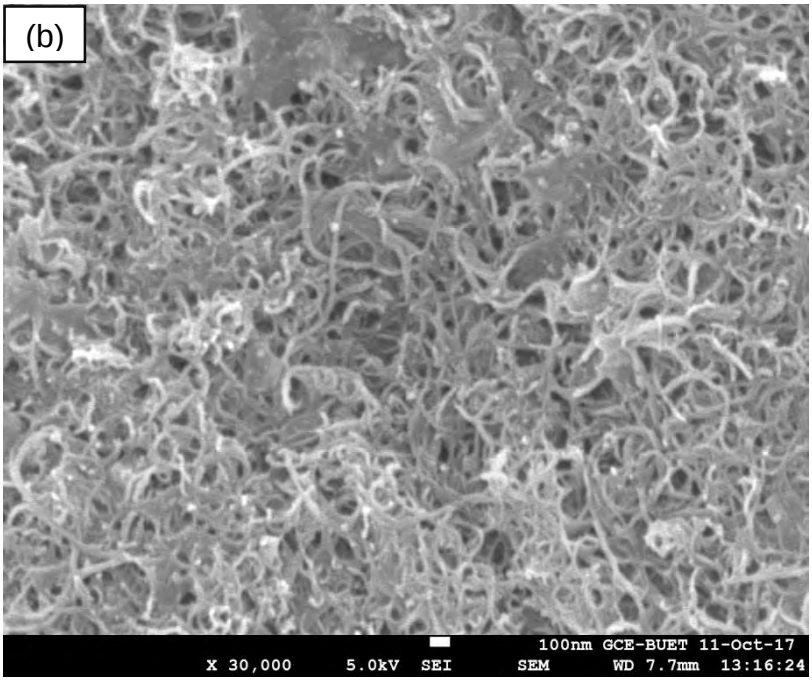

Figure 4.6: FESEM image of 1.5 wt% CNT/Cellulose nanocomposites at (a) ×10k magnifications and (b) ×30k magnifications.

High magnification image of the cellulose sheet shown in Figure 4.3 (b) represents clean surface of the cellulose fiber. The FESEM images of the CNT/cellulose composites reveal that due to 0.5 wt% of CNTs incorporation the cellulose fibers are not fully covered but in 1.0 wt% of CNTs the fibers are covered uniformly with CNTs. Further addition of CNTs may become extra layers on the already attached CNTs on the cellulose fibers.

4.3 Elemental Analysis

4.3.1 Energy Dispersive X-ray Analysis (EDX)

The elements in cellulose sheet and composite are examined by EDX analysis. From the EDX spectra of the cellulose sheet and CNT/cellulose composites shown in Figures 4.7, 4.8 and 4.9, two strong peaks can be noticed corresponding to C and O. There is also a small content of Ca and S, this may be due to the chemical treatment of pulp with $CaCO_3$ and Na_2S usually done in the papermaking process (Kraft process).

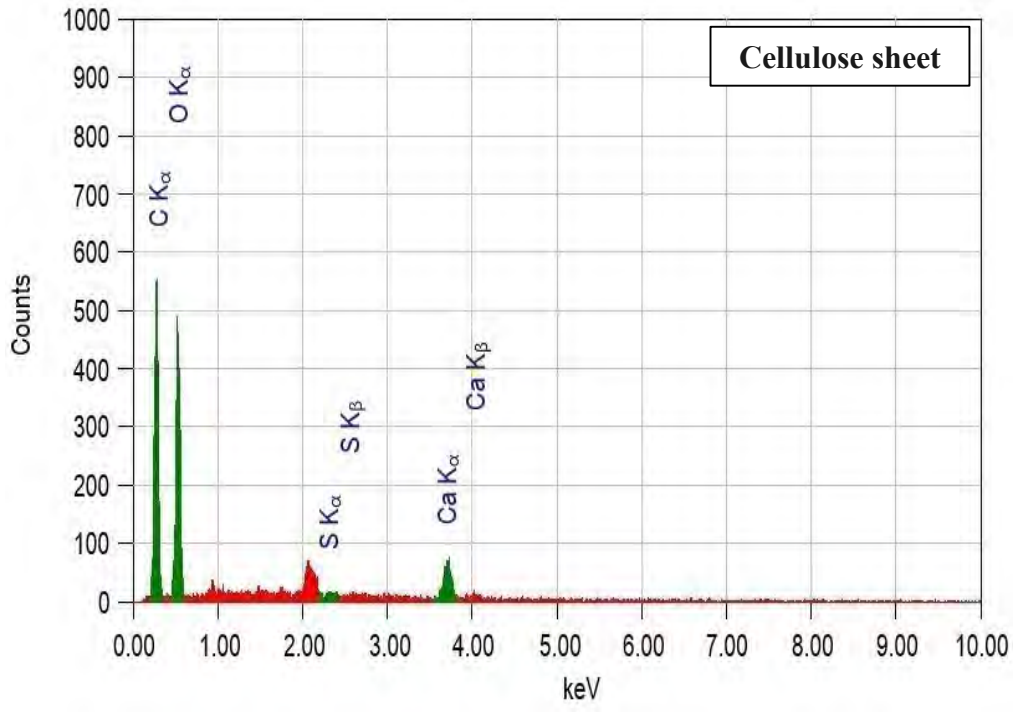

Figure 4.7: EDX spectrum of Cellulose sheet.

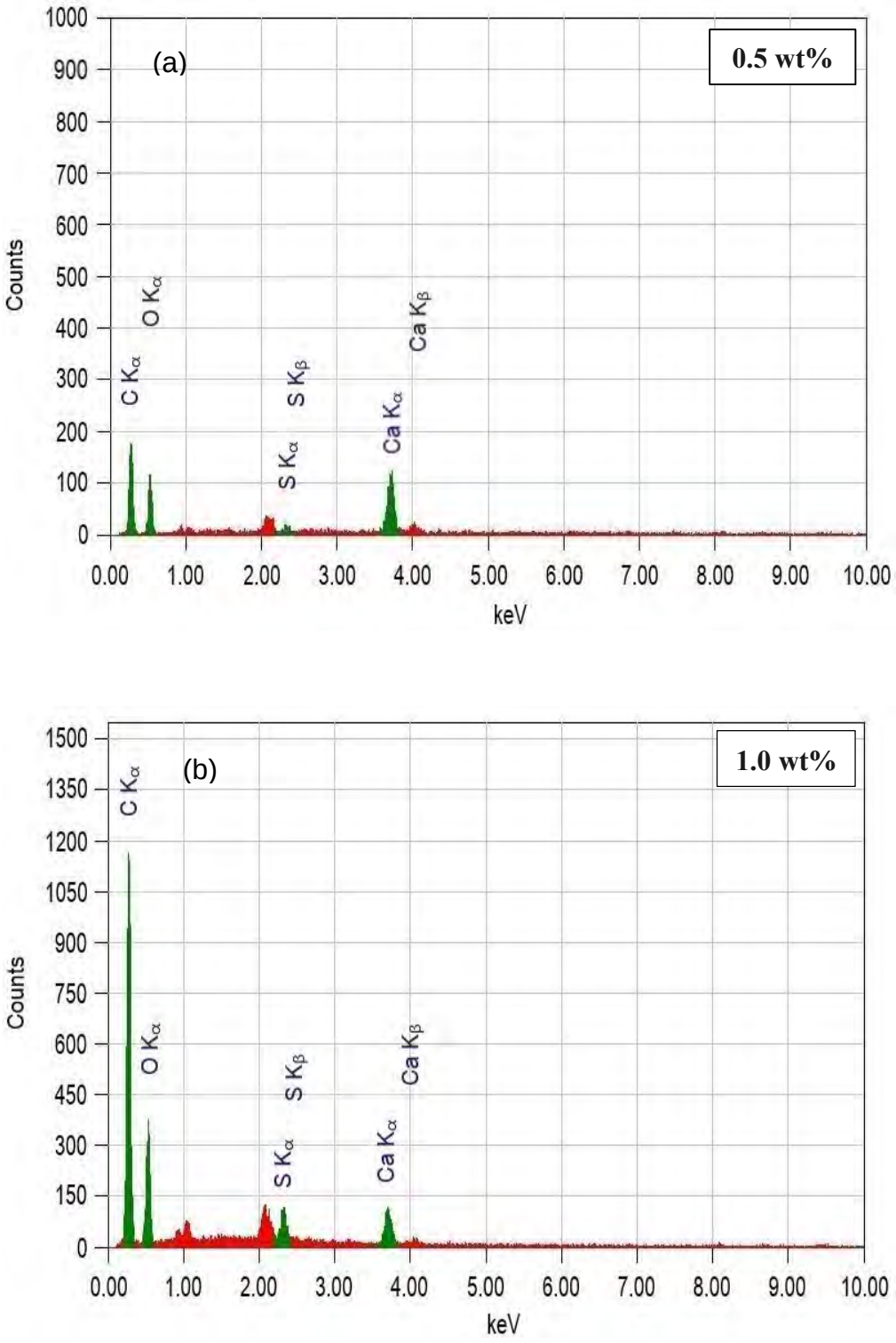

Figure 4.8: EDX spectra of (a) 0.5 wt% and (b) 1.0 wt% CNT/Cellulose nanocomposites.

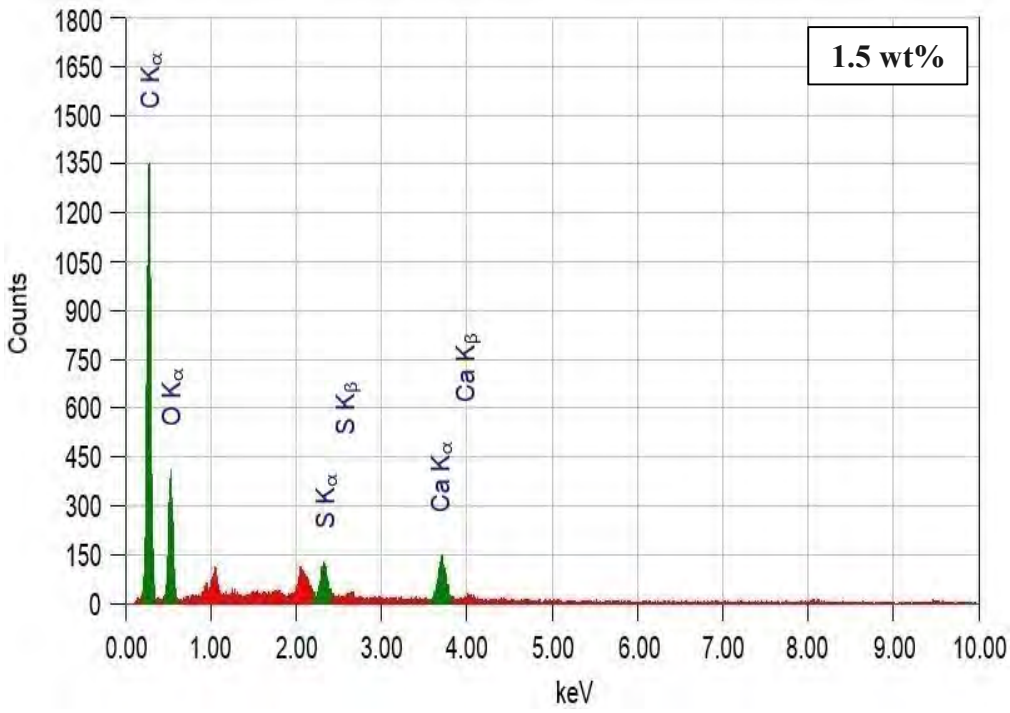

Figure 4.9: EDX spectrum of 1.5 wt% CNT/Cellulose nanocomposites.

Table 4.1: Elemental analysis data of cellulose sheet and CNT/cellulose nanocomposites

Sample	Elements in the nanocomposites with various wt% of CNTs			
	C	O	S	Ca
Cellulose sheet	53.38	43.24	0.18	3.20
0.5 wt%	72.38	19.66	0.67	7.29
1.0 wt%	85.68	11.93	0.88	1.51
1.5 wt%	85.77	11.91	0.91	1.41

Elemental analysis data of the composites is presented in Table 4.1. It is observed that the atomic percentage of C is increased with the increase of the CNTs in the composites and the percentage of O is observed to decrease with the increase of CNTs. Also the percentage of S is increased with increasing wt% of the CNTs because SDS has been used to disperse nanotubes.

4.4 Structural Analyses

4.4.1 Fourier Transform Infrared Spectroscopy (FTIR)

FTIR is used to study the structural composition of the composites. Figure 4.10 shows transmittance FTIR spectra of the *p*-CNTs, cellulose sheet and CNT/cellulose nanocomposites after baseline correction.

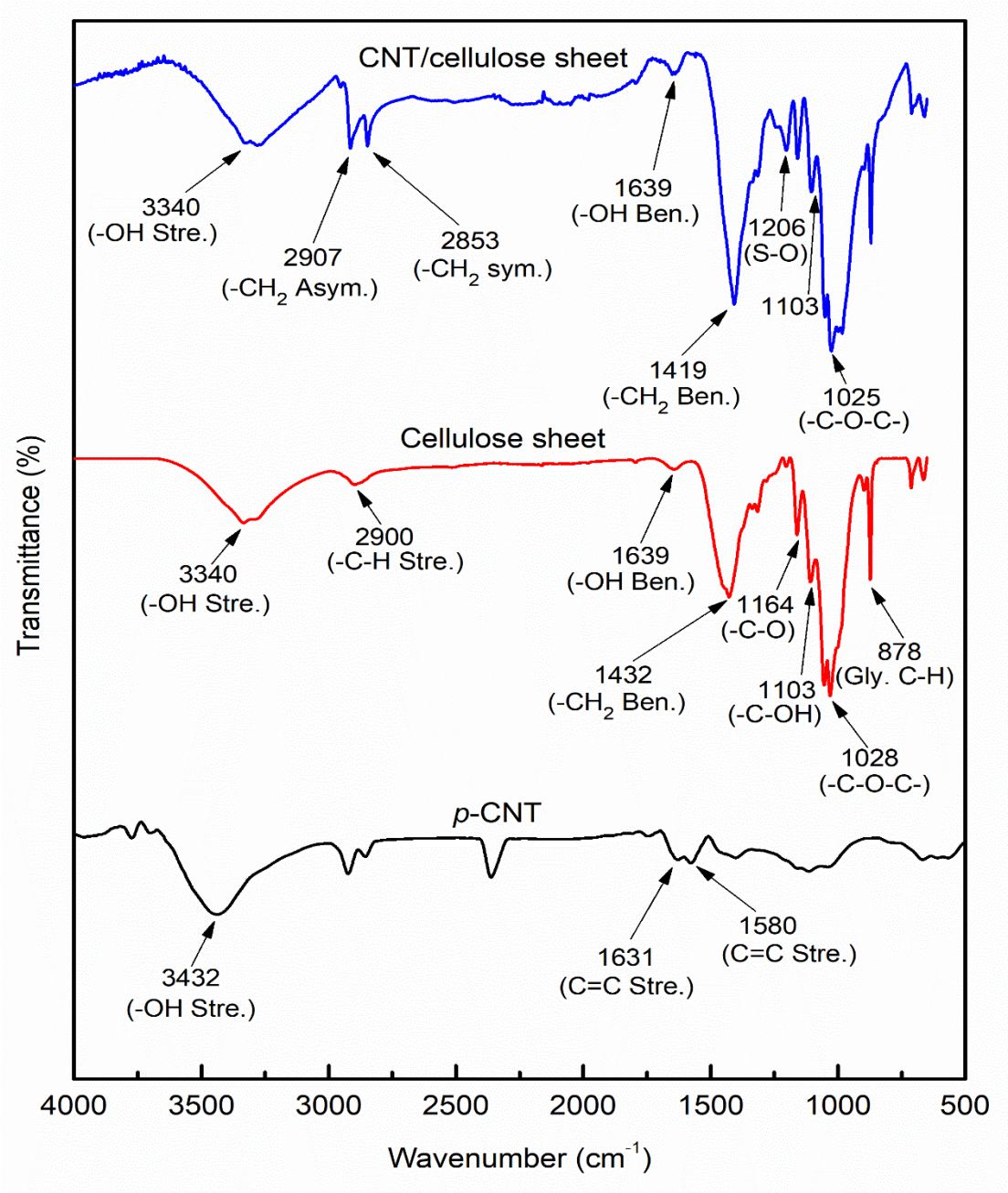

Figure 4.10: FTIR spectra of the *p*-CNTs, cellulose sheet and 2.0 wt% CNT/Cellulose nanocomposites.

FTIR spectrum of *p*-CNTs is featureless [1,2]. An absorption band at 3432 cm^{-1} for the spectrum of *p*-CNTs which represents O−H stretching [3] and also two small peaks at

1631 cm^{-1} and 1580 cm^{-1} are attributed to C=C stretching vibration [4,5], which are observed because *p*-CNTs are oxidized during the purification of the CVD synthesized CNTs [6]. The spectrum of the cellulose shows the characteristic peaks of cellulose molecules at 3340 cm^{-1}, 2900 cm^{-1}, 1432 cm^{-1}, 1164 cm^{-1}, 1103 cm^{-1}, 1028 cm^{-1}, 878 cm^{-1} [7-9]. Absorption band around 3340 cm^{-1} can be ascribed to O−H stretching. Additionally, the band at 2900 cm^{-1} is attributed to the characteristic C−H stretching of $–CH_2$ group. The peak at 1639 cm^{-1} is related to −OH bending of absorbed water. The absorption band at 1432 cm^{-1} exhibits $–CH_2$ bending mode. A band at 1164 cm^{-1} represents C−O bond vibrations and at 1103 cm^{-1} C−OH bond vibrations. A peak at 1028 cm^{-1} is associated to −C−O−C pyranose ring skeletal vibration. The absorption peak at 878 cm^{-1} is assigned to the vibration of glycosidic C−H deformation. The spectrum of the CNT/cellulose composites do not show any significant changes in the band position, but intensities of the bands at 3340 $cm^{-1}$and 1639 cm^{-1} are increased and C−H stretching mode at 2900 cm^{-1} is shifted to higher wavenumber at 2913 cm^{-1}. The peak at 2853 cm^{-1} is assigned to the symmetric stretching vibration of C−H bond. Also, the band at 1432 cm^{-1} is shifted to lower wavenumber at 1419 cm^{-1}, which is related to $–CH_2$ bending vibration. A new peak is found at 1206 cm^{-1} which indicates asymmetric S–O stretching vibration of hydrophilic sulfonate head group of SDS [10]. The bands at 4000-2995 cm^{-1}, 2900 cm^{-1} and 1430 cm^{-1} are especially sensitive to crystallinity [11]. The bands at 3340 cm^{-1}, 2913 cm^{-1} and 1432 cm^{-1} are increased in absorbance indicating that the crystallinity of the composites might be enhanced by the incorporation of CNTs in the cellulose matrix.

4.4.2 X-ray Diffraction (XRD) Analysis

Figure 4.11 represents the X-ray diffractograms of the *p*-CNTs, cellulose sheet and CNT/cellulose nanocomposites with different weight percentage of CNTs. *p*-CNTs exhibit characteristic assignments of (002), (100) and (004) crystallographic planes appeared at scattering angle of 25.95°, 42.78° and 56.8°. The characteristic peaks are identified from the JCPDS card no. 41-1487 for CNTs. (200) plane is the 2θ reflection of a graphite structure. This narrow peak indicates the neat arrangement of C atoms in the *p*-CNTs.

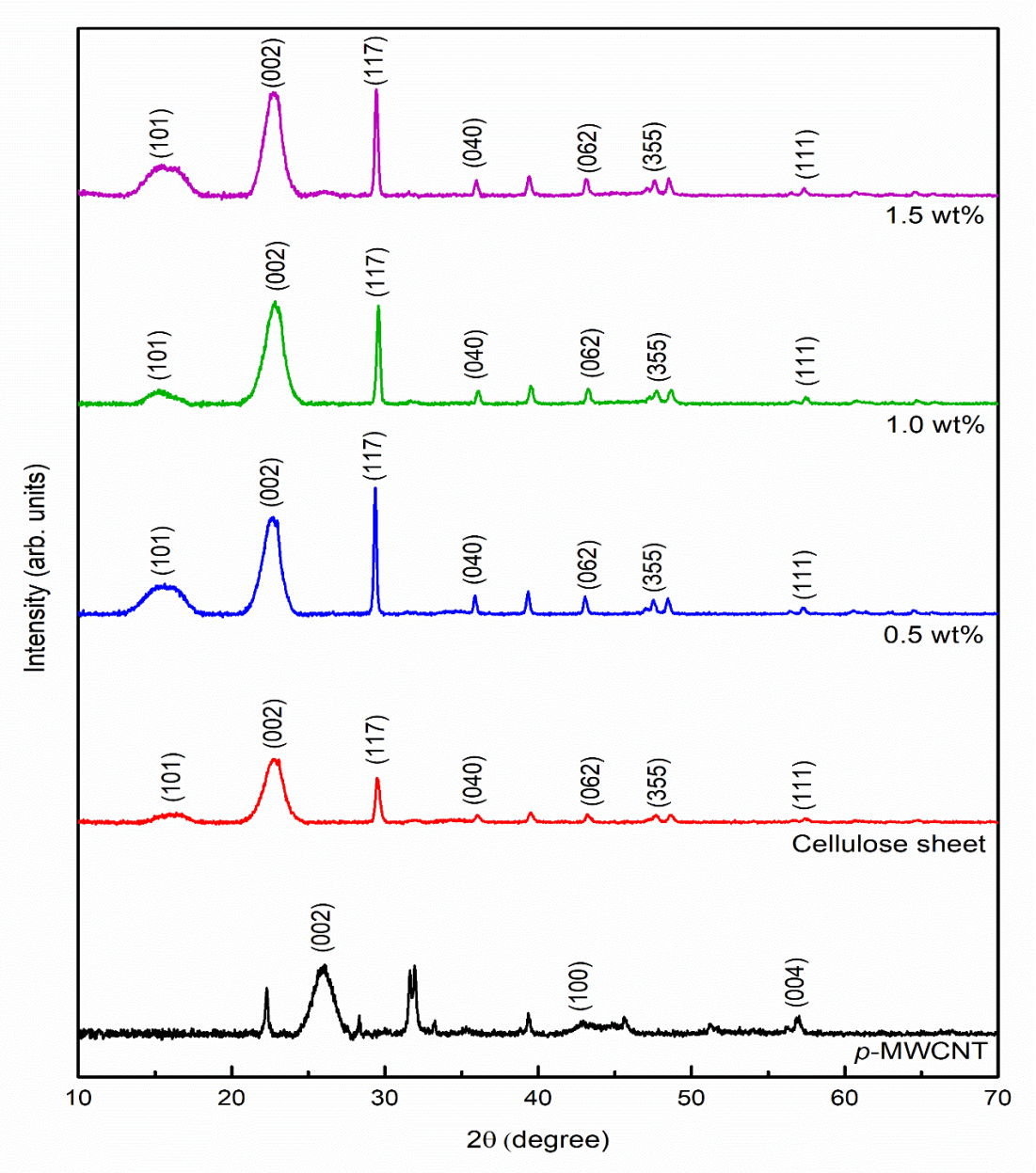

Figure 4.11: XRD patterns of the *p*-CNTs, cellulose sheet and 0.5 wt%, 1.0 wt%, 1.5 wt% CNT/cellulose nanocomposites.

The characteristic diffraction peaks are observed as (101), (002) planes at 2θ values of 15.64° and 22.69° respectively. [12,13]. These two planes are indicating the typical cellulose I structure. The plane (040) at 35.92° is related to the longitudinal structure of polymer [14]. The peaks at 2θ = 29.30°, 43.06°, 47.71°, 57.40° correspond to the (117), (062), (355) and (111) planes of sulfur respectively [15]. These sharp peaks are observed for both cellulose sheet and CNT/cellulose composites. The increasing peak intensities of sulfur are observed owing to the usage of SDS to disperse the CNTs, which also indicates the crystalline feature of the sulfur in the composites. The

diffraction patterns of the nanocomposites exhibit similar crystalline structure of cellulose. There is no corresponding peak for CNTs in the XRD patterns of the composites though the incorporation of CNTs in the cellulose matrix improves the crystallinity of the composites. The crystallite size of the samples is measured by using Debye-Scherrer equation.

$$\text{Crystallite size, } D = \frac{K\lambda}{\beta cos\theta} \quad \ldots\ldots\ldots\ldots\ldots\ldots\ldots\ldots\ldots\ldots\ldots\ldots\ldots\ldots \quad (4.1)$$

Where λ is the X-ray wavelength, K is the shape factor (0.94), β is the line broadening at the half maximum intensity in radians and θ is the Bragg angle. The values of the crystallite size of 0.5 wt%, 1.0 wt%, 1.5 wt% CNT/cellulose nanocomposites for (002) plane are found to be 6.50 nm, 6.82 nm and 6.91 nm, respectively which are larger than that of the cellulose sheet (6.24 nm).

4.5 Thermal Analyses

4.5.1 TGA and DTG

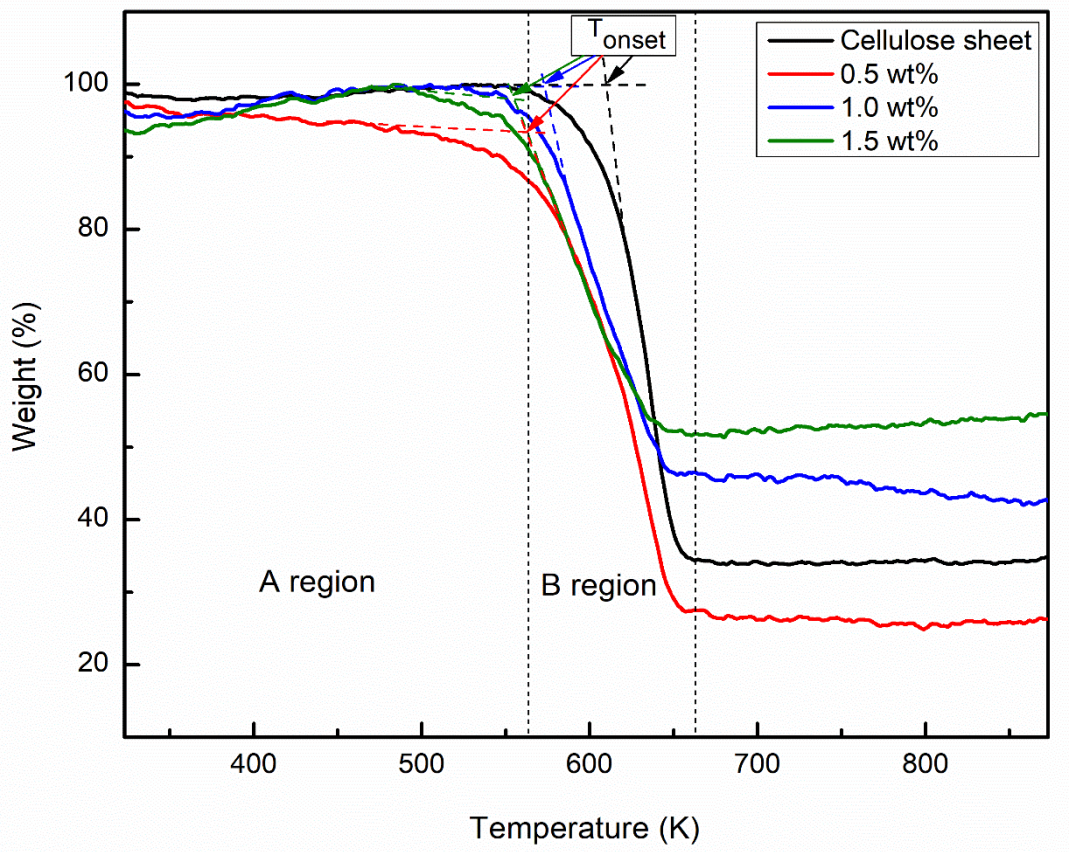

Figure 4.12: TGA curves of the cellulose sheet and 0.5 wt%, 1.0 wt%, 1.5 wt% CNT/Cellulose nanocomposites.

The thermal behavior of the cellulose sheet and cellulose composite sheets with different CNTs contents have been investigated using the techniques of TGA and DTG and the corresponding curves are shown in Figures 4.12 and 4.13. The initial weight loss of about 8 % at the temperature range of 298-393 K is observed due to the evaporation of surface bound moisture of cellulose, since the moisture regain of cellulose is known to be ~11% [16,17] or may be due to removal of water molecules released in the composites. The second dominant weight loss is observed at 566-663 K, leading to the formation volatile chemicals of low molecular weight owing to the pyrolysis of cellulose. Generally, thermal degradation of cellulose involves dehydration, depolymerization and decomposition of glycosyl-units and then formation of a charred residue. TGA curves for cellulose sheet, 0.5 wt%, 1.0 wt% and 1.5 wt% composites show residue of 33.9%, 25.9%, 43.2% and 53.7%, respectively after 773K.

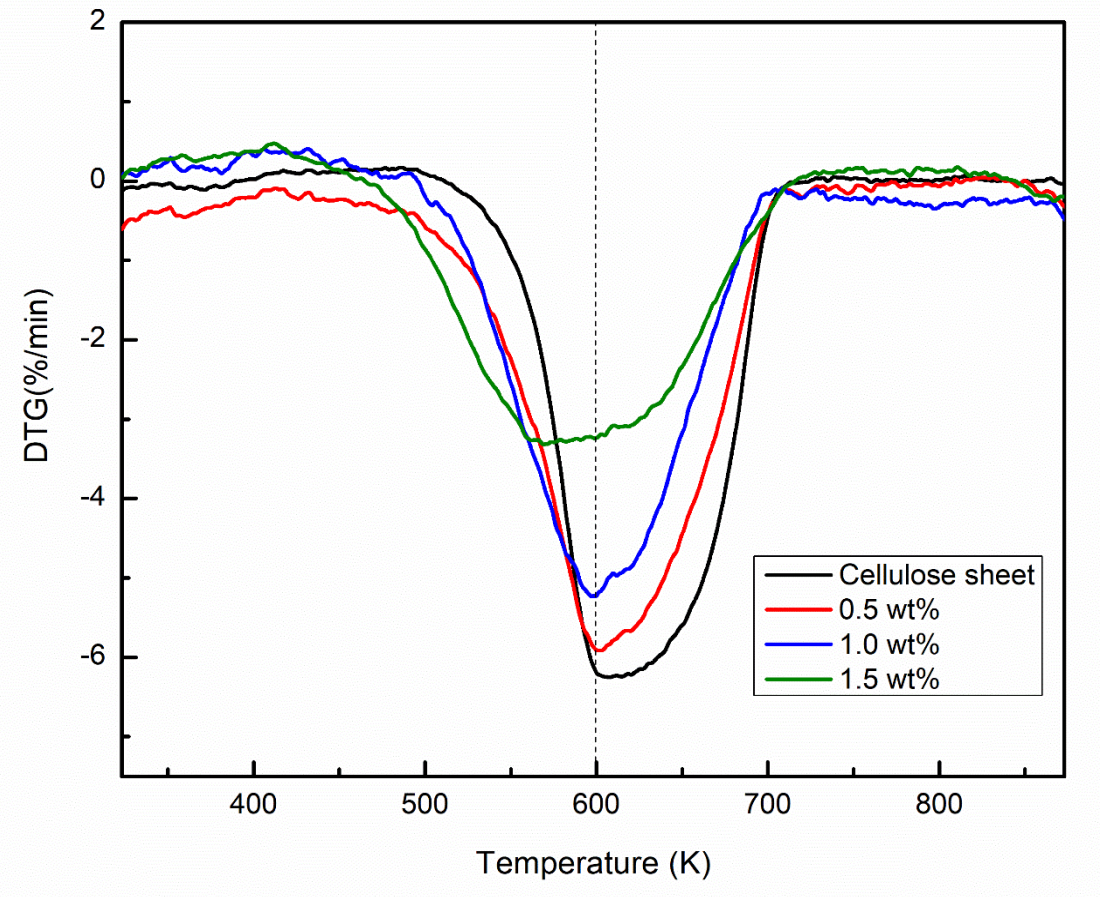

Figure 4.13: DTG curves of the cellulose sheet and 0.5 wt%, 1.0 wt%, 1.5 wt% CNT/cellulose nanocomposites.

From the DTG thermograms of cellulose sheet, 0.5 wt% and 1.0 wt% CNT/cellulose composites show degradation peaks at about 600 K and for 1.5 wt% composites

degradation reaches its peak at 569.2 K, which is lower than other three samples. This may be due to the presence of high content CNTs in the composites, which tend to display aggregation behavior of CNTs and the formation of effective interconnecting CNT networks in the polymer matrix with higher thermal conductivity, because the network density increases further with higher CNTs concentration. T_{onset} is the temperature from where the main degradation starts and $T_{50\%}$ indicates the degradation temperature for 50% weight loss. T_{onset} and $T_{50\%}$ values of the composites are presented in Table 4.2.

Table 4.2: Data of weight loss calculation for cellulose sheet and CNT/cellulose nanocomposites

Sample	First Stage (A)		Second Stage (B)		T_{onset} (K)	$T_{50\%}$ (K)
	Temperature (K)	Weight Loss (%)	Temperature (K)	Weight Loss (%)		
Cellulose sheet	298-393	2.2	566-663	64.4	609	640
0.5 wt%		4.5		58.6	561	626
1.0 wt%		4.6		48.7	573	639
1.5 wt%		6.9		38.3	555	660

4.5.2 Flame Retardancy Test

Flame retardancy of polymeric materials is essential to minimize the hazardous effect of fire in modern technological applications. CNTs provides a remarkable effect on the improvement of the flame retardancy behaviour of the nanocomposites [18,19]. Dispersion of CNTs is very important due to the formation of continuous CNT network on polymer surface that creates a protective layer and reduces the flammability of the nanocomposites [20]. To compare the flammability of cellulose sheet and CNT/cellulose nanocomposites the fire retardancy test is conducted. Figure 4.14 shows the combustion process.

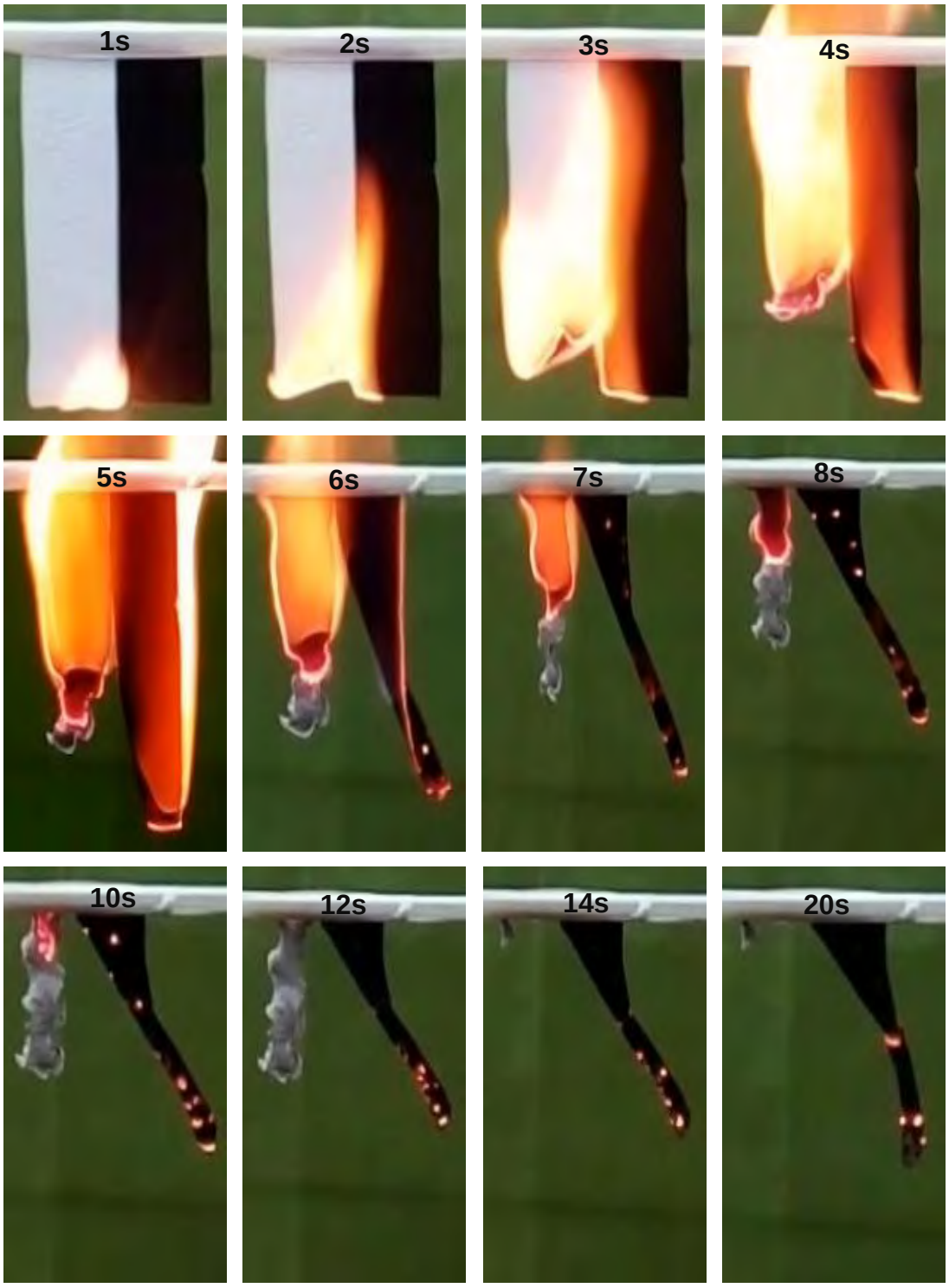

Figure 4.14: Flammability comparison of cellulose sheet (left) and CNT/cellulose composite sheet (right, CNT concentration of 3.0 wt%).

Both the samples are cut into strips of 8 cm long and 2.1 cm wide and are hanged parallel on a glass rod. To initiate combustion the samples are simultaneously ignited with a match at their lower edge. Cellulose sheet catches fire immediately and the entire

sample is engulfed within 4 seconds. For CNT/cellulose sheet, the flame dies out very soon (at 6s) and the sample turns to carbonaceous char residue, while cellulose sheet burns to ashes completely. The test reveals that CNT/cellulose composites exhibits an improved flame retardant performance.

4.6 DC Electrical Properties

4.6.1 Sheet Resistance

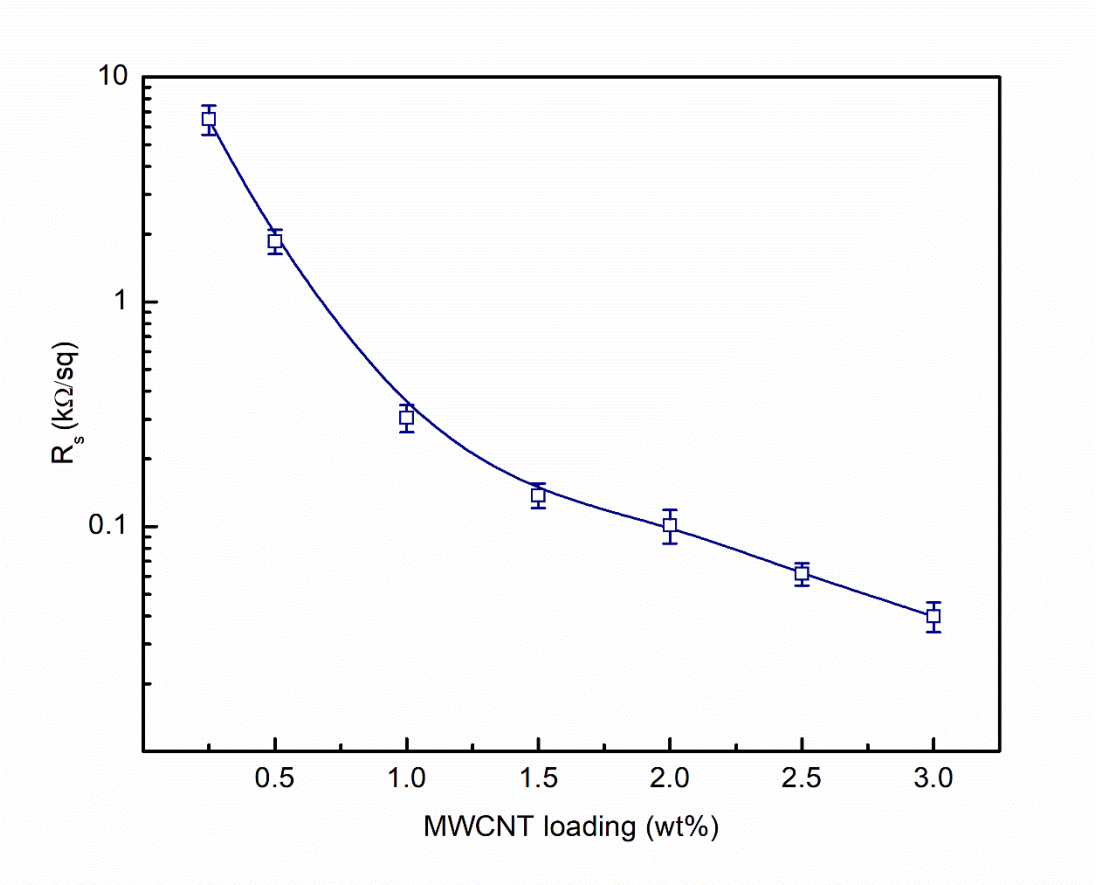

Figure 4.15: Sheet resistance vs composites with different weight percentages of CNTs.

Figure 4.15 represents the graph of sheet resistance vs composites with different weight percentages of CNTs. The sheet resistance is measured across the entire sample and at least 32 measurements are taken for each sample. The sheet resistance of the nanocomposites gradually decreases as the concentration of the CNTs increases in the cellulose matrix. The nanocomposites exhibit remarkably low sheet resistance varying from 6.5 kΩ/sq to 0.04 kΩ/sq.

4.6.2 Current Density – Voltage Characteristics

The current density-voltage (J-V) characteristics for cellulose sheet and CNT/cellulose nanocomposites at different temperatures are shown in Figures 4.16 and 4.17.

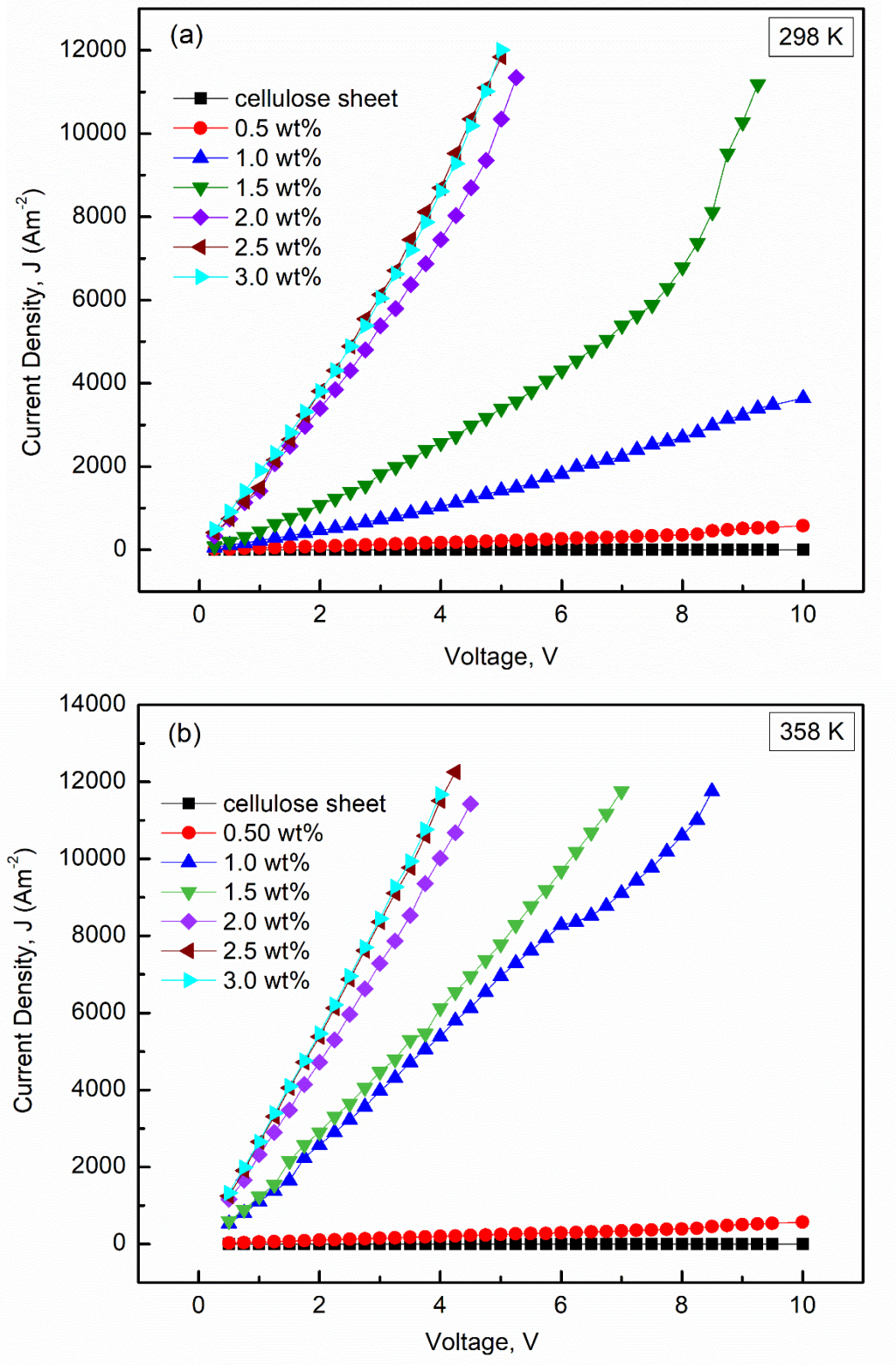

Figure 4.16: Plots of J-V characteristics for cellulose sheet and CNT/cellulose nanocomposites with various CNT content at (a) 298 K and (b) 358 K temperature.

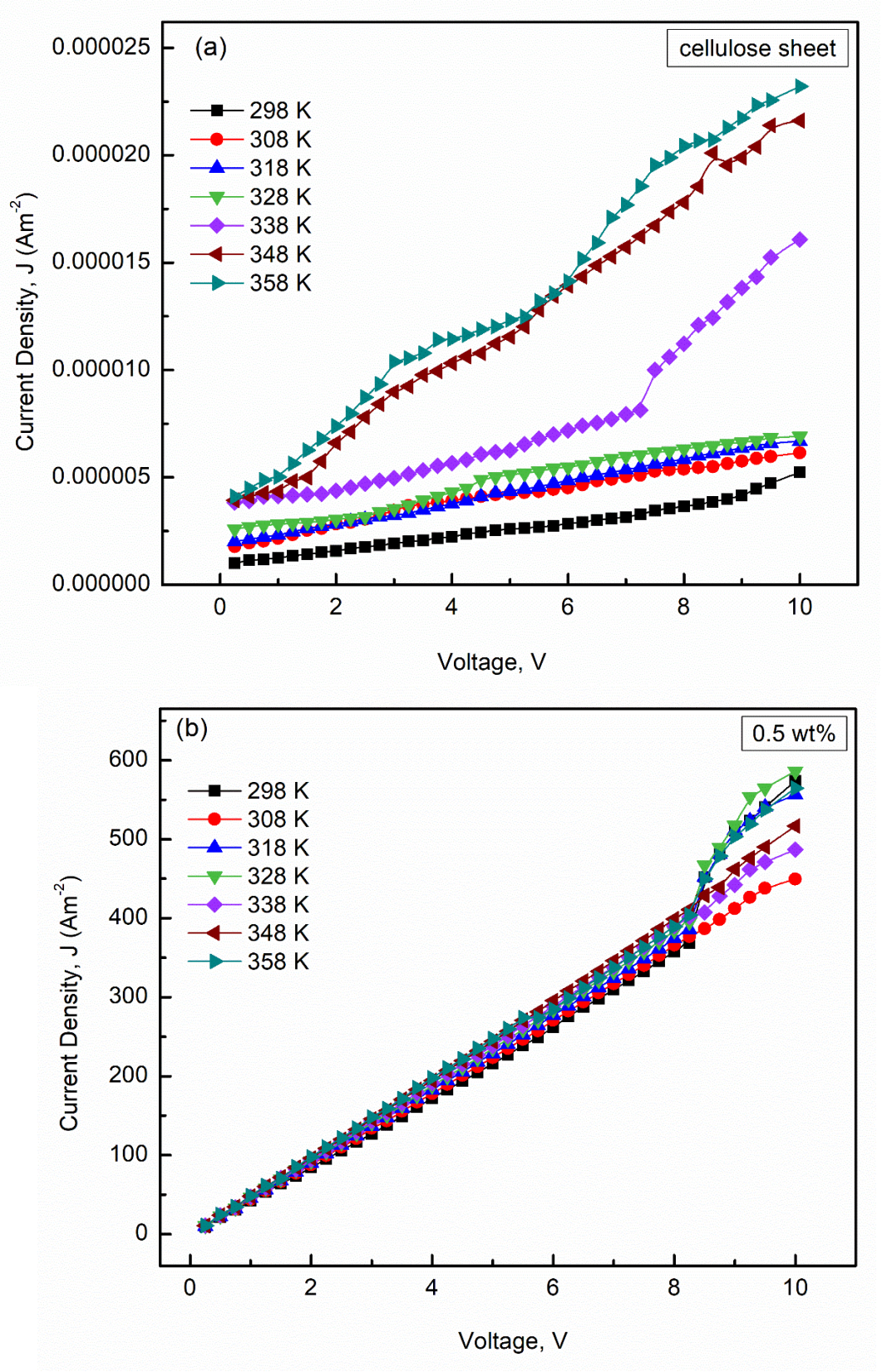

Figure 4.17: Plots of J-V characteristics at different temperature for (a) cellulose sheet and (b) 0.5 wt% CNT/cellulose nanocomposites.

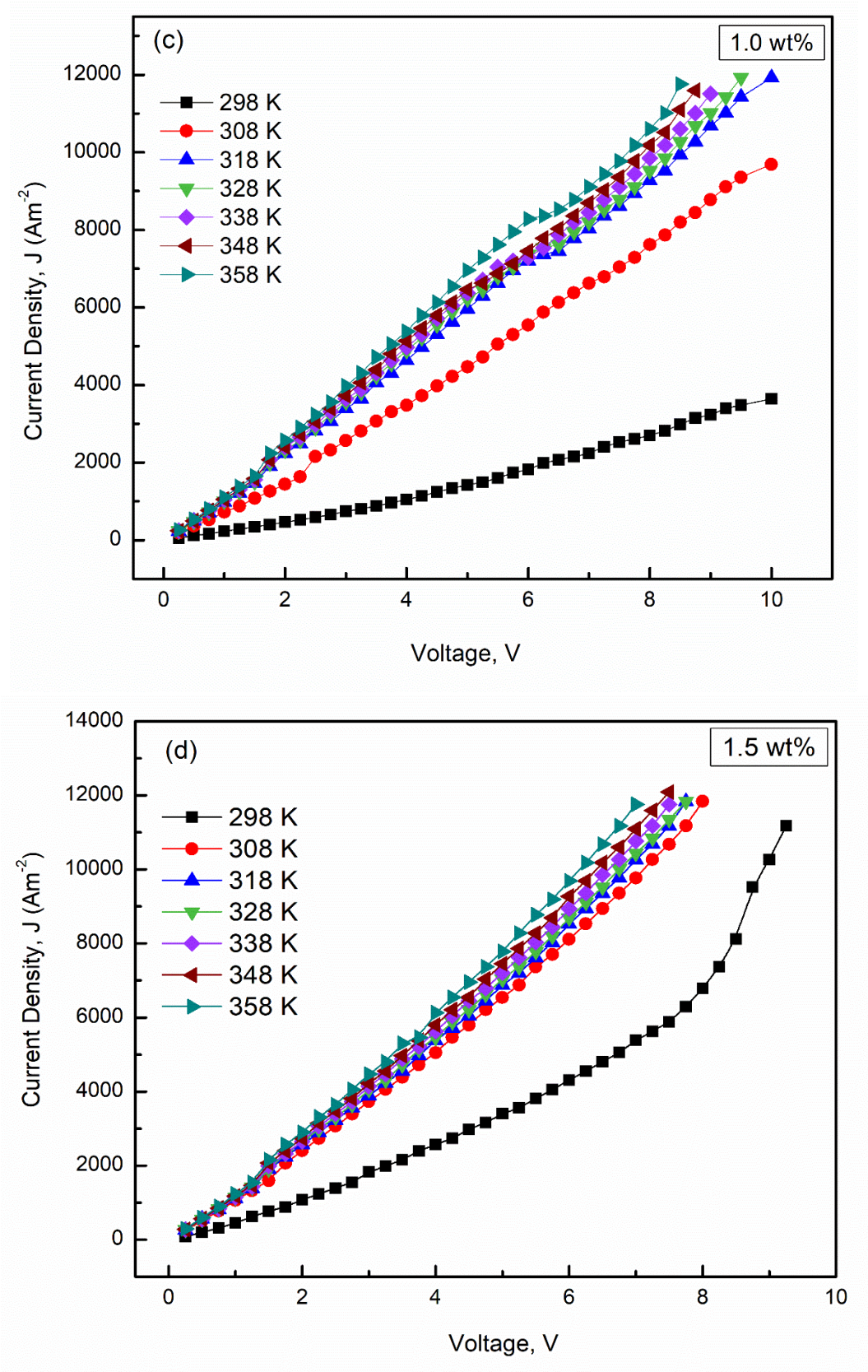

Figure 4.17: Plots of J-V characteristics at different temperature for CNT/cellulose nanocomposites (c) 1.0 wt% and (d) 1.5 wt%.

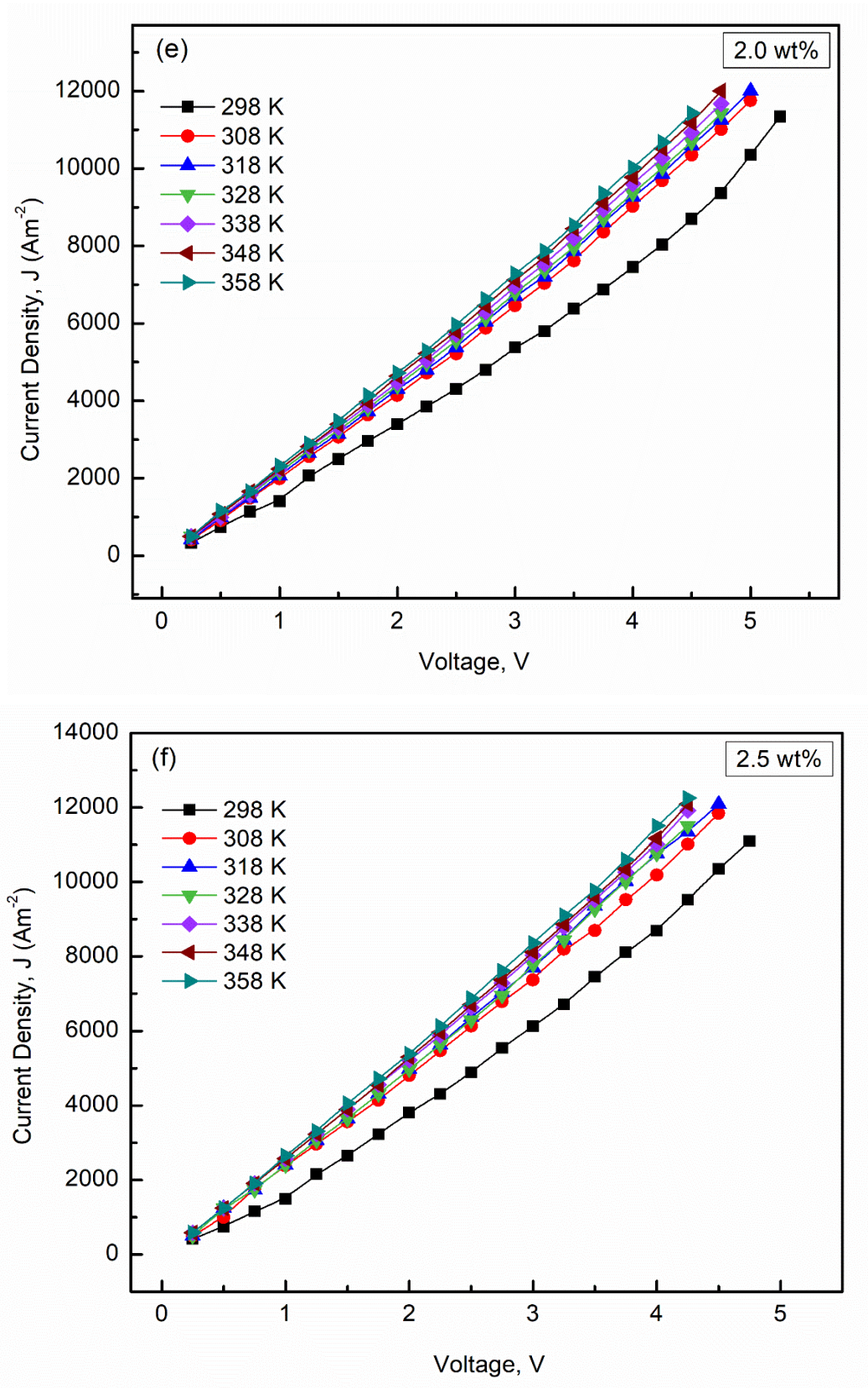

Figure 4.17: Plots of J-V characteristics at different temperature for CNT/cellulose nanocomposites (e) 2.0 wt% and (f) 2.5 wt%.

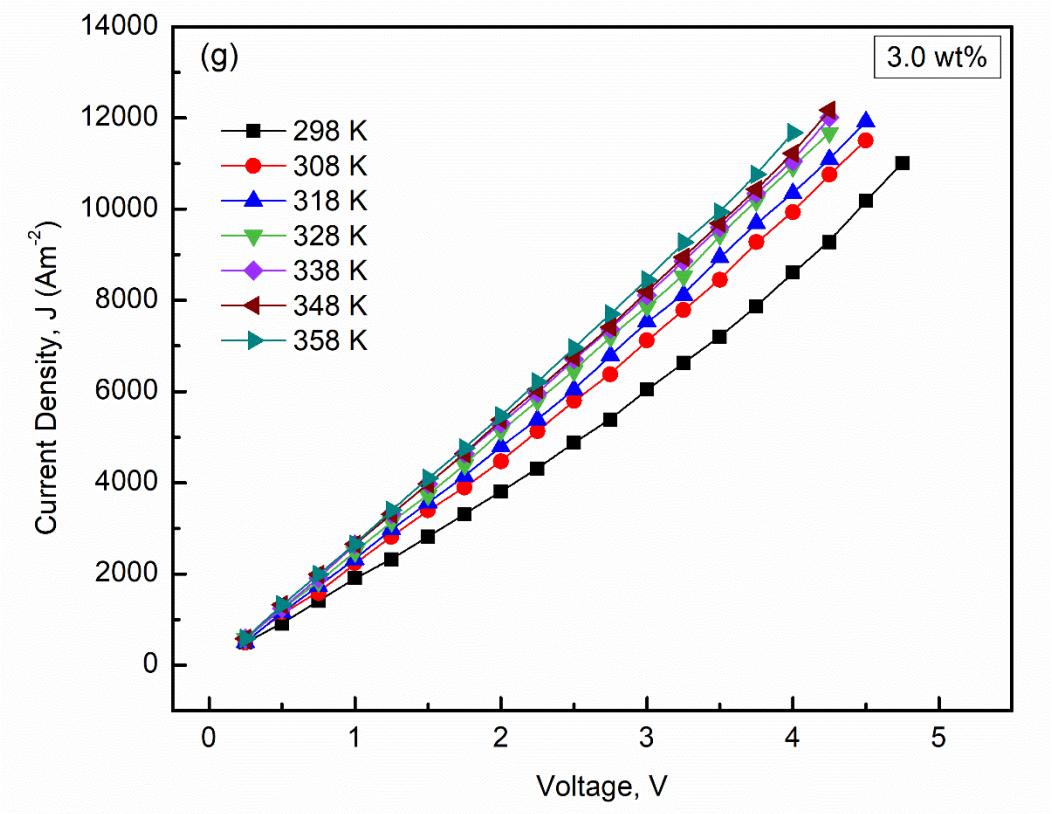

Figure 4.17 (g): Plot of J-V characteristics at different temperature for 3.0 wt% CNT/cellulose nanocomposites.

All the samples exhibit almost linear relationship between current density and voltage which indicate the Ohmic conduction. The J-V curve of the cellulose sheet represents insulating behaviour and no significant change is observed from the J-V curve of the 0.5 wt% composites which indicates that there is no effective conducting networks between the nanotubes because of very low integration of CNTs. The slopes of the J-V curve of 1.0 wt%, 1.5 wt%, 2.0 wt%, 2.5 wt% and 3.0 wt% CNT/cellulose nanocomposites are increased with increasing temperature.

4.6.3 Electrical Conductivity

Cellulose shows insulating nature which contains a very low concentration of free charge carriers. The incorporation of little amount of CNTs in the cellulose matrix exhibits significant improvement in the electrical conductivity of the sheet due to the formation of effective conducting network of CNTs.

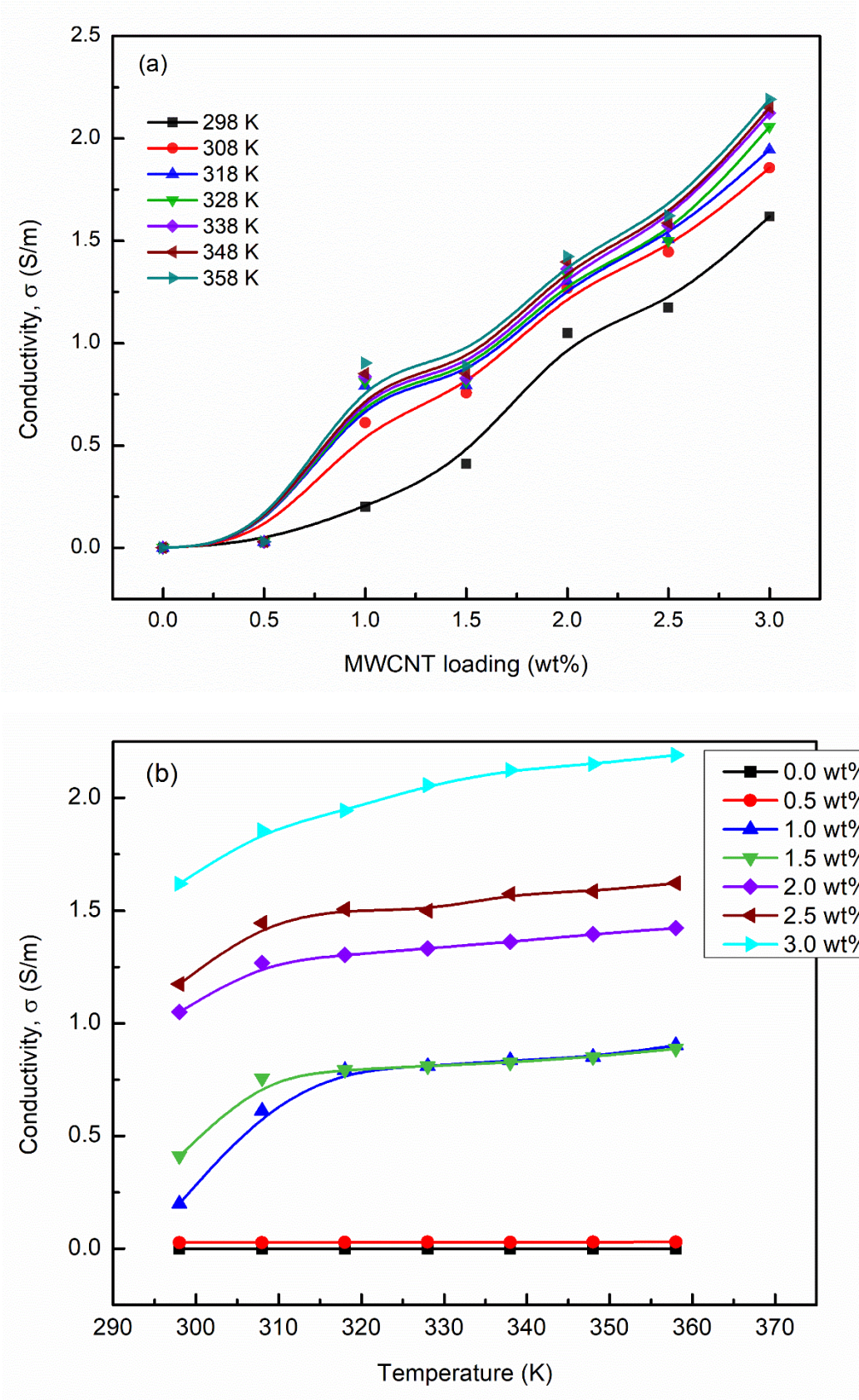

Figure 4.18: (a) Conductivity vs wt% of CNTs and (b) Conductivity vs temperature for cellulose sheet (0 wt%) and different wt% of CNT/cellulose nanocomposites.

The conductivity of the nanocomposites increases with the increase of incorporating wt% of CNTs in the cellulose matrix (Figure 4.18) and become 2.34 S/m at a very small applied voltage (5V). The temperature dependent electrical conductivity is shown in Figure 4.18. The electrical conductivity of the nanocomposites increases with the increase in temperature indicating the semiconducting nature of the composites.

4.6.4 Activation Energy

The activation energy is evaluated from the slopes of the current density versus inverse temperature curve (J vs 1000/T) by using the equation, $J = J_0\, e^{-\Delta E/kT}$. Figure 4.19 illustrates (a) Variation of current density with 1000/T and (b) variation of ΔE values of nanocomposite sheet with different concentrations of CNTs.

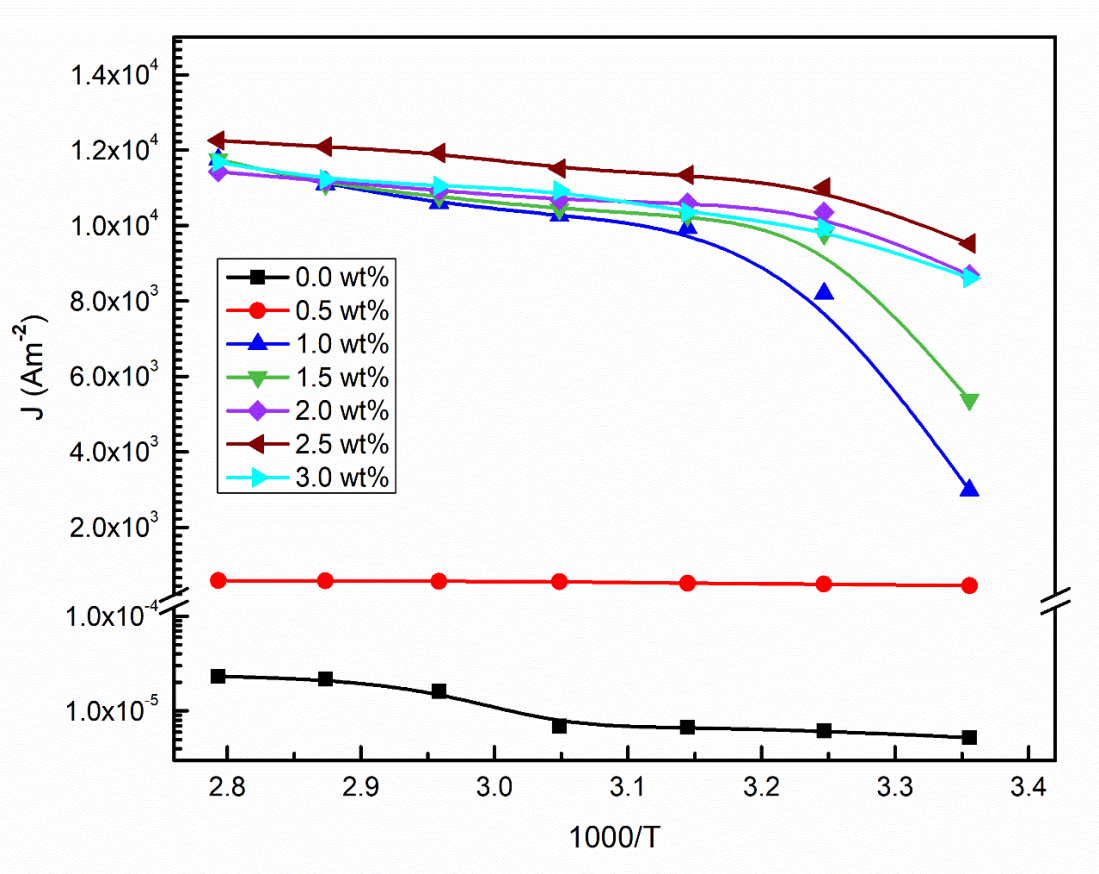

Figure 4.19: (a) Variation of current density with 1000/T.

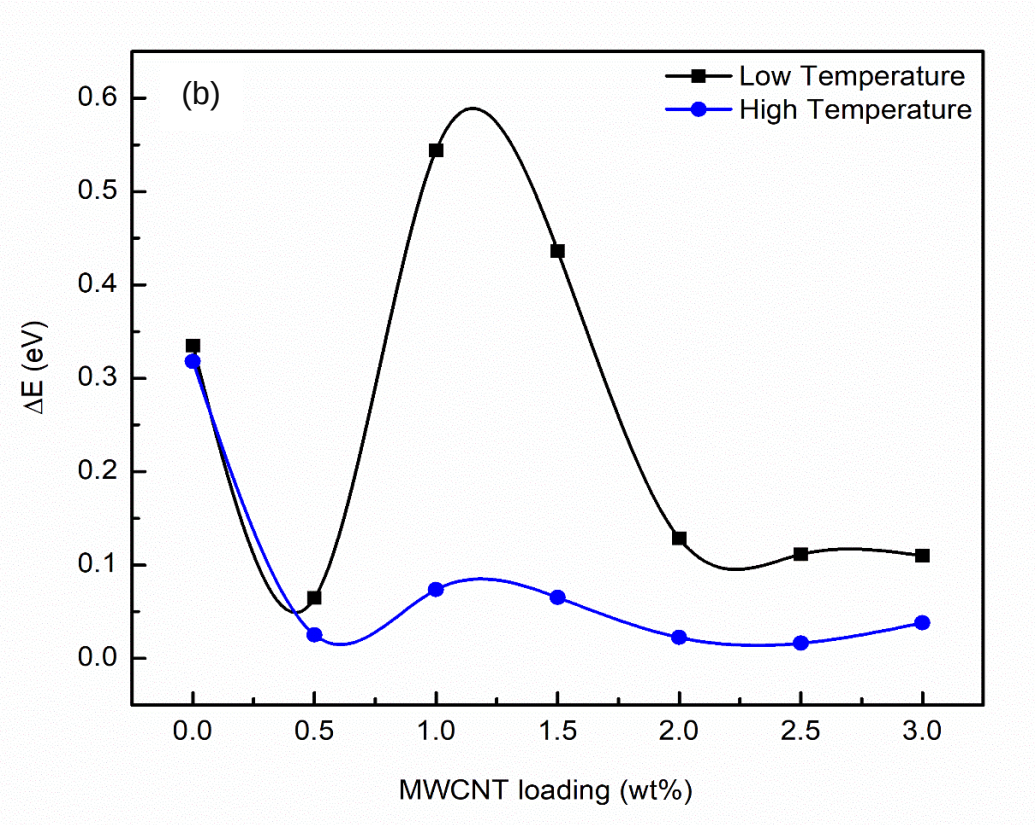

Figure 4.19 (b): Activation energy vs wt% of CNT in the cellulose matrix.

Table 4.3: Activation energy values of nanocomposites in two temperature regions.

Sample	Activation Energy, ΔE (eV)	
	Low Temperature	High Temperature
Cellulose sheet	0.335	0.318
0.5 wt%	0.065	0.025
1.0 wt%	0.544	0.074
1.5 wt%	0.436	0.065
2.0 wt%	0.128	0.022
2.5 wt%	0.111	0.016
3.0 wt%	0.109	0.038

Figure 4.19 (b) shows two regions of conduction indicated by different activation energies i.e. at low temperature region and high temperature region. The values of the activation energy are observed to decrease in the high temperature region owing to the thermally activated tunneling or hopping of the charge carriers through the connected network of conducting filler in the composites. The activation energy of cellulose sheet is found here 0.34 eV for low temperature region and 0.32 eV for high temperature region, which is quite close as Einfeldt et al. [21] mentioned for cellulose (0.47 eV). At 0.5 wt% the activation energy in the low temperature region reaches a minimum value, this may be because of a very well dispersion which is important for establishing the conductive network. From our result it can be said that the activation energy which is required for electrical conduction in the nanocomposites decreases with the increase in filler loading [22]. Beyond the percolation threshold, there is an increase in the activation energy for 1.0 wt% and 1.5 wt% composites. There is also a small increase of activation energy at 3.0 wt% composites because high concentration of CNTs lead to lack of the dispersion.

4.7 Flexibility Test

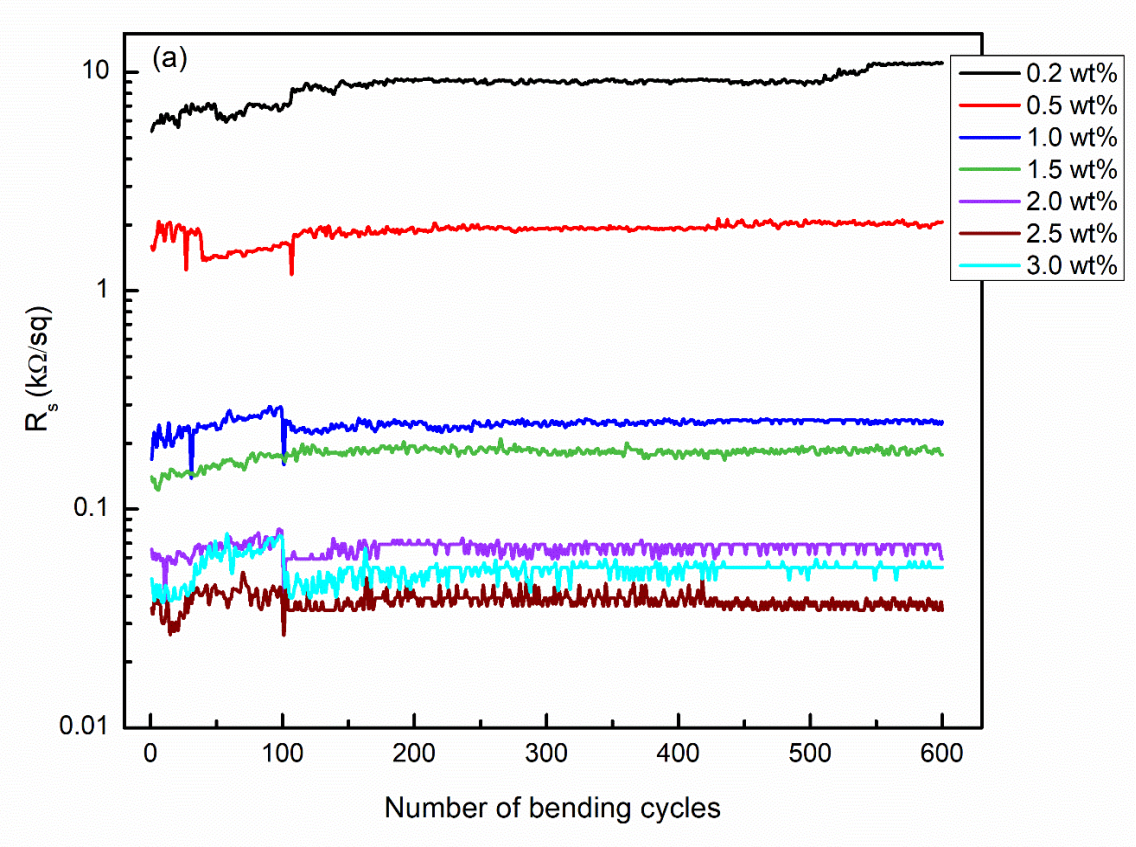

Figure 4.20: (a) Variation of sheet resistance of the nanocomposites according to the number of bending cycles.

The variation rate of sheet resistance according to the number of bending cycles is observed to investigate the mechanical flexibility of all the nanocomposites and shown in Figure 4.20 (a). Cyclic bending test is carried out at different bending angles (above 90°) and the variation of the sheet resistance is recorded with a digital multimeter (GW Instek GDM- 451, Taiwan). There is no significant change in the conductivity of the composites indicates the strong attachment of CNTs on the cellulose fibers and which also implies that the conducting CNT networks are not disrupted even after 600 bending cycles. This result demonstrates high flexibility of the composites. For 3.0 wt% composites, a slight increase in the sheet resistance is observed because high volume content of CNTs reduce the bending properties of the composites due to the hindrance caused by CNTs during densification [23]. High CNT loading increases the difficulty of dispersing CNTs in the composites and occurs agglomeration which interrupts the cohesion between CNTs and matrix leads to the loss of bonding.

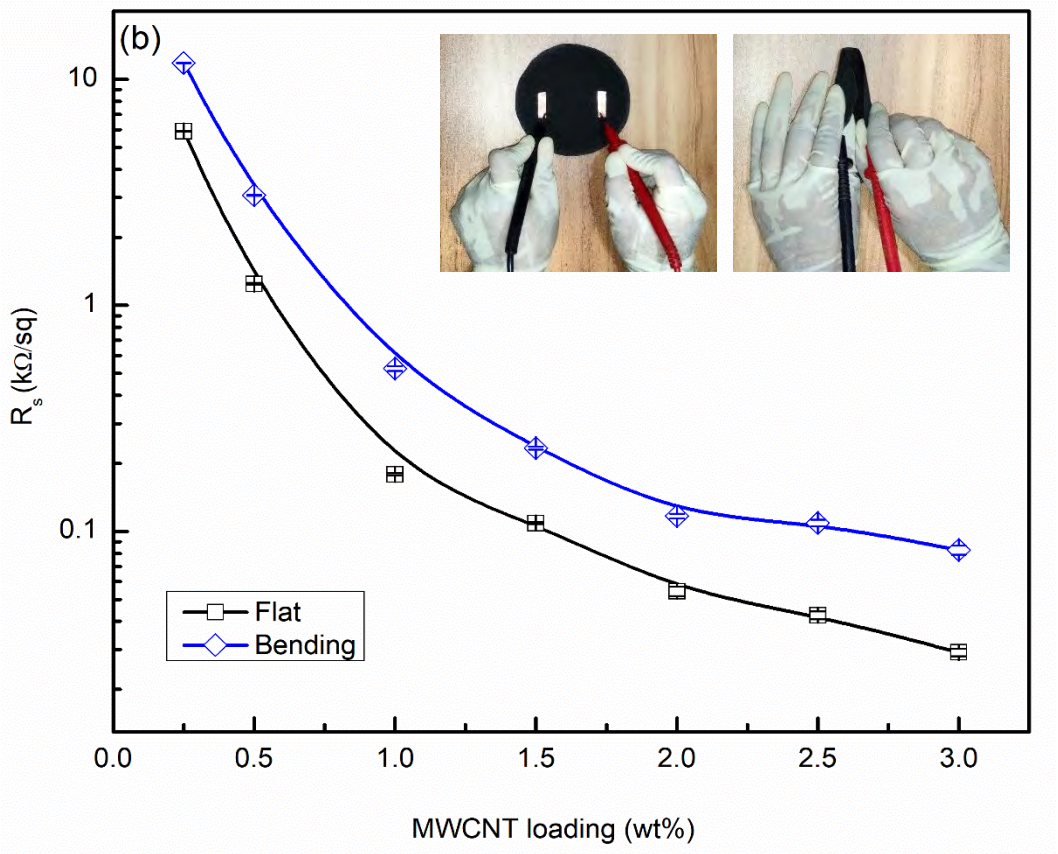

Figure 4.20: (b) Sheet resistance versus CNT concentration curves during flat and bending states, inset: photographs of sheet resistance measurement of the sample with flat and bending states.

Figure 4.20 (b) illustrates the influence of bending states on the sheet resistance curves of the composites. There is a minor change in sheet resistance between the two states. The slightly less conductivity of the composite samples at the bending state as compared to the flat sample probably due to the change in geometry and interconnections of CNTs in the matrix. Though the sheet resistance of the composites is reduced again upon returning to the flat state. This characteristics indicate high mechanical flexibility of the composites, which make them suitable for the applications in flexible energy storage devices.

References

[1] Jiang, H., X., Ni, Q., Q., Natsuki, T., "Design and evaluation of the interface between carbon nanotubes and natural rubber", Polymer Composites, Vol. 32, pp. 236-242, 2011.

[2] Naseh, M., V., Khodadadi, A., A., Mortazavi, Y., Pourfayaz, F., Alizadeh, O., Maghrebi, M., "Fast and clean functionalization of carbon nanotubes by dielectric barrier discharge plasma in air compared to acid treatment", Carbon, Vol. 48, pp. 1369-1379, 2010.

[3] Camacho, D., P. Velázquez, E., F., Félix1, D., E., R., Ortega1, M., C., Mundo, R., S., Castro, T., C., "Functionalization of multiwalled carbon nanotubes by microwave irradiation for lysozyme attachment: comparison of covalent and adsorption methods by kinetics of thermal inactivation", Advances in Natural Sciences: Nanoscience and Nanotechnology, Vol. 8, pp. 045011, 2017.

[4] Reddy, A., L., M., Ramaprabhu, S., "Hydrogen storage properties of nanocrystalline Pt dispersed multi-walled carbon nanotubes", International Journal of Hydrogen Energy, Vol. 32, pp. 3998 – 4004, 2007.

[5] Tian, R., Wang, X., Li et al., "An efficient route to functionalize singe-walled carbon nanotubes using alcohols," Applied Surface Science, Vol. 255, pp. 3294–3299, 2008.

[6] Yeoh, W-M., Lee, K-Y., Chai, S-P., Lee, K-T, Mohamed, A., R., "Synthesis of high purity multi-walled carbon nanotubes over Co-Mo/MgO catalyst by the catalytic chemical vapor deposition of methane", New Carbon Materials, Vol. 24, pp. 119-120, 2009.

[7] Liu, L., Gao, Z., Y., Su, X., P., Chen, X., Jiang, L., Yao, J., M., "Adsorption removal of dyes from single and binary solutions using a cellulose-based bioadsorbent", ACS Sustainable Chemistry & Engineering, vol. 3, pp. 432-442, 2015.

[8] Zhang, P., Dong, S., J., Ma, H., H., Zhang, B., X., Wang, Y., F., Hu, X., M., "Fractionation of corn stover into cellulose, hemicellulose and lignin using a series of ionic liquids", Industrial Crops and Products, Vol. 76, pp. 688-696, 2015.

[9] Lamaming, J., Hashim, R., Sulaiman, O., Leh, C., P., Sugimoto, T., Nordin, N., A., "Cellulose nanocrystals isolated from oil palm trunk", Carbohydrate Polymers, Vol. 127, pp. 202–208, 2015.

[10] Gao, X., Chorover, J., "Adsorption of sodium dodecyl sulfate (SDS) at ZnSe and a-Fe2O3 surfaces: Combining infrared spectroscopy and batch uptake studies", Journal of Colloid and Interface Science, Vol. 348, pp. 167–176, 2010.

[11] Oh, S., Y., Yoo, D., I., Shin, Y., Seo, G., "FTIR analysis of cellulose treated with sodium hydroxide and carbon dioxide", Carbohydrate Research, Vol. 340, pp. 417-428, 2005.

[12] Chena, W., Yua, H., Liua, Y., Chen, P., Zhang, M., Hai, Y., "Individualization of cellulose nanofibers from wood using high-intensity ultrasonication combined with chemical pretreatments", Carbohydrate Polymers, Vol. 83, pp. 1804–1811, 2011.

[13] Dutta, D., Hazarika, R., Dutta, P., D., Goswami, T., Sengupta, P., Dutta, D., K., "Synthesis of Ag-Ag_2S Janus nanoparticles supported on environmentally benign cellulose template and their catalytic applications", RSC Advances, vol. 6, pp. 85173-85181, 2016.

[14] Zavadskii, A., E., 'X-ray diffraction method of determining the degree of crystallinity of cellulose materials of different anisotropy", Fibre Chemistry, Vol. 36, pp. 425–430, 2004.

[15] Anilkumar, K., M., Jinisha, B., Manoj, M., Pradeep, V., S., Jayalekshmi, S., "Layered sulfur/PEDOT:PSS nano composite electrodes for lithium sulfur cell applications", Applied Surface Science, Vol. 442, pp. 556–564, 2018.

[16] Kim, D.-Y., Nishiyama, Y., Wada, M., Kuga, S., "High-yield carbonization of cellulose by sulfuric acid impregnation", Cellulose, Vol. 8, pp. 29-33, 2001.

[17] Lewin, M., "Handbook of fiber chemistry", Boca raton: CRC press, 2007.

[18] Visakh, P., M., Arao, Y., "Flame Reterdants: Polymer Blends, Composites and Nanocomposites", 2015.

[19] Beyer, G., "Short Communication: Carbon nanotubes as flame retardants for polymers", Fire and Materials, Vol. 26, pp. 291-293, 2002.

[20] Kashiwagi, T., Du, F., M., Douglas, J., F., Winey, K., I., Harris, R., H., Shields, J., R., "Nanoparticle networks reduce the flammability of polymer nanocomposites", Nature Materials, Vol. 4, pp. 928-933, 2005.

[21] Einfeldt, J., Meißner, D., Kwasniewski, A., "Polymerdynamics of cellulose and other polysaccharides in solid-secondary dielectric relaxation processes", Progress in Polymer Science, Vol. 26, pp.1419-1472, 2001.

[22] Nayak, L., Rahaman, M., Aldalbahi, A., Chaki, T., K., Khastgir, D., "Polyimide-Carbon nanotubes nanocomposites: electrical conduction behavior under cryogenic condition", Polymer Engineering and Science, Vol. 57, pp. 291-298, 2016.

[23] Ning, J., Zhang, J., Pan, Y., Guo, J., "Fabrication and mechanical properties of SiO_2 matrix composites reinforced by carbon nanotube", Materials Science and Engineering A, Vol. 357, pp. 392-396, 2003.

CHAPTER 5

CONCLUSIONS AND SUGGESTIONS FOR FUTURE WORK

5.1 Conclusions

In this research, CNT/cellulose composites are fabricated by varying the concentration of MWCNTs up to 3.0 wt% and different properties of the composites have been investigated.

Effective CNT dispersion in the polymer matrix leads to the novel properties of composites and in order to attain a uniform CNT dispersion in aqueous solvent anionic surfactant SDS is used here. By wrapping the nanotube surface with SDS molecules, the CNTs become dispersible in the polymer matrix.

The FESEM micrographs of cellulose sheet and CNT/cellulose composites exhibit clean surfaces of the cellulose fibers and uniform attachment of MWCNTs on the surfaces of all the fibers of cellulose sheet, respectively. All the samples are found with high content of C and O from the EDX analysis. S and Ca are also present in small contents, which may be due to the chemical treatment of pulp in the Kraft process or the use of SDS.

The FTIR spectrum of the CNT/cellulose composites do not show any significant changes in the band position but increase of absorption band intensities of –OH and $–CH_2$ groups are observed and a new peak for hydrophilic sulfonate group is also found.

The XRD patterns of the composites exhibit that the crystallinity of the composites is improved with increasing CNT concentration. The crystallite size of the nanocomposites is found to be larger than that of the cellulose sheet (6.24 nm) and 3.0 wt% CNT/cellulose nanocomposites represents maximum value of the crystallite size which is 6.91 nm.

The TGA thermograms show two-stage degradation for all the samples and the dominant weight loss is observed between 566-663 K.

Flame retardancy test indicates that the CNT/cellulose sheet exhibits an improved flame retardant performance where the flame dies out early (6s) and the sample turns to carbonaceous char residue as compared to the cellulose sheet.

From the electrical measurements, a gradual decrease of sheet resistance with increasing CNT concentration in the composites are observed and the value of the sheet resistance is varied from 6.5 kΩ/sq to 0.04 kΩ/sq. J-V curves of the CNT/cellulose

composites indicate Ohmic conduction. DC conductivity of the nanocomposites increases with the increase in temperature indicating the semiconducting nature of the composites.

The conductivity of the nanocomposites also increases with the increase of incorporated MWCNTs and becomes 2.34 S/m at only 5V. It is seen that the activation energy of all the samples are decreased in high temperature region (358 K) compared to the low temperature region (298 K).

Flexibility test shows that the conducting CNT networks of the composites are not disrupted even after 600 bending cycles and slightly less conductivity of the composite samples at bending state as compared to flat sample is observed, this is may be due to the change in geometry and interconnections of CNTs in matrix, which indicates high mechanical flexibility of the composites.

In summary, low cost, biodegradable, thin and flexible CNT/cellulose nanocomposites are fabricated and CNTs effectively reinforced the electrical, structural, thermal and mechanical properties of the composites. The presented results in this thesis indicate that the CNT/cellulose nanocomposites may find applications in foldable energy storage electronic devices as well as in other advanced technological fields such as paper battery, supercapacitor, transistors, actuators, multifunctional sensors, strain gauges, electric heater, power generators, and EMI shielding materials etc.

5.2 Recommendations for Future Work

Further investigations are required to better understand different features and to realize new capabilities of the composites for the development of applications in advanced technological fields. Therefore, the following studies may be carried out to understand the better implications of the composites —

- To perform AC electrical measurements.
- Transmission electron microscopy images analysis.
- It would be useful to measure specific capacitance.
- To study EMI shielding effectiveness.
- A comparative study can be done by adding other nanofillers in the cellulose matrix.